



Norwegian University of
Science and Technology

Ventilative Cooling of a Super Insulated Residential Building

Ventilasjonskjøling av superisolert bolig

Karoline Høva Bøhler

Master of Science in Mechanical Engineering

Submission date: February 2018

Supervisor: Hans Martin Mathisen, EPT

Norwegian University of Science and Technology
Department of Energy and Process Engineering

EPT-M-2017-123

MASTER THESIS

for

Student Karoline Høva Bøhler

Spring 2017

Ventilative Cooling of a Super Insulated Residential Building

*Ventilasjonskjøling av superisolert bolig***Background and objective**

In airtight residential buildings, controlled ventilation is a need to secure indoor air quality. Normally mechanical ventilation is the preferred solution, but operation of fans requires considerable amounts of electricity. The preferred solution for cooling of residential buildings is therefor through windows. In super insulated buildings the cooling season starts earlier and ends later in the year compared to older buildings. This means that air will be supplied with lower temperatures for certain periods. However, in periods with relatively low outdoor temperatures window opening is associated with draft problems and poor thermal comfort. Therefore, more research is required on this topic.

The objective of this master work is to study different solutions for air supply through window openings for cooling in super insulated buildings. Full scale measurements from ZEB Living Lab will be used to validate simulation models.

The following tasks are to be considered:

1. Update the literature study on window ventilation, and its simulation with CFD performed in the project work
2. Collect full scale measurements done by other master student and if necessary supplement with relevant data
3. Update existing IDA ICE model of Living Lab and perform some calculation for relevant conditions
4. Establish model in the CFD simulation tool
5. Perform simulations of air movements with special attention to thermal comfort

-- " --

Within 14 days of receiving the written text on the master thesis, the candidate shall submit a research plan for his project to the department.

When the thesis is evaluated, emphasis is put on processing of the results, and that they are presented in tabular and/or graphic form in a clear manner, and that they are analyzed carefully.

The thesis should be formulated as a research report with summary both in English and Norwegian, conclusion, literature references, table of contents etc. During the preparation of the text, the candidate should make an effort to produce a well-structured and easily readable report. In order to ease the evaluation of the thesis, it is important that the cross-references are correct. In the making of the report, strong emphasis should be placed on both a thorough discussion of the results and an orderly presentation.

The candidate is requested to initiate and keep close contact with his/her academic supervisor(s) throughout the working period. The candidate must follow the rules and regulations of NTNU as well as passive directions given by the Department of Energy and Process Engineering.

Risk assessment of the candidate's work shall be carried out according to the department's procedures. The risk assessment must be documented and included as part of the final report. Events related to the candidate's work adversely affecting the health, safety or security, must be documented and included as part of the final report. If the documentation on risk assessment represents a large number of pages, the full version is to be submitted electronically to the supervisor and an excerpt is included in the report.

Pursuant to "Regulations concerning the supplementary provisions to the technology study program/Master of Science" at NTNU §20, the Department reserves the permission to utilize all the results and data for teaching and research purposes as well as in future publications.

The final report is to be submitted digitally in DAIM. An executive summary of the thesis including title, student's name, supervisor's name, year, department name, and NTNU's logo and name, shall be submitted to the department as a separate pdf file. Based on an agreement with the supervisor, the final report and other material and documents may be given to the supervisor in digital format.

- Work to be done in lab (Water power lab, Fluids engineering lab, Thermal engineering lab)
 Field work

Department of Energy and Process Engineering, 4. September 2017



Hans Martin Mathisen
Academic Supervisor

Research Advisor:

Abstract

Passive cooling methods are preferred for super insulated, energy efficient buildings, to keep the energy consumption low. However, well insulated buildings are associated with longer cooling seasons, which means that air with lower temperatures will be supplied to the buildings for certain periods. For these periods, the use of ventilative cooling is associated with thermal discomfort and draught problems. The objective of this master thesis is to establish a reliable tool, by using Computational Fluid Dynamics, that can be used to study cooling by window opening in super insulated buildings in cold climates. The CFD tool ANSYS Fluent will be used to establish a CFD model and carry out simulations, where the data from the simulations will be used for thermal comfort analysis.

The CFD model is based on the geometry of the ZEB Living Laboratory building facility, located in Trondheim, Norway. This is a research facility that was built with the purpose of investigating how users interact with low-energy buildings. The CFD model will be validated with full-scale experimental measurements.

Three models have been established in this master thesis. A set of simplifications to the model geometry and the simulation setup have been carried out, due to limitations in computer capacity and time restrictions. Model A verified the setup to simulate the mechanical ventilation system, and the appropriate boundary conditions for the walls and roof. Model B investigated the effect of solar load on the model and verified the setup of the solid surface material characteristics. The transient simulation with solar load revealed a risk of thermal discomfort due to overheating in the building. Model C carried out the simulations that are compared with the full-scale experiment measurements. Ventilative cooling with cross ventilation by 25% opening (of measured maximum) of the north window and 100% opening of a kitchen skylight window was investigated. Different boundary conditions were tested at the inlet of the north window opening. The compared results from the simulated cases and the experiment revealed that the CFD model is not yet able to predict the flow to an acceptable accuracy. The sources of errors are discussed and the ones that are presumed the most dominant are identified.

The data from the case that was concluded to predict the flow best, compared with the experiment, are used to explain how thermal comfort investigations with CFD solutions can be carried out. For the draught rate calculations, both the directional (attained from the simulation data) and the omnidirectional (calculated with correction formulas) values are considered, to investigate the turbulence effects of the flow. These are again compared with the full-scale experiment values.

Sammendrag

Passive kjølemetoder er foretrukket i superisolerte, energi effektive bygninger, for å holde energiforbruket lavt. Imidlertid er godt isolerte bygninger forbundet med kjølesesonger som varer over lengre tid, noe som betyr at luft med lavere temperaturer vil bli levert til bygningene i bestemte perioder. I disse periodene vil bruk av ventilativ kjøling være assosiert med termisk ukomfort og trekk problemer. Formålet med denne masteroppgaven er å etablere et pålitelig verktøy, ved bruk av numerisk fluiddynamikk (CFD), som kan brukes til å studere kjøling med vindusåpninger i superisolerte bygninger i kaldt klima. CFD verktøyet ANSYS Fluent er brukt til å etablere CFD modeller og kjøre simuleringer, der resultatene fra simuleringene skal brukes for termisk komfort analyser.

CFD modellen er basert på geometrien til ZEB Living Lab, en bygning som befinner seg i Trondheim, Norge. Bygningen er et forskningsanlegg som ble bygd med det formål å undersøke hvordan brukere opplever det å forholde seg til lav energi bygg. Validering av CFD modellen vil skje med full-skala målinger utført i bygget.

Tre modeller har blitt etablert i denne masteroppgaven. Forenklinger preger både modelgeometrien og deler av simuleringsoppsettet, først og fremst på grunn av begrensninger i datakapasitet og tid. Modell A verifiserte oppsettet for å simulere det mekaniske ventilasjonssystemet, samt grensebetingelsene for veggene og taket i modellen. Modell B undersøkte effekten solbelastning har på modellen og verifiserte hvordan overflatene til de solide materialene skulle bli definert. Fra en transient simuleringen med solbelastning, ble det avklart at det er en risiko for termisk ukomfort på grunn av overoppheting i modellbygningen. Modell C utførte simuleringer som har blitt sammenlignet med full-skala forsøksmålinger. Ventilativ kjøling med kryss ventilasjon, der 25% åpning (av målt maksimal) for nord vindu og 100% åpning for himmellys vindu, ble undersøkt. Ulike grensebetingelser ble testet ut ved åpningen av nord vinduet. De sammenlignede resultatene fra simuleringene og forsøket viste at CFD-modellen foreløpig ikke klarer å estimere luftstrømmen nøyaktig nok. Feilkildene til CFD modellen blir diskutert, og de som antas å være mest dominerende blir identifisert.


Dataen fra den simuleringen som ble konkludert til å estimere luftstrømmen best, sammenlignet med forsøket, er brukt til å forklare hvordan termisk komfort analyser med CFD beregninger kan utføres. Når trekk risiko blir regnet ut, blir de vektor baserte målingene (hentet fra CFD simuleringen) sammenlignet med verdier regnet ut med korreksjonsformler, for å undersøke effekten av turbulens. Disse verdiene blir igjen sammenlignet med resultatet fra full-skala forsøket.

Preface

This master thesis is written at the Department of Energy and Process Engineering at the Norwegian University of Science and Technology. The master thesis is the final work before completing the Master of Science degree in Mechanical Engineering. Although it has been a pleasure to immerse myself in the fields of CFD and natural ventilation, the work have shown itself to be larger than first expected. This have caused the final result to be somewhat less than was originally intended. However, the master thesis has been a great learning experience.

I would like to show my appreciation to my academic supervisor Hans Martin Mathisen, for coming up with the idea of investigating cooling methods in ZEB Living Lab, and for good guidance and advise during the master work. Thanks to Solveig Blandkjenn for supplying the measurement data from the full-scale experiments, and for helping with the questions I've had in regards to this data. I also wish to thank Eugen Uthaug for facilitating me with computer equipment, and access to the Living Lab Database.

Trondheim, 2018-02-05


Karoline Høva Bøhler

Contents

Master Project Description	i
Abstract	iii
Sammendrag	v
Preface	vii
Table of Contents	xiii
List of Figures	xvii
List of Tables	xx
Acronyms	xxi
Nomenclature	xxiii
1 Introduction	1
1.1 Background	1
1.1.1 Problem formulation	2
1.1.2 Literature survey	2
1.2 Scope	3
1.2.1 Limitations	4
1.3 Approach	4
1.4 Structure of the Thesis	4
2 Background	7
2.1 Zero Emission Buildings	7
2.1.1 Concept	7
2.1.2 ZEB Living Laboratory	8
2.2 Ventilative Methods	9

2.2.1	Mechanical ventilation	9
2.2.2	Natural ventilation	10
2.2.3	Hybrid (Mixed-mode) ventilation	12
2.3	Cooling in Buildings	13
2.3.1	Thermal balance of a room	13
2.3.2	Cooling methods	14
2.3.3	Existing buildings using passive cooling	14
2.4	Ventilative Cooling in ZEB Living Lab	16
2.5	Thermal Comfort	17
2.5.1	Predicted mean vote (PMV)	17
2.5.2	Predicted percentage dissatisfied (PPD)	18
2.5.3	Local thermal discomfort	18
3	Simulation Theory	21
3.1	Introduction to CFD	21
3.1.1	CFD used in the building sector	21
3.2	CFD Analysis	23
3.3	The Fundamental Equations	23
3.3.1	Boussinesq approximation	24
3.4	Models	25
3.4.1	Energy	25
3.4.2	Viscous	25
3.4.3	Radiation	25
3.5	Turbulence Modelling	26
3.5.1	Reynolds averaged Navier–Stokes equation	26
3.5.2	The \bar{k} - ϵ turbulence model	27
3.5.3	RNG	28
3.5.4	Standard Wall Modeling	29
3.6	Radiation	29
3.6.1	Surface-to-Surface (S2S) Radiation Model	29
3.6.2	Solar Load model	29
3.7	The Grid	30
3.7.1	Important considerations	31
3.7.2	Grid quality	31
3.7.3	Grid independence	32
3.8	Discretization Schemes	32
3.8.1	Finite volume method	32
3.8.2	Solvers	32
3.8.3	Gradients and derivatives	34
3.8.4	Spatial discretization	34
3.8.5	Temporal discretization	34
3.9	Numerical Analysis	35
3.9.1	Consistency	35
3.9.2	Stability	35
3.9.3	Convergence	35
3.9.4	Verification and validation	36

3.10	Choice of Boundary Conditions	36
4	ZEB Living Laboratory	39
4.1	ZEB Living Laboratory	39
4.1.1	The concept	39
4.1.2	Location	39
4.1.3	The facility layout	40
4.1.4	Thermal specifications for the building envelope	43
4.1.5	HVAC specifications	44
4.1.6	Sensor locations	45
4.2	Full-scale Measurements	47
4.2.1	Ventilative cooling with north window	48
4.2.2	Ventilative cooling with south window	48
4.3	The Experiments Used For Validation	49
4.3.1	Sources of error for the experimental data	50
5	The Method	51
5.1	Introducing the CFD Model Geometry	51
6	Model A	53
6.1	General Info About the Model	54
6.2	Additional Simplifications and Comments to Model A	58
6.3	Grid	60
6.4	CASE 1: Air Flow Investigation	62
6.4.1	Input values for Case 1	62
6.4.2	The simulation result for Case 1	63
6.4.3	Case 1 Comment on the presented results	65
6.5	CASE 2: Energy Calculation Effects	66
6.5.1	Input values for Case 2	66
6.5.2	Data extraction	67
6.5.3	Case 2.1 Setup and Results	68
6.5.4	Case 2.2 Setup and Results	72
6.5.5	Case 2 Comment on the presented results	74
7	Model B	77
7.1	General Info About the Model	78
7.2	Grid	78
7.3	CASE 3: Effect of Solar Load	81
7.3.1	Input values for Case 3	81
7.3.2	Data extraction	82
7.3.3	Case 3 The simulation results	83
7.3.4	Case 3 Comment on the presented results	88

8	Model C	89
8.1	General Info About the Model	90
8.1.1	South window	90
8.1.2	Skylight windows	91
8.1.3	North windows	91
8.2	CASE 4: Ventilative Cooling with the North Window	92
8.2.1	Grid	92
8.2.2	Input values for Case 4	95
8.2.3	Data extraction	99
8.2.4	Case 4: The simulation results	100
8.2.5	Comment on the results	106
9	Discussion of the Models	107
9.1	The CFD Investigations	107
9.1.1	Case 1	107
9.1.2	Case 2	107
9.1.3	Case 3	108
9.1.4	Case 4	108
9.2	Sources of Error	109
9.2.1	Sources of error that result in under- and over- estimating heat loss in the simulation	109
9.2.2	Sources of error related to the simulation setup and solution .	110
9.2.3	The assumed most dominant sources	111
10	Thermal Comfort Investigation	113
10.1	Contours of Case 4.5	113
10.1.1	Velocity contours at plane 1	114
10.1.2	Turbulent kinetic energy contours at plane 1	116
10.1.3	Temperature contours at plane 1	118
10.2	Draught Rate Calculations	120
10.2.1	Correction formulas for turbulence intensity I_o and mean air velocity V_o	120
10.2.2	Draught rate comparison	122
10.2.3	Local thermal discomfort calculations for Case 4.5	124
11	Conclusion	127
11.1	Conclusion	127
11.2	Suggestion for Further Works	128
	Bibliography	129
A	Living Lab	137

B	Material Setup Information	139
B.1	Material properties	139
B.2	North window point measurement coordinates	140
C	Window Opening Calculations	141
C.1	Skylight windows	141
C.2	North windows	142
	C.2.1 Opening area found in [Blandkjenn, 2017]	142
	C.2.2 Opening angle calculations for the model	142
C.3	South windows	143
	C.3.1 Opening area found in [Blandkjenn, 2017]	143

List of Figures

2.1	ZEB life cycle	7
2.2	Picture of ZEB Living Lab	8
2.3	Principles of buoyancy driven (stack effect) and wind driven natural ventilation	11
2.4	Principles of single-sided and cross-flow natural ventilation	12
2.5	Thermal balance of a room	13
2.6	Predicted percentage of dissatisfied people (PPD) as a function of the predicted mean vote (PMV)	18
3.1	3D cell types available in ANSYS Fluent	30
3.2	The Pressure-Based Solution Method algorithm steps	33
4.1	Location of Trondheim, on the map of Norway	40
4.2	Illustration of the layout of the Living Laboratory facility	41
4.3	Illustration of the facility section	41
4.4	Double-skin window on the south facade	42
4.5	The north facades of ZEB Living Lab	43
4.6	Layout of the supply and exhaust duct network	45
4.7	Location of the windows used in ventilative cooling measurements	47
4.8	Measurement locations for ventilative cooling with north facade windows	48
6.1	Model A geometry	53
6.2	Floor dimensions of Model A	54
6.3	Details and dimensions of important geometries in the CFD model	54
6.4	Cross section dimensions of Model A	55
6.5	Location and dimensions of north and south windows in Model A	56
6.6	Location and dimensions of skylight windows in Model A	56
6.7	Locations of air supply and extraction in the CFD model	57
6.8	Mesh of Model A, viewed from south-west	60
6.9	Mesh of Model A, viewed from north-east	61

6.10	Case 1 - Velocity streamlines	64
6.11	Case 1 - Streamline distribution for the supply vents	65
6.12	Case 2 - Location of the planes used to evaluate the results	68
6.13	Case 2.1.1 - Temperature contours	69
6.14	Case 2.1.2 - Temperature contours	69
6.15	Case 2.1.1 - Temperature contour, plane 1	70
6.16	Case 2.1.2 - Temperature contour, plane 1	70
6.17	Case 2.1 - Flux Report, Mass flow rate	71
6.18	Case 2.1 - Flux Report, Heat transfer rate	72
6.19	Case 2.2 - Temperature contours	72
6.20	Case 2.2 - Temperature contour, plane 1	73
6.21	Case 2.2 - Temperature contours, viewed from the south	73
6.22	Case 2.2 - Flux Report, Mass Flow Rate & Total Heat Transfer Rate	74
7.1	Model B geometry	77
7.2	Mesh of Model B, viewed from south-west	79
7.3	Mesh of Model B, viewed from north-east	79
7.4	Mesh of Model B, cross-section	80
7.5	Case 3.1 - Temperature contours (steady state)	83
7.6	Case 3.1 - Temperature contour, plane 1 (steady state)	83
7.7	Case 3.1 - Temperature contours, viewed from the south (steady state)	84
7.8	Case 3.1 - Heat conduction over the solid windows	84
7.9	Case 3.2 - Temperature contours, plane 1 (transient)	85
7.10	Case 3.2 - Temperature contours, viewed from south (transient)	86
7.11	Case 3.2 - Temperature contours (transient)	87
7.12	Case 3 - Flux Reports, Mass Flow Rate	88
8.1	Model C geometry	89
8.2	South window cross section	90
8.3	North window open - New boundary surfaces	91
8.4	Mesh of Model C, north window 25%, viewed from south-west	93
8.5	Mesh of Model C, north window 25%, viewed from north-east	93
8.6	Mesh of Model C, north window 25%, cross-section	94
8.7	Mesh of Model C, north window 25%, details of the north window	94
8.8	Plot I - Velocity and temperature at B1	100
8.9	Plot II - Velocity and temperature at B1	101
8.10	Plot I - Velocity and temperature at B2	102
8.11	Plot II - Velocity and temperature at B2	103
8.12	Plot I - Velocity and temperature at B3	104
8.13	Plot II - Velocity and temperature at B3	105
10.1	Case 4.5 - Velocity profile at t=15 s	114
10.2	Case 4.5 - Velocity profile at t=29 s	114
10.3	Case 4.5 - Velocity profile at t=45 s	115
10.4	Case 4.5 - Velocity profile at t=59 s	115
10.5	Case 4.5 - Turbulent kinetic energy profile at t=15 s	116

10.6	Case 4.5 - Turbulent kinetic energy profile at t=29 s	116
10.7	Case 4.5 - Turbulent kinetic energy profile at t=45 s	117
10.8	Case 4.5 - Turbulent kinetic energy profile at t=59 s	117
10.9	Case 4.5 - Temperature profile at t=15 s	118
10.10	Case 4.5 - Temperature profile at t=29 s	118
10.11	Case 4.5 - Temperature profile at t=45 s	119
10.12	Case 4.5 - Temperature profile at t=59 s	119
10.13	Comparison of mean air velocity	121
10.14	Comparison of turbulence intensity	122
10.15	Comparison of draught rate	123
10.16	Comparison of draught rate	125
C.1	Skylight window opening	141
C.2	North window cross section from [Blandkjenn, 2017]	142
C.3	North window cross section of simulation model	142
C.4	South window opening from [Blandkjenn, 2017]	143

List of Tables

2.1	Seven-point thermal sensation scale	17
2.2	Categories of thermal environment	19
3.1	Model constants for RNG \bar{k} - ϵ model	29
4.1	Solar radiation in Trondheim	40
4.2	Thermo-physical specifications of the building envelope	43
4.3	Internal heat loads of ZEB Living Lab	44
4.4	Ventilation rates in ZEB Living Lab	45
4.5	The window arrangement for the ventilative cooling measurements	47
4.6	Data from Living Lab Database	49
6.1	Vent characteristics	57
6.2	Grid operations - Model A	60
6.3	Mesh statistics - Model A	61
6.4	Fixed setup settings for all the simulation cases	62
6.5	Extraction outlet B.C. calculations - new mass flow rates	64
6.6	Case 2 - Solid material properties	66
6.7	Case 2 - Plane locations for post-processing	67
7.1	Window thickness	78
7.2	Grid operations - Model B	78
7.3	Mesh statistics - Model B	80
7.4	Case 3 - Thermal condition specifications	81
7.5	Case 3 - Input values for the solar load model	82
8.1	Case 4 - Grid operations - Model C	92
8.2	Case 4 - Mesh statistics - Model C	95
8.3	Case 4 - Thermal condition specifications	97
8.4	Case 4 - Input values for the solar load model	97
8.5	Case 4 - Boundary conditions for the north window	98

8.6	Case 4 - North window measurement points (in coordinates)	99
A.1	Integrated sensors in Living Lab	137
A.2	Measuring Equipment for the Full-scale experiment	137
B.1	Material properties	139
B.2	Overview of the north window point location in coordinates	140
C.1	Calculated opening angles for the north window	143

Acronyms

B.C. boundary condition.	FVM finite volume method.
CAD Computer-Aided Design.	GHG green house gases.
CAE Computer-Aided Engineering.	HVAC Heating, ventilation, and air conditioning.
CAV Constant Air Volume.	LES large-eddy simulations.
CFD Computational Fluid Dynamics.	N-S Navier–Stokes.
CO₂ carbon dioxide.	PD percentage dissatisfied.
DNS direct numerical simulations.	PDE partial differential equation.
DO Discrete Ordinates.	PMV Predicted mean vote.
DTRM Discrete Transfer Radiation Model.	PPD Predicted percentage dissatisfied.
F fluorinated.	RANS Reynolds averaged Navier–Stokes.
FDM finite difference method.	RH relative humidity.
	RNG Re-Normalization Group.
	RSM Reynolds Stress Model.
	S2S Surface-to-Surface.
	VAV Variable Air Volume.
	ZEB Zero Emission Building.

Nomenclature

Greek symbols

β	thermal expansion coefficient, $\approx \frac{1}{T}$ for ideal gases $[\frac{1}{K}]$
δ_{ij}	Kronecker delta function, $\delta_{ij} = 1$ if $i = j$ and $\delta_{ij} = 0$ if $i \neq j$
μ	dynamic viscosity $[\frac{kg}{m \cdot s}]$
μ_T	turbulent dynamic viscosity $[\frac{kg}{m \cdot s}]$
∇	vector differential operator
Φ_{ci}	conductive flux through the walls $[\frac{W}{m^2}]$
Φ_{cv}	convective flux exchange between internal surfaces and air $[\frac{W}{m^2}]$
Φ_{pc}	total convective internal gains $[\frac{W}{m^2}]$
Π	stress tensor
ρ	fluid density $[\frac{kg}{m^3}]$

σ Stefan-Boltzmann constant
 $[5.67036713 \times 10^{-8} \frac{W}{m^2 K^4}]$

τ_{ij} Reynolds stress tensor

ϕ dissipation function

τ viscous stress tensor

Superscript

' defines a fluctuating quantity

- defines a time averaged quantity

Symbols

\mathbf{V}	velocity vector $[\frac{m}{s}]$
C_p	pressure coefficient [-]
c_p	specific heat capacity $[\frac{J}{kg \cdot K}]$
E_s	short-wavelength radiation $[\mu m]$
g	gravitational acceleration $[\frac{m}{s^2}]$
h	Specific enthalpy $[\frac{J}{kg}]$
h, H	height [m]
hc_i	convective exchange coefficient $[\frac{J}{K \cdot m^2 \cdot s}]$
I_o, T_u	local turbulence intensity [%]
I_V	turbulence intensity (vector) [%]
k	thermal conductivity $[\frac{W}{m \cdot K}]$
l, L	length [m]
p	pressure [Pa]
Q_m	total mass flow rate of air $[\frac{kg}{s}]$
S_{ij}	mean strain rate tensor
T	temperature [K or °C]
t	time [s]
$t_{a,l}$	local air temperature [°C]

u, v, w velocities in x-, y-, and z-
direction $[\frac{m}{s}]$

V velocity, free stream $[\frac{m}{s}]$

$V_o, \bar{v}_{a,l}$ local mean air velocity $[\frac{m}{s}]$

V_V mean velocity vector $[\frac{m}{s}]$

x, y, z directional coordinates $[m]$

V volume of the a room $[m^3]$

Subscripts

i, j, k denoting the Cartesian coordi-
nates

Introduction

1.1 Background

One of the biggest threats the world is facing today is climate changes. The impact and consequences of global warming will not only be noticed by changes to the global temperatures, but in some regions, changes in the precipitation, relative humidity, wind speed and potential evaporation will be significant, and there are many uncertainties coupled to how species and ecosystems will handle these changes [Hulme, 2005]. The building sector account for more than one-third of the final energy consumption globally [International Energy Agency, 2013], and in 2010 the energy-related GHG emissions, CO₂ emissions, and F-gases emissions in the building sector were measured to be 19%, 33% and 12.5-33%, respectively [Intergovernmental Panel on Climate Change, 2015].

One way to tackle the problem is to build more energy efficient buildings. The increasing focus on low-energy, and low-emission buildings shows that there is much potential in making more energy efficient and climate-friendly commercial and residential buildings. The ZEB Living Lab located in Trondheim, Norway was built as a research facility, with the main purpose of investigating how users interact with low-energy buildings that have integrated state-of-the-art technologies. The aim of the building design was to reach a Zero Emission target. This was realized by implementing measurements for energy conservation and exploitation of renewable energy sources [Goia et al., 2015]. Because of the air-tight, well insulated envelope that is typical for Zero Emission Buildings, research and experiments have shown that risk of overheating is a big problem for the buildings, event in cooler climates.

Overheating in buildings causes thermal discomfort. To reduce the energy demand for the buildings, passive methods for removing the excess heat and cooling down the building is preferred. The cooling strategy for ZEB Living Lab is to apply ventilative cooling. For super insulated buildings, the need for cooling span over

a longer time period, compared with older buildings. This means that cooling by window ventilation may have to be utilized when outdoor temperatures are quite low (early spring/late autumn). Supplying air with low temperatures to buildings, is a risk as it may cause the occupants inside the building thermal discomfort as a result of draught [Nilsson and Group, 2003].

To find the optimal solution for cooling with natural ventilation, investigations on the distribution of the temperature and velocity in the indoor environment needs to be performed, to be able to conclude if there are risks of thermal discomfort when ventilative cooling is utilized. This can either be done by carrying out experiments or by the help of simulation tools. With Computational Fluid Dynamics (CFD) analysis, detailed descriptions of the flows inside the building envelope are possible to acquire [Chen, 2009]. This information may then be used for thermal comfort predictions.

The utilization of CFD methods to study the indoor environment are popular, as it is a cheaper method of investigation compared to experiments, and offers the possibility of making changes to the model geometry in an cost- and time efficient manner [Hilgenstock and Ernst, 1996]. However, care must be taken when setting up CFD simulations, as it is recognized that the simulations tend to be sensitive to the many computational parameters that must be defined. It is therefore imperative to verify and validate the CFD model, and perform sensitivity studies on the computational parameters [Ramponi and Blocken, 2012].

1.1.1 Problem formulation

The motivation behind this master thesis is to establish a model of ZEB Living Lab that can accurately predict the flow pattern and temperature distribution inside the building, removing the need for expensive and time consuming lab experiments, to find the optimal ventilative cooling arrangement for different outdoor conditions, when special attention is made to thermal comfort.

The aim of this master thesis is to replicate the full-scale experiments carried out by [Blandkjenn, 2017], by using a numerical software tool, that may in the future be used in investigations on the indoor thermal environment in ZEB Living Lab when ventilative cooling is utilized. Measurements from the experiments will be used to validate the CFD model.

1.1.2 Literature survey

An investigation into the passive cooling technologies available, and a small introduction to buildings (found in [Kolokotroni and Heiselberg, 2015]) who are using these technologies, are given in Section 2.3. Previous studies on ventilative cooling in Living Lab are presented in Section 2.4. Both experiments and simulations have been performed, concluding that draught risks exist, but are possible to avoid. It is suggested that further investigations on ventilative cooling in Living Lab should

be done to understand how the temperature difference between the outdoor and indoor and the window opening areas affect the indoor thermal environment. Literature study on CFD used in the building sector in general and more specified in regards to ventilation and thermal comfort are done in Chapter 3. How other studies have carried out the simulation setup will be important to the final decision for the simulation setup of the CFD model of ZEB Living Lab.

The literature survey shows that it is the setup of the CFD simulation that should be given the most attention, ensuring that the simulated results are accurate and reliable. With complex CFD models, it is necessary to make simplifications and certain assumptions, to avoid to computationally expensive simulations. These alterations will to some unknown degree affect the end result. When creating the model in this master thesis, the assumptions made to the geometry and setup will be carefully determined, and the simulation solutions will be assessed to draw conclusions on the validity of the final model.

1.2 Scope

The objective of this report is to develop a reliable tool that can be used in numerical calculations. By accomplishing this, one consequently obtains a cheaper method for attaining accurate results compared with the costs of running lab experiments.

The information obtained by previous studies on ventilative cooling in ZEB Living Lab (see Section 2.4), will in this master thesis be used to create a simulation model of the building, that can be applied for thermal comfort investigations, by utilizing a CFD tool. The experimental measurements obtained during the master thesis work of [Blandkjenn, 2017] will be used to validate the model setup. Literature investigating similar problems related to natural ventilation and passive cooling methods with CFD, will be used to substantiate the choices of the decided computational parameters.

In the beginning of this master thesis there was an intention of performing new CFD simulations, investigating different configurations (new opening area sizes, different windows included, different outdoor conditions, etc.) of ventilative cooling in Living Lab, with special attention made to the thermal comfort. It was also intended that IDA ICE simulations should be used for validation of these CFD simulations. Unfortunately, because the CFD model is not finished, this part of the assignment was never started on, and is therefore not included in the master thesis. Creating the model, and finding the appropriate computational parameters for the CFD model turned out to be more time consuming than first anticipated. Although the model are able to run, the validation of the model was never completed. Before further investigations can be performed, the model must be finalized.

1.2.1 Limitations

The final result of this master thesis is affected by the need for simplification and making assumptions to the CFD model, to reduce the computational cost of the simulations. The work is restricted due to limitations in available computer capacity and time constraints, and assumptions to the model is made accordingly.

1.3 Approach

Theory on super insulated buildings, ventilation and passive cooling methods, and the utilization of CFD in the building sector were reviewed to get a better comprehension of the problem. To understand how far the research have come and what the limitations are in relation to passive cooling in highly insulated buildings, focusing on natural ventilation in cold climate with computational fluid dynamic modelling, literature studies on relevant topics were performed. The choice of an acceptable CFD tool was made, based on certain criterias such as availability, previous knowledge, what the industry prefer/uses, dependability, and what the problem consist of. CFD models were then created, and a number of simulations were set up to verify that the models solves the problem correctly. After this, the final model performed simulations with different boundary conditions and the data was compared with the results measured in the full-scale experiment, to evaluate the CFD model. The case that predicted the flow best, compared with the experiment, were used to explain how the data from the CFD models may be used in thermal comfort analysis.

1.4 Structure of the Thesis

The first chapter introduces the background for this thesis, as well as the problem formulation, scope, limitations and other aspects that should be included in an introduction. The next two chapters provide theory related to the thesis problem. In Chapter 2 zero emission buildings, ventilative methods, cooling methods in buildings, literature review on real buildings utilizing passive cooling and on previous studies on ventilative cooling in Living Lab, and thermal comfort theory is included. Chapter 3 introduces CFD, how it may be employed in the building sector, the choice of software, theory related to creating the model and literature review to help with the simulation simplifications, assumptions and setup. Some of the ventilation theory and some of the CFD theory is taken from the project work of [Böhler, 2017]. Where this theory was lacking or missing, new information have been added during the thesis work. Relevant information about ZEB Living Lab is described in Chapter 4. The experimental setup used for validating the CFD model is also presented in this chapter. A brief introduction to the method of this thesis and the CFD models used can be found in Chapter 5. Chapter 6 and 7 presents Model A and Model B, and the cases simulated with these models. The simulations verify the case setups. The final model, Model C, is provided in Chapter 8. Model C is set up to match the conditions of the full-scale experiment

(see Section 4.3), so the simulation can be validated. In Chapter 9 the results from the models and sources of errors are discussed. Chapter 10 explains how the CFD results can be evaluated in regards to thermal comfort investigations. Draught rate calculations are carried out for the simulation and the experiment. The conclusion of the master thesis is presented in Chapter 11. The chapter also include a section where suggestions for further work is listed.

Background

2.1 Zero Emission Buildings

2.1.1 Concept

The concept Zero Emission Building (ZEB) is an attempt to reduce the high primary energy use and greenhouse gas emissions that exists in today’s building sector [Riedy et al., 2011]. Compared to Zero Energy Buildings, where the aim of the building is to produce on-site renewable energy equivalent to the building energy demand, the Zero Emission Building concept take it one step further. It considers the emissions related to all the energy used for operations, i.e. equipment, material, construction (which includes construction installation processes, and transport of materials and products to the construction site), and deconstruction of the building (at the end of the building’s life cycle), and require these emissions to be compensated with on-site renewable energy generation, see Figure 2.1 [Woods and Samdal, 2017].

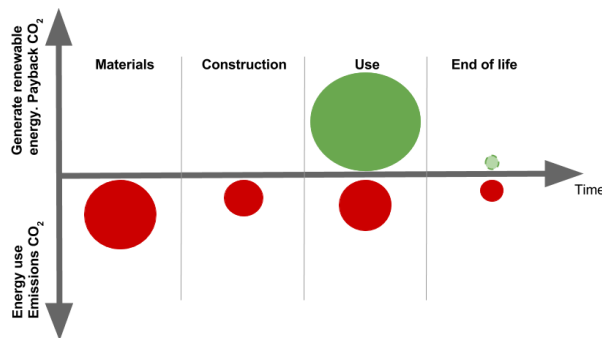


Figure 2.1: ZEB life cycle. Illustration indicating the generated emissions and renewable energy at different building phases [Admin, 2017]

The time frame for achieving zero impact is typically defined as 50-60 years (or a building life time) [Riedy et al., 2011].

2.1.2 ZEB Living Laboratory

The Living Laboratory, located at the Norwegian University of Science and Technology (NTNU), was developed and built as a multipurpose experimental center. The full-scale residential building, representing a detached, single family house, was designed to reach a Zero Emission target. To achieve a low carbon build environment, state-of-the-art technologies were integrated for energy conservation and solar energy exploitation (both active and passive technologies). The building materials and systems were selected based on minimization of embodied emissions, as well as the ability to achieve a lower energy demand for operations. The facility offers the possibility of running experiments on different design levels, e.g. investigating the building envelope, user interaction in a low energy building, window ventilation strategies, etc. [Goia et al., 2015].



Figure 2.2: Picture of ZEB Living Lab

A more thorough description of the building design and other building characteristics relevant to this master thesis will be introduced in Chapter 4.

2.2 Ventilative Methods

The TEK10 regulations state that a satisfactory air quality must be established within a building. A well designed ventilation system will remove heat, polluted air and moisture from a room by extraction, supplying new fresh air for the occupants [Direktoratet for Byggkvalitet, 2011]. While the required flow rate of air for respiration for an individual is about 7.5 liters/sec, a much larger air flow rate is needed to achieve a satisfactory level in regards to thermal comfort. Highly insulated buildings requires at least ten times the respiration flow rate to achieve air changes needed for thermal comfort [Linden, 1999].

The methods used to ventilate an occupied space are either mechanical ventilation, natural ventilation, or a combination of these two methods known as hybrid ventilation. Mechanical ventilation systems requires electricity to operate mechanical machinery to supply fresh air to a building, whereas natural ventilation systems utilize natural driving forces together with window and door openings to supply fresh air, i.e. no mechanical assistance or energy consumption is needed [Romano and Duval, 2012, Evola and Popov, 2006].

2.2.1 Mechanical ventilation

Ventilation through electrically driven fans supply fresh air to the building. The velocity and the psychometric properties of the air jet can be modified to achieve a desirable indoor environment that account for variables such as changes in seasons, number of occupants within certain zones of the building, internal loads, etc. [Norton et al., 2007].

Air distribution method

The airflow pattern in ventilated rooms affects both the air quality and the perception of thermal comfort. It is therefore important to choose a flow distribution that does not jeopardize the thermal comfort, while providing good indoor air quality. The airflow patterns can generally be divided up to three types: *piston flow*, *displacement flow* and *mixing flow* [Nilsson and Group, 2003].

Piston flow is characterized by the air moving in a piston, from one surface of the room to the opposite surface (floor-to-ceiling, ceiling-to-floor, wall-to-wall). The supply air is distributed with uniform air velocity across the inlet surface area [Nilsson and Group, 2003]. The method is not commonly used, as it requires a large amount of air and energy to operate [Novakovic et al., 2007]. For *displacement flow*, the air is supplied either through the floor or near to the floor and exhausted from the room near the ceiling. The air is supplied with a temperature lower than the room temperature, then heated within the room by a heat source, making the air flow toward the ceiling because of buoyancy forces [Nilsson and Group, 2003]. The flow is used for both ventilate purposes and for cooling purposes, and is well suited

for Variable Air Volume systems [Novakovic et al., 2007]. The *mixing flow* supply air with a velocity high enough to move all of the air volume in the room. The mixing of air results in a uniform distribution of the temperature and concentration of contaminants in the air volume [Nilsson and Group, 2003]. The air is usually supplied with jets, and located outside the zone of occupancy to limit the risk of draught that would cause thermal discomfort [Novakovic et al., 2007].

The mechanical ventilation applied in the Living Lab is mixing flow. The air is supplied high up on the walls in the two bedrooms and the living room. For the CFD model, because of certain assumptions and simplifications made to the model layout, a combination of the mixing flow (for the living room) and displacement flow (for the two bedrooms) simulate the mechanical ventilation.

Control methods

For a *Variable Air Volume (VAV) System*, the temperature is set to a constant value while the air flow rate varies. The amount of air can be controlled by e.g. time schedules, heat loads in the zone, and movement sensors. With a *Constant Air Volume (CAV) System*, a constant airflow rate is supplied to the room. The system allows for varied supplied air temperatures, in response to the heat surplus/deficit in the different ventilation zones [Nilsson and Group, 2003, Novakovic et al., 2007].

2.2.2 Natural ventilation

The driving forces for natural ventilation originates from the freely available resources of wind and solar energy [Stavarakakis et al., 2008]. The pressure differences produced by wind and/or buoyancy forces, drives the air flow in and out of the building [Jiang and Chen, 2003]. The benefits of using natural ventilation in buildings are that it may improve the energy performance of a building while providing a good indoor air quality, and maintaining an acceptable thermal comfort. It has great cooling potential, as ventilation and air infiltration is strongly coupled with the thermal behaviour of a building [Santamouris and Allard, 1998]

Stack ventilation

The buoyancy induced flow is a result of density differences inside and outside of a building, where the high density medium (cold area) will move toward the low density medium (warm area), see Figure 2.3a [Santamouris and Allard, 1998]. The low density air will be heated by incoming convective and radiative fluxes, most likely from technical equipment, occupants, and/or other heat sources within the warm domain [Norton et al., 2007]. The flow configuration is highly unpredictable, as there is also often temperature differences within the room. However, a stable stratification is usually established because of the natural tendency of hot air rising and accumulating in the upper areas of the space [Linden, 1999]. The stack pressure is given as

$$P_s = -\rho g H (T_i - \frac{T_0}{T_i}) = -\rho g H (\frac{\Delta T}{T_i}) \quad (2.1)$$

Here T_0 = Outdoor air temperature (K)
 T_i = Indoor air temperature (K)
 H = Height between two openings (m)
 ρ = density of free stream (kg/m^3)

Wind-induced ventilation

For the wind induced flows, the external wind exerts pressure variations over the building envelope, resulting in forced air flow through the building. A positive pressure will be generated on the windward side of the building while a negative pressure or suction occurs on the leeward wall and on the roof, resulting in a ventilation flow from the positive pressure area to the negative, see Figure 2.3b [Norton et al., 2007]. The wind pressure is calculated with Eq.(2.2)

$$P_W = \frac{1}{2}\rho V^2 C_p \quad (2.2)$$

where ρ is the air density, wind speed V represent the velocity at the opening height or at a reference point on the building, and C_p is the pressure coefficient [Awbi, 2010] given as

$$C_p = \frac{p_w - p_0}{\frac{1}{2}\rho V^2} \quad (2.3)$$

Here p_w = Static pressure at some point on the building (Pa)
 p_0 = static pressure of the free stream (Pa)
 V = free stream velocity normally calculated at building height or other reference height (m/s)

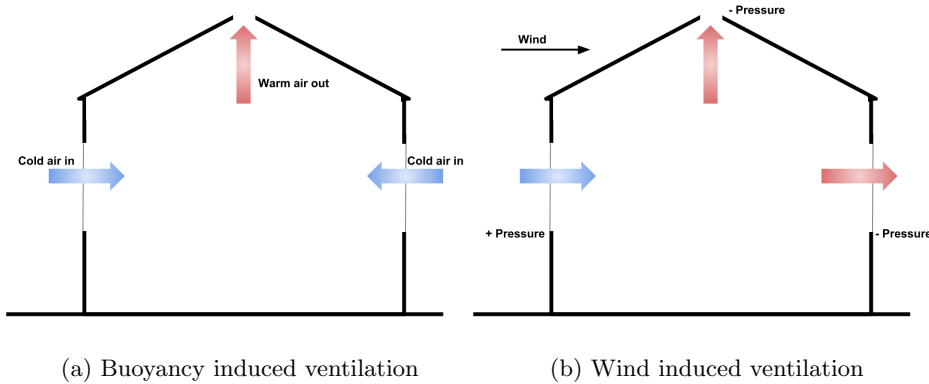


Figure 2.3: Principles of buoyancy driven (stack effect) and wind driven natural ventilation

Single-sided ventilation

Stack air flow is dominant, while influence of the wind is less important. The openings may be at the same height or at different levels. When the outdoor

temperature is lower than the indoor temperature, cool air will enter the opening at a lower part, while the warm air will escape at a higher level, see Figure 2.4a. The flow is due to pressure differences that are created by the temperature difference [Santamouris et al., 1996]. This is what will happen in the cases where only the skylight windows will be open (i.e. when the outdoor temperature is really low).

Cross-flow ventilation

The air flow is dependent on pressure differences at the openings. The influencing factors to the air flow include the surface opening of the inlet and outlet, the wind magnitude and direction, the indoor and outdoor temperature difference, the position of the opening and the relative wind shadowing of the building, see Figure 2.4b [Santamouris et al., 1996]. When the south or north windows are used in combination with skylight windows for ventilative cooling, the air flow will be due to cross-ventilation.

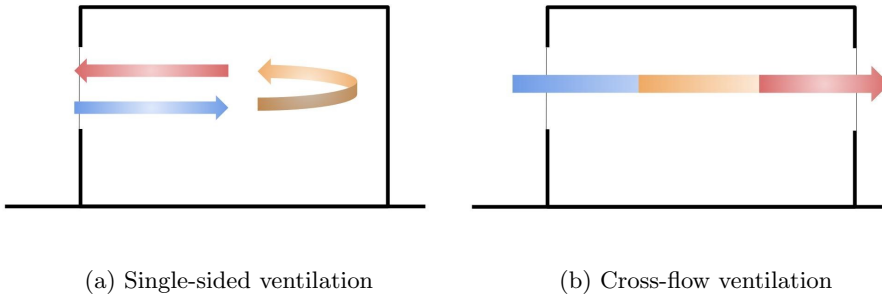


Figure 2.4: Principles of single-sided and cross-flow natural ventilation

2.2.3 Hybrid (Mixed-mode) ventilation

As mentioned earlier, the hybrid ventilation system is a combination of mechanical and natural ventilation. ZEB Living Lab operates with a CAV system that supply the two bedrooms and the living room with a constant air flow rate of 52 m³/h, 52 m³/h and 26 m³/h, respectively [Blandkjenn, 2017]. The inlet air temperature varies, depending on outdoor conditions (seasonal dependent). To keep the energy demand at a low level, ventilative cooling was decided upon as the preferred method for removing excess heat. The cooler outdoor conditions that exists in Norway, gives a great potential for cooling down overheated, super insulated buildings by ventilative ventilation, without additional use of electricity.

The windows in ZEB Living Lab are chosen and designed to yield optimal ventilation, and placing special considerations into their orientation and height location.

2.3 Cooling in Buildings

2.3.1 Thermal balance of a room

When a room is in thermal equilibrium, all the heat that enters the room and that is generated inside the room is equivalent to the heat leaving the room. When overheating becomes a problem in a building, it is because not enough heat are transferred from the building, causing a heat surplus. Figure 2.5 shows the thermal balance of a room. The global enthalpy balance of the room is given in Eq(2.4) [Santamouris and Allard, 1998].

$$V c_p \frac{dT_a}{dt} = \Phi_{pc} + \sum_{i=1}^{nS} h c_i S_i (T_{si} - T_a) + Q_m c_p (T_e - T_a) \quad (2.4)$$

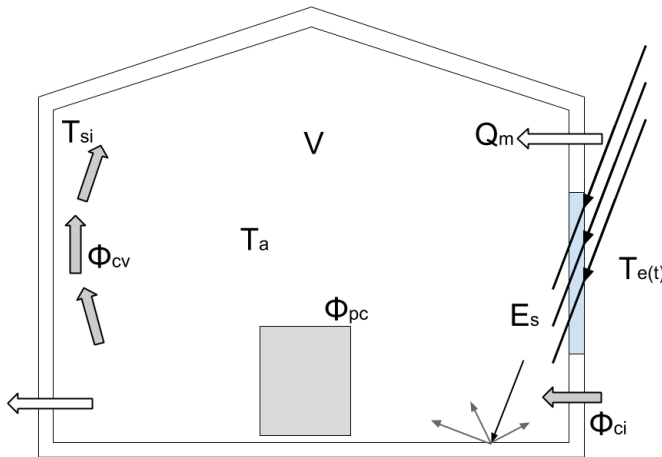


Figure 2.5: Thermal balance of a room [Santamouris and Allard, 1998]

- Here
- E_s = represent the short-wavelength radiation [μm]
 - Φ_{cv} = the convective flux exchanged between the internal surfaces and the air [W/m^2]
 - Φ_{pc} = the total convective internal gains (occupants+equipment) [W/m^2]
 - Φ_{ci} = the total conductive flux through the walls [W/m^2]
 - Q_m = the total mass flow rate of air at temperature T_e [kg/s]
 - V = the volume of the room [m^3]
 - T_a = the air temperature [K]
 - T_{si} = the interior surface temperature [K]
 - c_p = the specific heat capacity [$J/kg-K$]
 - $h c_i$ = the convective exchange coefficient at surface S_i [J/Km^2-s]

2.3.2 Cooling methods

Mechanical cooling in buildings is achieved by vapor compression systems (like air conditioning systems), and thermoelectric systems (like heat pumps). Passive and natural cooling in buildings are techniques that is used to prevent heat gains and modulate heat gains in the building, and that uses natural heat sinks to remove excess heat in the buildings. The first technique, preventing heat gains, include considerations into the microclimate, site design of the building, solar control, thermal insulation, behavioural and occupancy patterns, and internal gain control. The second technique is achieved by using the thermal mass of the building, where the buildings thermal inertia absorbs and store the heat during day time and releases the heat during night time. The natural heat sinks include ground cooling, evaporative cooling, radiative cooling, and ventilation [Santamouris et al., 1996]. The benefit with the passive systems, is that they have great energy savings potential.

For cooling by natural ventilation, the generated air flows, that are due to pressure differences, wind or a combination of the two, introduces cooler air to the indoor spaces and removes heat from the building, when the indoor air have a higher temperature than the outdoor. The natural ventilation may also directly cool down the building structure, the occupants inside the building through convection and evaporation, and by using thermal mass as a storage medium (nighttime ventilation for office buildings) [Santamouris and Allard, 1998].

2.3.3 Existing buildings using passive cooling

The use of passive methods for cooling down buildings have existed since the early periods of civilization. In more modern times, the principles remain the same, but the techniques have been enhanced and optimized to provide the best results for the buildings [Santamouris et al., 1996]. With an increasing interest in constructing low-energy buildings, the interest for utilizing passive cooling systems also increased. Office buildings and residential homes have been studied for a range of different climatic settings. Some of the buildings that are designed to use passive cooling and that have been monitored, are presented in the following text. The performance of the cooling systems and their possible problems will be addressed.

C-Ddl ArFrisol PSA (2007, dry hot summers and cold winters)

The building is located in Tabernas, Spain, and is a one floor office building. The design of the building results in protection from the sun by shading, and solar collectors are operated as radiant coolers by night. A solar chimney releases stored energy at night-time, that have been absorbed during day-time summer, inside chimney channels to force ventilation in the offices, reducing the indoor air temperature of the rooms. The building achieves a high degree of thermal comfort with the utilized cooling strategies during the whole year. The biggest challenge for the building is related to developing an optimal control algorithm for the complex systems [Kolokotroni and Heiselberg, 2015].

Maison Air et Lumière (2012, oceanic climate - warm summers and cool winters)

The residential building is located in Verrières-le-Buisson, France, and is designed to achieve energy and environmental objectives at the top ambition levels for new detached houses for 2020. A hybrid ventilation system supply air to the house by mechanical ventilation during the winter, with heat recovery, and during the summer, natural ventilation provides a good indoor air quality and ventilative cooling, by using window openings. In addition, cooling demand is also reduced by using solar shading, thermal mass and automatic control with a building management system. During a one year period, a family of four have been monitored while living in the building. No overheating was experienced during the summer period. The temperature was measured to be a little low during the winter period. However, it is assumed that the family chose the lower temperature, as they had access to control the heating system and temperature [Kolokotroni and Heiselberg, 2015].

Home for Life (2009, temperate coastal climate)

The single-family house is located in Lystrup, Denmark. The idea of the design is to have a low energy building that works as a residential home, considering especially the indoor environmental qualities, the experience, and the functionality, while maintaining a low energy consumption. A combination of controlled solar protection, natural ventilation (automatic control) and moderate thermal building mass reduces the risk of overheating inside the building (even outside summer season), and consequently avoiding cooling demand. The control system for the house is managed to ensure minimum use of heat and electricity. However, the users may override the system. During a two year monitoring period, with families living in the building, the users have been very satisfied, and the thermal performance have been very good. The risk of overheating is still present, which shows that improvement to the control may still be required [Kolokotroni and Heiselberg, 2015].

Solstad (2011, cold climate)

The kindergarten is a two-storey, low-energy building, located Larvik, Norway. The building's goal was to achieve an energy consumption corresponding to half of the set requirement given in the Norwegian building code, TEK07. A hybrid ventilation system operates with mechanical ventilation when natural ventilation is inadequate or the outdoor temperatures are too low. Motor controlled windows removes cooling demand for medium low outdoor temperatures, and the natural ventilation is driven by both cross and stack ventilation. From simulations and measurements, the control algorithm for the window openings is concluded to be optimized for ensuring a good indoor climate. Because of the passive cooling methods, the hybrid system managed to keep an average lower temperature, while keeping the energy consumption low during the summer period, reducing the annual energy consumption by 13% [Kolokotroni and Heiselberg, 2015].

2.4 Ventilative Cooling in ZEB Living Lab

For Zero Emission Buildings, the ventilation system should be as little energy demanding as possible. A highly insulated building combined with an energy production on-site equivalent to the emissions resulting from the different stages of the building's life cycle, makes the use of ventilative cooling a preferred option for removing the excess heat accumulating in the building. The overheating is in part due to solar irradiation, as investigated by [Rodriguez-Ubinas et al., 2014, Orme et al., 2003], limited ventilative options [Larsen et al., 2012], and internal heat gains [Janson, 2010].

For the case of ZEB Living Lab, a hybrid ventilative system is incorporated. The mechanical ventilation part consist of a balanced Constant Air Volume (CAV) system, where a constant air flow rate is supplied to the different rooms in the building. The supply temperature depends on the season, and thus the temperature of the outdoor environment [Goia et al., 2015].

Previous studies investigating cooling by means of window openings in ZEB Living Lab have shown that the use of cross-flow ventilation is quite effective. However, there are eminent risk of thermal discomfort, because of draught. Ventilative cooling in ZEB Living Lab have been investigated by [Kirkøen, 2015, Risnes, 2016, Blandkjenn, 2017]. [Kirkøen, 2015] and [Blandkjenn, 2017] used the simulation tool IDA ICE to investigate thermal comfort and energy consumption in the building. The results from Kirkøen (2015) showed that the building would be at risk of overheating and that utilizing ventilative cooling would reduce the occurrence of overheating, while keeping energy demand down. A mixed-mode system were found to be the best way of applying window ventilation. Windows should be opened during the day when indoor air temperatures reached 24°C and closed when the the air temperature dropped to below 22°C. With this system, simulations revealed that the recorded overheated hours were reduced with 99%.

In addition to IDA ICE simulations, Blandkjenn (2017) did a set of full scale experiments in the test facility ZEB Living Lab, where the cooling effect of different window openings were tested. The experiment concluded that a cross-stack ventilation method was preferred to a cross-wind ventilation, and that the best cooling effect occurred when opening the north window and kitchen skylight window. Ventilative cooling with the south window had negative effect on the hottest days, as the double-skin window preheated the outdoor air before it entered the building. To avoid local thermal discomfort on really cold days, only the skylight windows could be opened. Draught rate calculations showed that the window on the south facade could be used for lower outdoor air temperatures, compared to the window on the north facade. Window openings up to 25% of maximum opening surface gave acceptable results in regards to thermal comfort, for temperature difference up to 10°C (between indoor and outdoor air), a solar irradiance above 70 W/m², and wind speed less than 2m/s. For the north window, an opening of 50% of maximal opening area was acceptable when the temperature difference was

below 6°C. The measured draught rates at the north window was contingent on the temperature difference.

Risnes (2016) performed a study on the indoor environment in ZEB Living Lab, which concluded that draught risks were high in the shoulder seasons (early spring and late fall) when ventilative cooling by windows were used. Blandkjenn (2017) recommend that a more thorough evaluation on smaller window openings should be investigated before discarding the use of ventilative cooling for these periods, to see if the draught risks can be reduced.

2.5 Thermal Comfort

Controlling the indoor climate to achieve a satisfying thermal environment requires understanding of the interactions of all climatic variables, combined with how the occupants perceive thermal comfort [Norton et al., 2007]. Thermal comfort is usually described with the indices PMV and PPD, introduced by Fanger (1972), where the indices can be used to specify the quality of the thermal climate in a building or the degree the thermal environment satisfies human requirements [Nilsson and Group, 2003].

2.5.1 Predicted mean vote (PMV)

The first index predicts the mean value of the votes of a large group of persons. It uses a seven-point thermal sensation scale, see Table 2.1, to describe the thermal sensation for the entire body. The index is based on the heat balance of the human body, where thermal neutrality is obtained when the body's internal heat generation is equivalent to the body's heat losses to the environment.

Table 2.1: Seven-point thermal sensation scale [NS-EN ISO 7730, 2006]

+3	Hot
+2	Warm
+1	Slightly warm
0	Neutral
-1	Slightly cool
-2	Cool
-3	Cold

Thermal neutrality being equal to zero and the comfort zone recommended within the limits of $-0.5 < \text{PMV} < +0.5$ [NS-EN ISO 7730, 2006, Nilsson and Group, 2003].

2.5.2 Predicted percentage dissatisfied (PPD)

The second index predicts the percentage of thermally dissatisfied people that feel uncomfortably warm or cool in a large group of people. These people are the ones that voted -3, -2, +2, and +3 on how they perceived the thermal climate with the PMV index. The PPD can be calculated with Eq.(2.5),

$$PPD = 100 - 95 * \exp(-0.03353 * PMV^4 - 0.2179 * PMV^2) \quad (2.5)$$

which gives the following distribution

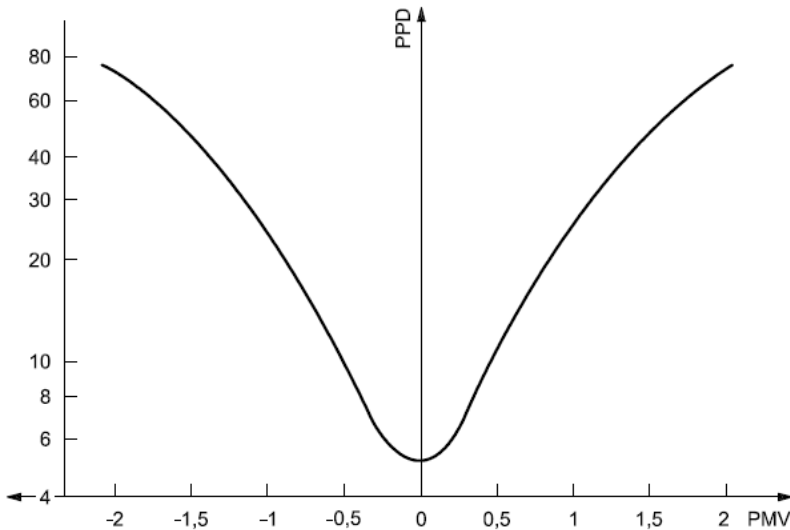


Figure 2.6: Predicted percentage of dissatisfied people (PPD) as a function of the predicted mean vote (PMV) [NS-EN ISO 7730, 2006]

From Figure 2.6, a $PMV = 0$ indicates a $PPD = 5\%$. This is due to inter-personal variations in preferred temperatures, i.e. for an optimal temperature, it is impossible to satisfy more than 95% of the people [NS-EN ISO 7730, 2006, Nilsson and Group, 2003].

2.5.3 Local thermal discomfort

Local thermal discomfort is the perceived thermal dissatisfaction that occurs in specific areas of the body. This type of discomfort is usually caused by draught, large vertical temperature differences between feet and head, too cool/hot floor or too high radiant temperature [NS-EN ISO 7730, 2006].

Draught rates

The draught rate is expressed by Eq.(2.6) and indicates the percentage of people that feel discomfort due to draught. This is assumed to be the most dominant cause of thermal discomfort when ventilative cooling is carried out in ZEB Living Lab.

$$DR = (34 - t_{a,l})(\bar{v}_{a,l} - 0.05)^{0.62}(0.37 \cdot \bar{v}_{a,l} \cdot T_u + 3.14) \quad (2.6)$$

where $t_{a,l}$ = local air temperature [°C] 20°C - 26°C
 $\bar{v}_{a,l}$ = local mean air velocity [m/s] 0.005 m/s < $\bar{v}_{a,l}$ < 0.5 m/s
 T_u = local turbulence intensity [%] 10%-60% (if unknown, set to 40%)

Depending on the environment and type of space, the desired thermal environment may be split into three categories; A, B, and C. These categories give the maximum PPD for the body as a whole and a maximum PD for the local discomfort types. Table 2.2 gives the criterias.

Table 2.2: Categories of thermal environment (from [NS-EN ISO 7730, 2006])

Category	Thermal state of the body as a whole		Local discomfort			
	PPD %	PMV	DR %	Vertical air temperature difference	PD % Warm or cool floor	radiant asymmetry
A	<6	-0.2 < PMV < +0.2	<10	<5	<10	<5
B	<10	-0.5 < PMV < +0.5	<20	<5	<10	<5
C	<15	-0.7 < PMV < +0.7	<30	<10	<15	<10

Each of the categories require that all the criterias are satisfied simultaneously [NS-EN ISO 7730, 2006].

Simulation Theory

3.1 Introduction to CFD

The development of Computational Fluid Dynamics (CFD) provided more accurate solutions of complex mathematical problems compared to previous methods. Before, the calculation of the problems required great approximations and simplifications to be solve, or the results had to be obtained from empirical measurements from tests in small- and full-scale, where the solutions usually ended up being inaccurate. The capability of CFD, growing with faster computers, improved turbulence models, and faster numerical methods, results in the possibilities of achieving more accurate solutions for the problems, while keeping the costs low. It is an inexpensive way to see how a new solution to a problem is compared to old technology [Li and Nielsen, 2011].

3.1.1 CFD used in the building sector

In the building sector, CFD can be used to get a detailed description of the flow field in three dimensions. The application of CFD can provide information about cooling- and heating loads, pollutant flow, particle transport, and distribution of air flow and temperature inside a building, to name some [Fouquier et al., 2013]. The information from the CFD simulations are then often used to assess indoor air quality, thermal comfort and the buildings energy consumption (depending on the study's area of interest) [Zhai and Chen, 2006].

Challenges connected to CFD in the building design include large modelling domains that require sufficiently fine grids, which results in long simulation time, the difficulties in defining appropriate boundary conditions, and the wide range of physical processes (unsteady flows, atmospheric boundary layers, radiation, buoyancy effects, etc.) [Gaspar et al., 2003].

The benefits with employing CFD, compared to other methods (empirical methods and other building simulation programs), are mainly (1) the CFD method's ability to predict detailed descriptions of flow and thermal systems inside the building [Foucquier et al., 2013], and (2) that CFD modelling can be a reliable tool and a relatively inexpensive method to use in design changes investigations, compared to experimental studies [Griffiths and Boysan, 1996].

CFD is widely employed for studies involving ventilation in buildings, usually to predict the ventilation performance of the building. By controlling the indoor air parameters, CFD may be used to assess the thermal environment, even before the building is constructed, to find the acceptable indoor air quality. Because of the detailed descriptions CFD gives of the air flow velocities and temperature distribution inside the building, it is a great tool for investigating draught risks when employing ventilation by passive means or ventilative cooling.

[Stavarakakis et al., 2008] examined the steady-state air flow and the indoor thermal environment in an enclosed space subjected to wind and buoyancy forces. [Allocca et al., 2003] applied CFD to simulate the steady-state ventilation rates and indoor conditions for a building. Effects of buoyancy, wind and a combination of the two were considered. [Jiang and Chen, 2003] ran a full-scale experiment and used CFD to evaluate the natural ventilation effect with large openings, on a warm day with no wind present. [Anderson et al., 2014] carried out a steady-state study where they examined how the opening aspect ratio and temperature difference between the indoor and the surroundings affect the heat loss from a room due to natural convection. [Ziskind et al., 2002] studied the possibility of using solar radiation to generate buoyancy driven flow through a one story building. Both steady-state and transient flow simulations were investigated. [Gilani et al., 2016] studied the steady flow from two displaced openings, where air is heated by local heat sources in the floor. [Lin et al., 2011a] performed CFD simulation on stratum ventilation, to investigate the space cooling load and energy consumption over a year, for an office, a class room and a retail shop in Hong Kong. [Stavridou and Prinos, 2017] examined, by transient simulations, the flow field and temperature distribution in a naturally ventilated room. The study looks into the simulation process, the use of natural ventilation and the thermal comfort of the space.

From the literature, there is still a shortage when it comes to investigations in the field of natural ventilation in colder climates, and what this means for the thermal comfort. The lack of investigations on the temporal flow effects found in the literature is another field that needs future research.

3.2 CFD Analysis

The software used in the CFD modeling and simulations is ANSYS®Workbench 18.1. With this software the users have the opportunity to work on and complete end-to-end Computer-Aided Engineering (CAE) processes, by using the task moduls available, i.e. creating the CAD model and mesh, setting up and running the simulation, and post-processing the final results. The *DesignModeler* was used to create the geometry, and the simulation grid used the task modul *Mesh*. The simulations were completed with ANSYS®Fluent commercial code, and a post-processing task modul named *Results* was used to review the results [Inc., 2005]. The Fluent code is designed to be easy to use, and its ability to perform is similar to the other codes in the market. The program uses the fundamental equations (mass, momentum and energy) to predict characteristics of the fluid flow and heat transfer. The solvers in ANSYS Fluent uses finite volume method to discretize the domain into a finite set of control volumes. The fundamental equations are then solved numerically for each of the discretized control volumes [ANSYS, 2015].

3.3 The Fundamental Equations

The universal laws of conservation of *mass*, *momentum* and *energy* are the basis for the *fundamental equations*. By applying mass conservation to a fluid flow, all mass entering the system must be equal to the mass leaving the system. This is represented by the *continuity equation*:

$$\frac{D\rho}{Dt} + \rho(\nabla \cdot \mathbf{V}) = 0 \quad (3.1)$$

When the assumption of incompressible flow is valid, Eq.(3.1) can be reduced to

$$\nabla \cdot \mathbf{V} = 0 \quad \text{or} \quad \frac{\partial u}{\partial x} + \frac{\partial v}{\partial y} + \frac{\partial w}{\partial z} = 0 \quad (3.2)$$

Here ρ = the density of free stream (kg/m³)
 t = time (s)
 \mathbf{V} = a velocity vector (m/s)
 u, v, w = velocities in x-, y-, and z-direction (m/s)
 x, y, z = directional coordinates (m)

The conservation of momentum is the same as Newton's 2nd law, which states that the rate of change of momentum on a fluid element equals the sum of forces acting on the same fluid element. This is represented by the *momentum equation*:

$$\rho \frac{D\mathbf{V}}{Dt} = \rho \mathbf{f} + \nabla \cdot \Pi_{ij} \quad (3.3)$$

The body force term \mathbf{f} in Eq.(3.3) will in this case be the same as the acceleration of gravity g for the y-momentum, and zero for x- and z-momentum. For a Newtonian

fluid, the stress tensor Π_{ij} becomes

$$\Pi_{ij} = -p\delta_{ij} + \mu \left[\left(\frac{\partial u_i}{\partial x_j} + \frac{\partial u_j}{\partial x_i} \right) - \frac{2}{3}\delta_{ij} \frac{\partial u_k}{\partial x_k} \right] = -p\delta_{ij} + \tau_{ij} \quad (3.4)$$

where $i, j, k = 1, 2, 3$. The *Navier–Stokes equation* can be obtained by the *continuity equation* and the *momentum equation*. Assuming incompressible flow, the N–S equation is reduced to

$$\rho \frac{D\mathbf{V}}{Dt} = \rho \mathbf{f} + \mu \nabla^2 \mathbf{V} \quad (3.5)$$

Here p = pressure (Pa)
 μ = dynamic viscosity (kg/m·s)
 δ_{ij} = Kronecker delta function
 τ_{ij} = Reynolds stress tensor
 i, j, k = denotes the Cartesian coordinates

The energy conservation law states that the rate of change of energy equals the rate of change of heat gained and lost, and the work done on the fluid particle (1st law of thermodynamics) [Pletcher et al., 2013]. This is represented by the *energy equation*:

$$\rho c_p \frac{DT}{Dt} = \nabla \cdot k \nabla T + \beta T \frac{Dp}{Dt} + \mu \phi \quad (3.6)$$

where the dissipation function ϕ in Cartesian coordinates is given by

$$\begin{aligned} \phi = 2 \left[\left(\frac{\partial u}{\partial x} \right)^2 + \left(\frac{\partial v}{\partial y} \right)^2 + \left(\frac{\partial w}{\partial z} \right)^2 \right] &+ \left[\left(\frac{\partial u}{\partial y} + \frac{\partial v}{\partial x} \right)^2 \right. \\ &+ \left. \left(\frac{\partial v}{\partial z} + \frac{\partial w}{\partial y} \right)^2 + \left(\frac{\partial w}{\partial x} + \frac{\partial u}{\partial z} \right)^2 \right] - \frac{2}{3} \left(\frac{\partial u}{\partial x} + \frac{\partial v}{\partial y} + \frac{\partial w}{\partial z} \right)^2 \end{aligned} \quad (3.7)$$

and the static temperature is the dependent variable [Pletcher et al., 2013]. The relationship between enthalpy and temperature being

$$h = c_p T \quad (3.8)$$

Here c_p = specific heat capacity (J/kg·K)
 T = temperature (K or °C)
 k = thermal conductivity (W/m·K)
 β = thermal expansion coefficient (1/K)

3.3.1 Boussinesq approximation

When having a natural convection problem, a flow can be induced as a result of density variations in the fluid flow. This motion is due to gravitational forces acting on the density variations. This must be considered when solving the *fundamental equations*. The Boussinesq Approximation solves natural convective problems by treating the *fundamental equations* as incompressible except for in the term where the density ρ and gravity g is multiplied (i.e. in the gravitation term in Eq.(3.3))

and Eq.(3.5)). This is an incorporated model in ANSYS Fluent that will replace the term ρg with

$$\Delta\rho g = (\rho - \rho_0)g \approx -\rho_0\beta(T - T_0)g \quad (3.9)$$

where ρ_0 and T_0 are the constant density and operating temperature of the flow, respectively [ANSYS, a].

3.4 Models

ANSYS Fluent is capable of solving modeling problems of a large variety, from basic fluid flow problems to pollutant formation and acoustic calculations, to mention some [ANSYS, 2009]. The models that will be included in this thesis are the energy model, viscous model and radiation model.

3.4.1 Energy

The energy model allows the users to solve problems related to energy or heat transfer [ANSYS, 2009]. The thermal boundary conditions, such as temperature, heat flux, and convection can be defined with this model activated [ANSYS, 2006].

3.4.2 Viscous

The viscous model offers the option of running inviscid, laminar or turbulent simulations. For turbulent flow, activation of relevant turbulence model (e.g. Spalart-Allmaras, \bar{k} - ϵ , \bar{k} - ω , LES, etc.) and options are necessary. When one of the \bar{k} - ϵ turbulence models or the Reynolds Stress Model (RSM) are used, and the flow involves walls, *Near Wall Treatment* must be defined. Further specifications relevant to the flow problem can be selected in Options [ANSYS, 2009].

3.4.3 Radiation

The radiation model should be included when radiation heat flux dominates the total heat transfer rate. In ANSYS Fluent this is done by simply activating radiation, followed by deciding on an appropriate radiation model. There are five radiation models in Fluent that can be used together with a heat transfer simulation; Discrete Transfer Radiation Model (DTRM), P-1 Radiation Model, Rosseland Radiation Model, Surface-to-Surface (S2S) Radiation Model, and Discrete Ordinates (DO) Radiation model [ANSYS, 2009]. The Solar Load Model can be used if it is of interest to include radiation effects from the sun's rays that enters the computational domain [ANSYS, a]. After the model is selected, further specifications such as emissivity and temperature must be stipulated at the appropriate boundaries.

3.5 Turbulence Modelling

Turbulence problems are generally quite complicated, and demand considerable computer power to obtain correct solutions. There are three main ways of approaching a turbulent problem; by direct numerical simulations (DNS), large-eddy simulations (LES) or Reynolds averaged Navier–Stokes (RANS). The DNS method resolves the unsteady Navier–Stokes equations by making the spatial grid and time step fine enough to resolve the smallest turbulent eddies and fastest fluctuations present in the flow [Versteeg and Malalasekera, 2007]. The model considers and calculates the turbulent properties as the eddies are becoming smaller and smaller, due to energy cascade, until they dissipate. The DNS method is rarely used in investigations involving distribution of air temperature and flow patterns inside buildings, as this type of method is known to be too computationally expensive to simulate, on account of the required computer resources needed [ANSYS, a, Pletcher et al., 2013]. The flow calculations required for buildings are also generally not needed to be at the level of accuracy the DNS method will solve. The LES method resolves the mean flow and the large eddies in the unsteady Navier–Stokes equation [Versteeg and Malalasekera, 2007]. The computational effort required to resolve large-eddy simulations is about 1/10 of that required for direct numerical simulations. For many flow situations, including the flow problem in this project, this is still too computationally expensive to simulate, and the Reynolds averaged Navier–Stokes (RANS) method would be the better option [Pletcher et al., 2013]. ANSYS Fluent provides the possibility of simulating problems with all three turbulence methods [ANSYS, a].

Both the LES method and the RANS method are used to investigated different natural ventilation situations. [Jiang and Chen, 2003] compared the LES turbulence model simulation with a standard \bar{k} - ϵ turbulence model simulation and concluded that the LES model was preferred for simple geometrical problems, while the RANS turbulence modeling with \bar{k} - ϵ was a good option for more complex problems. Most of the literature have used RANS models, because the LES method was too expensive to simulate.

3.5.1 Reynolds averaged Navier–Stokes equation

The Reynolds averaged Navier–Stokes (RANS) equation solves the time-averaged Navier–Stokes for fluid flow by decomposing the dependent variables in the equations into its time averaged and fluctuating components (i.e. \bar{f}_i and f'_i , respectively) [Pletcher et al., 2013].

$$f_i = \bar{f}_i + f'_i \tag{3.10}$$

The unknown quantity f_i might be switched out with velocities u, v and w , pressure p , density ρ , and temperature T . These decomposed components are then placed in the equations and all the terms are averaged. For the incompressible *continuity*

equation in the x-direction, the equation becomes

$$\frac{\partial \bar{u}}{\partial x} = \frac{\partial(\bar{u} + u')}{\partial x} = \frac{\partial \bar{u}}{\partial x} + \frac{\partial \bar{u}'}{\partial x} = \frac{\partial \bar{u}}{\partial x} = 0 \quad (3.11)$$

Note: $\bar{u}' = 0$. Although the solved properties are not nearly as detailed as those obtained with LES, they are usually good enough for most engineering purposes [Versteeg and Malalasekera, 2007]. The available models for RANS in ANSYS Fluent includes Spalart-Allmaras, different variants of \bar{k} - ϵ and \bar{k} - ω , and the RMS [ANSYS, 2006].

[Gilani et al., 2016] performed a sensitivity analysis where Standard-, 'Realizable-', and RNG \bar{k} - ϵ turbulence models, and Standard- and SST \bar{k} - ω turbulence models were applied. The study concluded that the SST \bar{k} - ω turbulence model was the best to predict buoyancy turbulence interaction. [Stavarakakis et al., 2008] simulated for and compared the Standard-, 'Realizable-', and RNG \bar{k} - ϵ turbulence model, and concluded that the RNG \bar{k} - ϵ turbulence model provided the best temperature predictions. The preferred RANS turbulence model for most of the literature was the \bar{k} - ϵ model. [Allocca et al., 2003] and [Meng et al., 2016] simulated with the RNG \bar{k} - ϵ model, because the turbulence model was recommended by other literature. [Lin et al., 2011a] based its simulation setup on a RNG \bar{k} - ϵ model previously developed and validated by [Lin et al., 2011b].

Based on previous studies on ventilation and CFD, the chosen turbulence model is the RANS method with RNG \bar{k} - ϵ turbulence model, because of its ability to predict the temperature and air flow distribution for simulations investigating natural ventilation.

3.5.2 The \bar{k} - ϵ turbulence model

In the RANS equations, six new unknowns will be introduced, all relating to the effects of turbulence [ANSYS, a]. These are the Reynolds stresses

$$\tau_{ij} = -\rho \overline{u'_i u'_j} \quad \text{for } i = 1, 2, 3 \text{ and } j = 1, 2, 3 \quad (3.12)$$

To close the system new equations must be introduced. Boussinesq (1877) suggested that the turbulent or 'eddy' viscosity might relate the turbulent sharing stresses to the rate of mean strain. This was called the Boussinesq assumption

$$-\rho \overline{u'_i u'_j} = 2\mu_T S_{ij} - \frac{2}{3}\delta_{ij} \left(\mu_T \frac{\partial u_k}{\partial x_k} + \rho \bar{k} \right) \quad (3.13)$$

where the turbulent viscosity is $\mu_T = \rho v_T l$. v_T and l are the characteristic velocity- and characteristic length scales of turbulence. The kinetic energy of turbulence is given as

$$\bar{k} = \frac{\overline{u'_i u'_i}}{2} \quad (3.14)$$

and

$$S_{ij} = \frac{1}{2} \left(\frac{\partial u_i}{\partial x_j} + \frac{\partial u_j}{\partial x_i} \right) \quad (3.15)$$

is the mean strain rate tensor [Pletcher et al., 2013].

For predictions of buoyancy driven flow, the \bar{k} - ϵ turbulence model is a very popular turbulence model to use. The two equation model solves equations for turbulent kinetic energy \bar{k} and dissipation rate ϵ . The standard model is as follows:

Turbulent kinetic energy

$$\rho \frac{D\bar{k}}{Dt} = \frac{\partial}{\partial x_j} \left[\left(\mu + \frac{\mu_T}{Pr_k} \right) \frac{\partial \bar{k}}{\partial x_j} \right] + \left(2\mu_T S_{ij} - \frac{2}{3} \rho \bar{k} \delta_{ij} \right) \frac{\partial u_i}{\partial x_j} - \epsilon \quad (3.16)$$

Turbulent dissipation rate of kinetic energy

$$\rho \frac{D\epsilon}{Dt} = \frac{\partial}{\partial x_j} \left[\left(\mu + \mu_T / Pr_\epsilon \right) \frac{\partial \epsilon}{\partial x_j} \right] + C_{\epsilon 1} \frac{\epsilon}{k} \left(2\mu_T S_{ij} - \frac{2}{3} \rho \bar{k} \delta_{ij} \right) \frac{\partial u_i}{\partial x_j} - C_{\epsilon 2} \rho \frac{\epsilon^2}{k} \quad (3.17)$$

The relationship between the turbulent dissipation rate and turbulent kinetic energy is given by $\epsilon = C_D \bar{k}^{3/2} / l$. The turbulent viscosity can now be found with

$$\mu_T = C_\mu \rho \bar{k}^2 / \epsilon \quad (3.18)$$

where $C_\mu = C_D^{4/3}$. $C_{\epsilon,1}$, $C_{\epsilon,2}$, C_D , C_μ , Pr_k , Pr_ϵ and Pr_T are model constants calculated to satisfy consistency checks [Pletcher et al., 2013].

3.5.3 RNG

The RNG model is a favorable turbulence model for indoor air simulations. It is derived using re-normalized group theory, and differs from the standard \bar{k} - ϵ model (Eq.(3.16) and Eq.(3.17)) by

1. adding an additional term in the dissipation rate of kinetic turbulence equation (Eq.(3.17))
2. including effects of swirl on turbulence
3. providing an analytical way of obtaining turbulent Prandtl numbers (Pr_k , Pr_ϵ and Pr_T)
4. being able to solve for low-Reynolds-numbers effects (Standard is only a high-Reynolds-number model)

All these differences results in more reliable and accurate solutions compared to the Standard \bar{k} - ϵ model [ANSYS, 2009]. The values of model constants for the RNG \bar{k} - ϵ model are found in Table 3.1.

Table 3.1: Model constants for RNG \bar{k} - ϵ model [ANSYS, 2009]

C_μ	$C_{\epsilon 1}$	$C_{\epsilon 2}$
0.00845	1.42	1.68

3.5.4 Standard Wall Modeling

ANSYS offers two methods to model the region near the wall, when the applied turbulence model is not suitable on its own (as is the case with the \bar{k} - ϵ model). The Wall Function approaches the problem by not resolving the inner region consisting of the viscous sublayer and buffer layer. Wall functions are instead used to connect the wall and the fully developed turbulent region through the viscous-affected region. The Near-Wall model resolves the inner region all the way from the fully turbulent region to the wall by making the mesh fine enough. It is worth noting that for high-Reynolds number flows, the preferred method would be the Wall Function approach, because of the significantly reduced computational cost [ANSYS, 2009].

3.6 Radiation

3.6.1 Surface-to-Surface (S2S) Radiation Model

The Surface-to-Surface model uses view factors to account for the radiation exchange in an enclosure of gray-diffuse surfaces. Gray surfaces have properties independent of wavelength and diffuse surfaces have properties independent of direction. The S2S model assumes that only surface to surface radiation needs to be considered, because the absorption, emission and scattering of radiation can be ignored [ANSYS, 2006].

3.6.2 Solar Load model

The solar model in ANSYS Fluent offer two options for solar radiation modelling; Solar Ray Tracing and DO Irradiation. The DO Irradiation model is only available when the Direct Ordinates radiation model is selected. The solar load can be included in both steady and unsteady flow, but is only available in the 3D solver [ANSYS, 2006].

Solar Ray Tracing

The algorithm used in the solar ray model allows for effects of direct solar illumination and diffuse solar radiation to be included in the simulation. It applies the solar load as a heat source in the energy equation, where the sun's position vector and solar intensity may be defined by either the user or computed by a solar calculator. The materials defined for the solid outer surfaces determines if the sun rays are shaded for the rest of the domain (opaque characteristics) or if the rays are able to enter the domain (semi-transparent characteristics).

A set of input values are required for the solar ray tracing to work. Among these are the sun direction vector, direct and diffuse solar irradiation, the spectral fraction, direct and IR absorptivity and transmissivity, scattering factor and ground reflectivity. When using the solar calculator, input values for the global position of the domain (latitude, longitude, time zone), starting date and time, orientation of the domain, solar irradiation method and sunshine factor must be included [ANSYS, 2006].

3.7 The Grid

To assure accurate solutions from the simulation, the mesh must be small enough to avoid large discretization errors. Fluent is an unstructured solver, i.e. the use of indexes (i,j,k) is not required, which leads to flexibility in creating mesh topology that is best suited for the given problem. For 3D grids, the available cells in ANSYS Fluent are hexahedral, tetrahedral, pyramid, wedge, and polyhedral. These are depicted in Figure 3.1 [ANSYS, a].

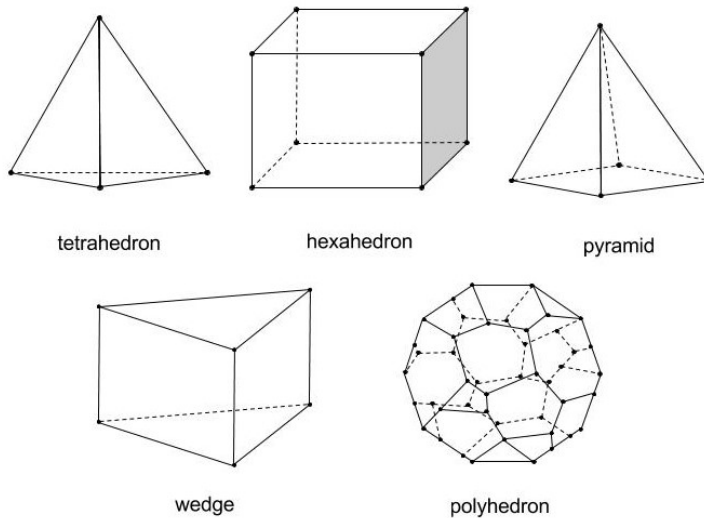


Figure 3.1: 3D cell types available in ANSYS Fluent

3.7.1 Important considerations

An appropriate mesh for a problem depends on the application of the given problem, and certain issues should be considered when deciding the mesh type. Creating structured meshes (only hexahedral elements) are normally very time-consuming when the geometry is complex. By employing unstructured meshes (tetrahedral and/or triangular cells), the setup time will be reduced significantly. Regarding computational expense it is desirable to have a mesh consisting of as few cells as possible. The general practice recommended by Fluent User's Guide 16.2 (from ANSYS Fluent Documentation) are that hexahedral meshes should be used for simple geometries, unstructured hexahedral meshes should be used for moderately complex geometries, tetrahedral meshes are a good option for relatively complex geometries with wedge elements in the boundary layers, and for the extremely complex geometries it is best to use only tetrahedral meshes. The presence of numerical diffusion (also known as false diffusion), should be considered as it is one of the dominating sources of error in 3D situations. The resolution of the mesh, and the amount of false diffusion are inversely related. By refining the mesh, the error will be reduced. Meshes aligned with the flow (hexahedral meshes), minimizes the false diffusion. For complex problems this is not a possibility [ANSYS, a].

3.7.2 Grid quality

If the mesh is of poor quality, the numerical computation will not be accurate or stable. Therefore, it is essential to check the mesh quality to ensure good results. Different mesh quality indicators can be applied in ANSYS Fluent, such as orthogonal quality, skewness, and aspect ratio [ANSYS, a].

Orthogonal quality is the minimum value that is calculated with either

$$\frac{\vec{A}_i \cdot \vec{f}_i}{|\vec{A}_i| |\vec{f}_i|} \quad \text{or} \quad \frac{\vec{A}_i \cdot \vec{c}_i}{1 \vec{A}_i \cdot \vec{c}_i} \quad (3.19)$$

where \vec{A}_i is the face normal vector, \vec{f}_i is a vector from the centroid of the cell to the centroid of the face, and \vec{c}_i is a vector from the centroid of the cell to the centroid of the adjacent cell that shares the face [ANSYS, b]. Values close to 0 indicates bad quality of the cells, and cells with orthogonal quality near 1 are of good quality [ANSYS, a].

Skewness is a measurement determining how ideal a cell is [ANSYS, b]. This is done by comparing the shape of the cell with the shape of an equilateral cell of equivalent volume [ANSYS, a]. Values close to 0 indicates close to equilateral cells, i.e. good quality mesh, and skewness close to 1 means a highly skewed mesh [ANSYS, b] that will decrease the solution accuracy and lead to a destabilized solution [ANSYS, a].

Aspect ratio measures the degree a cell is stretched. For most problems it is best to avoid large aspect ratios [ANSYS, a]. A general rule of thumb is to keep the aspect ratio below 5:1.

3.7.3 Grid independence

Grid independence studies investigate the grid quality combined with the number of elements of the mesh. When the solutions of the CFD simulations, where the only difference is the number of mesh elements, give the same results, the CFD model is concluded to be grid independent. A study like this will reduce the computational cost of the simulation, by simulating with the lowest number of elements while still getting the same result.

3.8 Discretization Schemes

In Fluent it is possible to select discretization schemes for the convective terms in the different fundamental equations. By default, the viscous terms have a second order accuracy and the turbulence quantities a first order accuracy. Fluent also allows the users to choose between different pressure schemes, when the pressure-based solver is used [ANSYS, a].

3.8.1 Finite volume method

The finite volume method (FVM) is a discretization technique for partial differential equations that is quite similar to the more well known finite difference method (FDM), except it is applicable to unstructured grids. The method divides the domain into control volumes (fixed regions in space), where the fundamental equations are solved for each one. The FVM is usually represented with integrals, that are evaluated over the finite volume or its boundaries [Pletcher et al., 2013].

3.8.2 Solvers

It is the pressure-based solver that will be used to solve the governing equations. There are four pressure-based segregated algorithms available in ANSYS Fluent; SIMPLE, SIMPLEC, PISO, and FSM. The two first are recommended for steady-state calculations, while PISO and FSM should be used for transient calculations. In this algorithm, the governing equations are solved sequentially (i.e. \mathbf{u} , \mathbf{v} , \mathbf{w} , \mathbf{p} , \mathbf{T} , \bar{k} , ϵ , etc. are solved one after another) [ANSYS, 2006]. Fluent also provides the option of using a pressure-based coupled algorithm that enables pressure-velocity coupling, called Coupled algorithm [ANSYS, a]. This algorithm differs from the segregated algorithm by solving the momentum equations and the pressure-based

continuity equation together in a coupled system. The difference is illustrated in Figure 3.2.

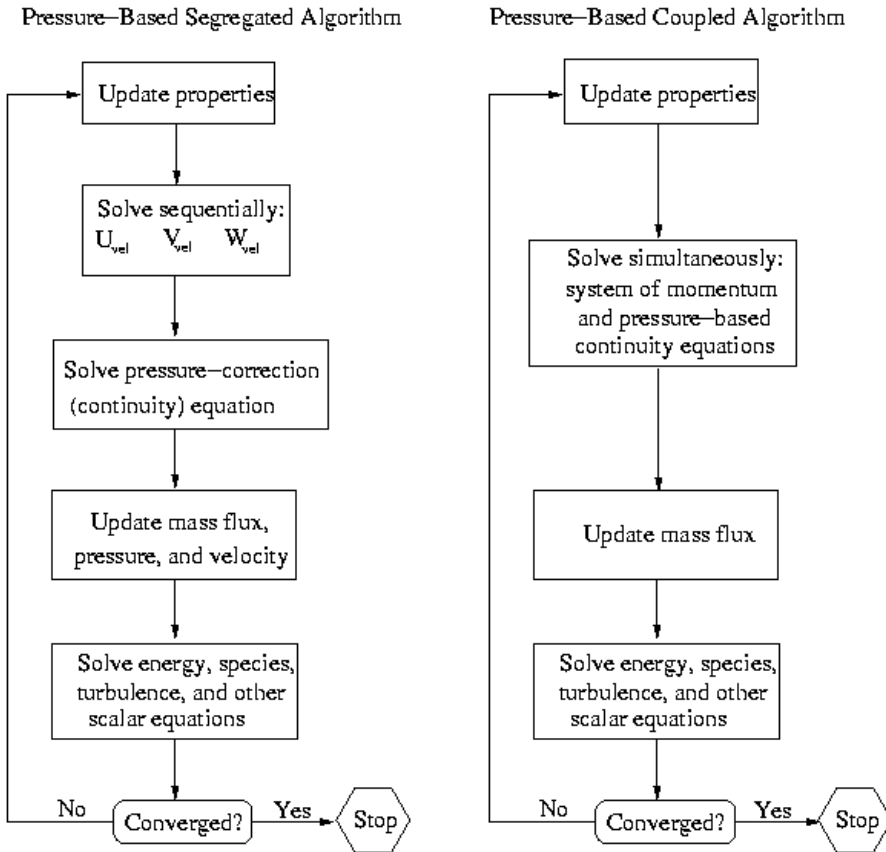


Figure 3.2: The Pressure-Based Solution Method algorithm steps [ANSYS, 2006]

The coupled algorithm is the chosen pressure-based solver. The scheme achieves a quicker convergence compared to the segregated algorithms, as a result of a full implicit coupling where the momentum and continuity equations are solved in a closely manner. A drawback is the increased memory requirement, resulting from needing to store all the momentum and continuity equations when solving pressure and velocity fields (memory increase of about 1.5-2 times). With transient flows, when the the mesh quality is poor or the time step is large, the coupled method is necessary to use [ANSYS, 2006].

3.8.3 Gradients and derivatives

Three methods (Green-Gauss Cell-Based, Green-Gauss Node-Based, and Least Squares Cell-Based) are available in ANSYS Fluent to compute the gradients in the fundamental equations. For unstructured meshes that are skewed and distorted, the node-based and least-squares gradient method are more superior to the cell-based gradient. Furthermore, the least-squares gradient is cheaper to compute compared to the node-based gradient [ANSYS, a].

3.8.4 Spatial discretization

The *Upwind Schemes* possess the characteristics of controlling numerical instabilities by adding dissipation. This makes the schemes a good option when running problems that might be unstable. The downside with the schemes is that they might produce excessive dissipation when solving viscous flows that will affect the natural dissipation in the boundary-layer regions. One way of solving this is by using higher-order upwind schemes [Pletcher et al., 2013].

PREssure STaggering Option (PRESTO!) Scheme is the preferred scheme when solving natural convection flow with high-Rayleigh-number [ANSYS, 2006]. The scheme computes the “staggered” or face pressure by calculating the pressure field with the discrete continuity equation [Andersson et al., 2011].

Pseudo-transient control

The pseudo-transient control is an option when running steady-state simulations with the pressure-based coupled solver. It will generate better convergence for meshes that have large aspect ratio cells, as well as converging the solution much faster [ANSYS, 2012]. A time step can be specified for both the solid zone and fluid zone, depending on the problem. For the steady-state simulations performed in this master, pseudo-transient will be used for the fluid zones, and a user specified pseudo time step will be used [ANSYS, a].

3.8.5 Temporal discretization

When the simulation solution is time dependent, the problem should be simulated transient, and the governing equations need to be discretized in both space and time. This works by integrating every term in the differential equations over a time step Δt . The temporal discretization will, based on the choice of solver (Pressure-Based coupling algorithm), be solved implicit, i.e. for a function $\mathbf{F}(\phi)$, the function will be evaluated at the future time level:

$$\frac{\phi^{n+1} - \phi^n}{\Delta t} = \mathbf{F}(\phi^{n+1}) \quad (3.20)$$

This scheme is unconditionally stable with respect to time step size [ANSYS, 2006].

3.9 Numerical Analysis

3.9.1 Consistency

A scheme is consistent when the size of the truncation error is made to approach zero by reducing the spatial and temporal step size [Ryaben'kii and Tsynkov, 2006]. The truncation error is a result of numerical approximation, by making the PDE into an equivalent differential equation [Kim, 2013].

3.9.2 Stability

By using numerical method to solve PDEs, the solution obtained will vary from the exact solution. These discrepancies are usually divided up into errors such as truncation error and round-off error. The numerical method is said to be stable if the errors decay while the computations are being performed. The round-off error is given as

$$\text{Round-off error} = \text{Numerical solution} - \text{Discretized solution} \quad (3.21)$$

The discretized solution is the exact solution for a given discretized equation the computer will obtain with infinite accuracy. The numerical solution is obtained by using a computer with finite accuracy.

3.9.3 Convergence

Convergence is a measurement used in CFD simulations that indicates when the iterations can be stopped. This is done by either setting a convergence criterion for the residuals that will automatically stop the iterations when reached, or by monitoring the iterations manually until residuals stabilize to a constant value [Andersson et al., 2011]. Fluent allows for different ways to evaluate convergence, but the most used method is by scaling the residual. The scaled residual use a scaling factor when comparing the old and new cell values, as shown in Eq.(3.22)

$$\mathbf{R}^\phi = \left| \frac{\phi_i^{new} - \phi_i^{old}}{\phi_i^{old}} \right| \quad (3.22)$$

where \mathbf{R}^ϕ is the scaled residual, and ϕ_i is a general variable at cell i . The default convergence criterion in Fluent is set to 10^{-6} for energy, and 10^{-3} for the other residuals. For most problems, these default values are sufficient. The situation for when this criterion might not be appropriate, usually happens when either a really good initial guess of the flow field variables have been made or a really bad initial guess for the turbulent quantities have been made. If this is the case, the criterias should be altered to ensure a properly converged solution [ANSYS, 2006]. The convergence criterion will be clearly stated for each simulation. When the criterion has been reduced, it is done to achieve a better solution. The default values are used when the CFD simulations are expected to require large amount of computer power and/or simulation time.

3.9.4 Verification and validation

To ensure that the model has been accurately solved, it is important to verify that the simulation is set up right and that it solves the equations correctly. This procedure is called verification. The model setup will be verified in Chapter 6 and Chapter 7. To check how accurate the simulated results are, the results should be compared to results collected from models representing the reality. This is known as validation [Andersson et al., 2011]. Full-scale measurements (from [Blandkjenn, 2017]) will be used to compare simulation results obtained with the CFD model, so the model can be validated.

3.10 Choice of Boundary Conditions

The final result of the CFD simulation depends strongly on the accuracy of the defined physical quantities for the model's flow domain boundaries. It is therefore highly important to understand the flow problem of the simulation to such a degree that the defined flow conditions for the solid boundaries and the fluid boundaries will solve the CFD model accurately, compared to real life flow situations [Santamouris and Allard, 1998].

The most common boundary condition for the solid boundaries are walls. The walls may be assumed to be still (where velocity at the wall surface = 0 m/s), or moving at a given speed (sliding wall). For defined inlets and outlets in the model, the flow conditions may vary between being inlets of velocity, pressure, mass flow and vent, while outlets can be defined as pressure, mass flow rate, pressure far-field, outflow, outlet vent and exhaust fan [ANSYS, 2006]. Appropriate physical quantities, such as the flow (velocity and mass) magnitude and direction, the thermal conditions (temperature, convection, heat generation, radiation), and the material properties (density, thermal conductivity, specific heat capacity, opaque/semi-transparent) must be selected.

When the heat transfer over the solid walls are assumed to be very small or not important for the simulation, the walls are given adiabatic characteristics, as is the case for [Allocca et al., 2003, Jiang and Chen, 2003, Meng et al., 2016]. [Ziskind et al., 2002] and [Gilani et al., 2016] applied constant temperatures found in experiments for the walls. For walls that experience conductive heat transfer, and where this information will matter for the final solution, the boundary condition require the information about the wall thickness, thermal conductivity of the wall material, the heat transfer coefficient over the wall surface and the free stream and radiation temperature [ANSYS, 2006]. [Gilani et al., 2016] set zero static pressure at the outlet and uniform velocity, calculated from experiment, with constant temperature at the inlet. The heat source was given a constant heat flux. [Ziskind et al., 2002] specified no-slip and no-penetration at all the walls. For the openings, zero pressure was imposed and a temperature corresponding to the surroundings was introduced at the inlet. [Allocca et al., 2003] ran two scenarios

with different domain sizes. The first model, a single-room, was simulated without outdoor surroundings, while the second model included an outer domain where the minimum dimensions of the domain were found to be $2l$ -, $2w$ -, and $1.5h$ of the single room. For the first model, the windows were defined as outlets with zero pressure and zero gradients for temperature and velocity. Outdoor temperature was set at the lower window. For the second model, the outside side boundaries were specified as walls with slip and temperature equal to the outdoor conditions. For the upper boundary, a zero pressure was applied and for the lower (i.e. ground) boundary, adiabatic, no-slip condition was set. The study concluded that the CFD model domain combining the surroundings and the building gave a better solution for the problem, compared with the single-room flow domain. The flow domain of [Stavridou and Prinos, 2017] consist of only the building. The heat source was set as a velocity inlet with air temperature equal to 320K and the air velocity equal to 0.01 m/s. At the low opening, velocity inlet with very low velocities were defined (to simulate no wind) and the temperature is set to outdoor temperature. At the high opening, zero static pressure was set. Most of the literature investigating buoyancy effects accept the simplification of only considering the room or building as the flow domain, while the studies investigating the effects of wind almost always include a larger part of the surroundings [Aldawoud, 2017, Stavrakakis et al., 2008].

ZEB Living Laboratory

4.1 ZEB Living Laboratory

Most of the information presented in this section is based on [Goia et al., 2015].

4.1.1 The concept

The testing facility was built as a detached, single family house, designed to represent a typical Norwegian home. The main focus and purpose of the facility is to study how well different groups of occupants adapts to living in the house, thus being able to draw a conclusion on whether a Zero Emission Building is a valid options as a residential building or not.

With the installed monitoring system in the Living Laboratory, other studies in regards to ZEB characteristics are easy to perform. The monitors collect relevant environmental quantities both outside and inside. It also measures the buildings energy demand and can record users' interaction and occupants' habits.

4.1.2 Location

The facility's location does affect the energy performance of the building. In Trondheim (63°25'N, 10°27'E, Figure 4.1) the temperature and solar radiation hours varies drastically over the entire year [Finocchiaro et al., 2016]. The winter is characterized with low temperatures and few hours of daylight around the winter solstice. The summer temperatures are relatively high, and because of the high latitude the sun might shine for 20 hours close to the summer solstice. [Finocchiaro et al., 2016] presented the quantities of the peak maximum and minimum direct solar radiation and the diffuse solar radiation for the summer and winter months. These are listed in Table 4.1.

Table 4.1: Solar radiation in Trondheim

	Summer	Winter
Direct solar radiation	432 kWh/m ² (June)	153 kWh/m ² (December)
Diffuse solar radiation	80 kWh/m ²	290 kWh/m ²

The diffuse solar radiation is dependent on the amount of cloudiness in the sky.



Figure 4.1: Location of Trondheim, on the map of Norway

4.1.3 The facility layout

The facility is a one story building, containing two bedrooms, an office area, living room area, kitchen area, bathroom, entrance and a technical room. In addition to this, a small mezzanine is placed above the small bedroom. Figure 4.2 illustrates the floor layout. The total length of the building is ≈ 16 m and the total width is ≈ 9.5 m. The roof is designed with a 30° angle, illustrated in Figure 4.3. The height of the indoor environment ranges between 2.45 m to 4.54 m. Total floor area is about 100 m², and the glass ratio of the building is around 20%.

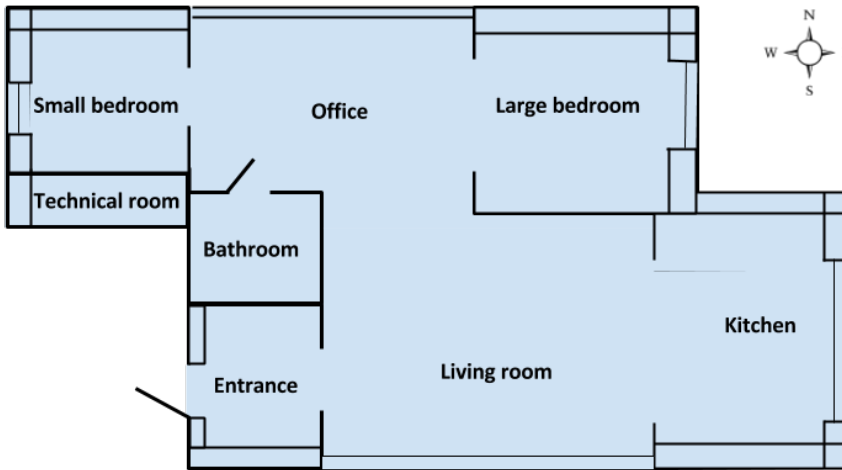


Figure 4.2: Illustration of the layout of the Living Laboratory facility

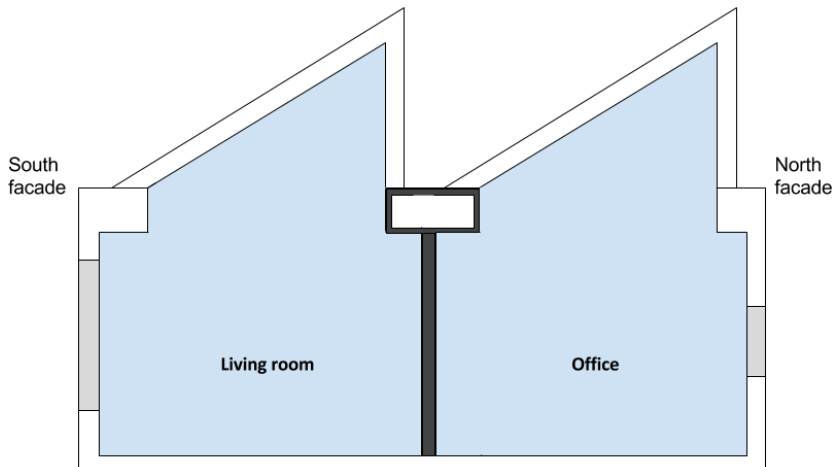


Figure 4.3: Illustration of the facility section

Window on the south facade

A double-skin window ($l=5.40$ m, $h=2.02$ m) is located at the south facade, along the living room wall. The window consists of two large glass surfaces at the outer

layer of the window, and four smaller glass surfaces at the inner window layer. Between these glass layers there is an air gap of approximately 400 mm. Two of the inner layer windows can be opened from the inside of the building, to be used for ventilation and cooling purposes. These windows are placed at the furthest right and left, and are side hung casement windows. The ventilated air gap between the inner and outer frames reduces the risk of condensation on both sides on the exterior glass. Outdoor air enters through a small opening at the bottom of the window and exits through a small opening at the top [Woods and Samdal, 2017]. Both the inlet and outlet opening consist of grills. When the inner windows are open, the outdoor air will flow into the living room. Because of heat transfer through the inner windows and solar irradiation outside, the outdoor air entering the indoor environment will have a higher temperature compared to the outdoor temperature [Carlos and Corvacho, 2013, Blandkjenn, 2017]. The supply air temperature influence the occupants perception of the indoor thermal environment, thus a higher temperature may reduce the risk of thermal discomfort when applying ventilative cooling for overheated rooms with cooler out conditions. The double-skin window is depicted from the outside and illustrated from the side in Figure 4.4.

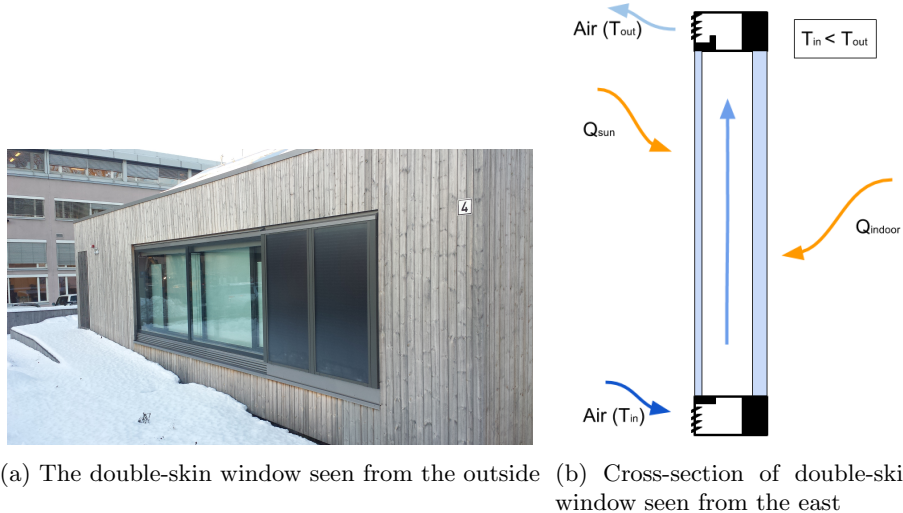


Figure 4.4: Double-skin window on the south facade

Windows on the north facade

On the north facades of the building there are placed four skylight pivot windows (each $l=0.59$ m, $h=0.99$ m) and two top hung windows (total $l=4.79$ m, $h=0.69$ m). Two of the skylight windows are located on the north wall of the kitchen, and the other two skylights are located on the north wall of the mezzanine, all four approximately 4.2 m above the floor. The top hung windows are located 1.05 m high at the north wall of the office, see Figure 4.5.



Figure 4.5: The north facades of ZEB Living Lab

4.1.4 Thermal specifications for the building envelope

The building follows the passive house standards [Finocchiaro et al., 2016]. To reduce the risk of overheating in the summers, ultra-insulated walls and ceiling with special material were used in the construction [Bazilchuk, 2017]. Table 4.2 gives the thermal specifications for the building envelope.

Table 4.2: Thermo-physical specifications of the building envelope

Building envelope	U-value [W/m ² K]	Comment
Walls	0.11	Wooden-frame inside and outside with a double layer rock wool insulation
Floors	0.10	
Roofs	0.11	
Window, south	0.65-0.69	Double-skin window. Value depending on the ventilation rate within the air cavity.
Window, north	0.97	Does not follow the passive house standard of <0.8 W/m ² K.
Window, skylight	1.0	
Other windows	0.80	In the bedrooms and kitchen. Not included in the simulation model.
g-value	0.5	Typical value for buildings in cooler climates
Air tightness	0.5 ach	Resistance to inward and outward leakage
Thermal bridges (normalized)	0.03 W/m ² K	

4.1.5 HVAC specifications

Two different heating systems are installed in the building, for the purpose of testing the systems efficiency: floor heating and a high-temperature radiator. Only floor heating will be investigated further in this master thesis. This system will make it possible to compare CFD result with full-scale experimental measurements taken by [Blandkjenn, 2017]. The floor heating uses underfloor heating panels in the all the rooms [Goia et al., 2015]. Other heat loads inside the building will contribute to the increase the indoor temperature, such as lighting, equipment, and occupants. Table 4.3 lists the assumed heat load values for ZEB Living Lab (taken from validated IDA ICE simulations [Kirkøyen, 2015, Risnes, 2016, Blandkjenn, 2017]).

Table 4.3: Internal heat loads of ZEB Living Lab (validated IDA ICE values)

Heat load	Value
Floor	20 W/m ²
Lights	200 W (10am-3pm, summer condition) Off (winter condition)
Occupants	1 MET and 0.85 clo (10am-3pm, living room, summer condition) 1 MET and 1.0 clo (3pm-4pm, living room, winter condition)
Equipment	Constant heat loads (both conditions): 20 W in entrance 200 W in technical room 20 W in home office 90 W in kitchen 15 W in living room + 45 W (10am-3pm, living room, summer condition)

The ventilation system, is a mixed mode (hybrid) ventilation system. The balanced mechanical system supplies air to the bedrooms, and living room, and extracts air at the bathroom and kitchen with ventilation rates within the TEK10 regulation requirements. These rates are listed in Table 4.4. The set temperatures for the supply air of the mechanical ventilation depends on the weather season. For cooler outdoor conditions (late autumn, winter and early spring) the supply temperature is 19°C. For warmer outdoor conditions (late spring, summer and early autumn) the supply temperature is set to 22°C [Blandkjenn, 2017]. The duct network for the building is illustrated in Figure 4.6. The blue lines indicate the air supply duct network and the yellow lines indicate the exhaust network.

Table 4.4: Ventilation rate of ZEB Living Lab. Determined and validated by [Blandkjenn, 2017]

Name	Supply/extract rate	Comment
Large bedroom	52	Two people. Overflow to office, under the door
Small bedroom	52	Two people. Overflow to office, under the door
Living room	26	Additional air supplied to achieve a balanced system
Kitchen	-52	Constant extraction of air
Bathroom	-78	Constant extraction of air
SUM	0	The system is balanced

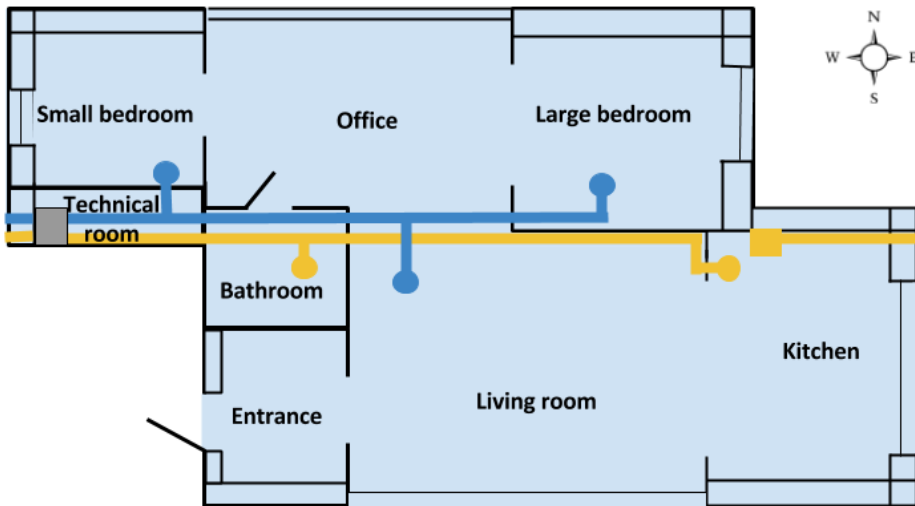


Figure 4.6: Layout of the supply and exhaust duct network

The building have no cooling system, and rely only on using ventilative methods for removing the surplus heat that may accumulate inside the building.

4.1.6 Sensor locations

A weather station is installed above the roof of the building, measuring outdoor air temperature, relative humidity, barometric pressure, wind velocity, and global solar irradiance. Air temperatures are also measured on the north and south facade, and two additional sensors measures the global solar irradiance, one on the roof slope plan and one on the south facade [Goia et al., 2015].

Integrated sensors indoor collects data on the indoor climate parameters. Air temperatures are measured in the office (six sensors), living room (six sensors), kitchen (two sensors), bathroom (two sensors), and the bedrooms (two sensors). Air temperatures and velocities are also measured near and inside the ventilation system. The temperature, flow rate, energy and power are measured for the hydronic system. Electrical energy is measured for lighting, appliances and other equipment. It is the National Instrument LabVIEW programming code that controls the data acquisition system and the control system [Goia et al., 2015]. The information on the measuring equipment for temperature, wind conditions and solar irradiance is given in Appendix A in Table A.1.

4.2 Full-scale Measurements

[Blandkjenn, 2017] collected data inside the ZEB Living Laboratory for different ventilative cooling arrangement. These are listed in Table 4.5.

Table 4.5: The window arrangement for the ventilative cooling measurements from [Blandkjenn, 2017]

South window	North window	Kitchen skylight
12.5%	-	100%
25%	-	100%
37.5%	-	100%
50%	-	100%
75%	-	100%
-	25%	100%
-	50%	100%

Only one of the south windows and one of the north windows were opened during the experiments. The same is the case for the kitchen skylight. The windows used for ventilative cooling measurements are marked red in Figure 4.7.

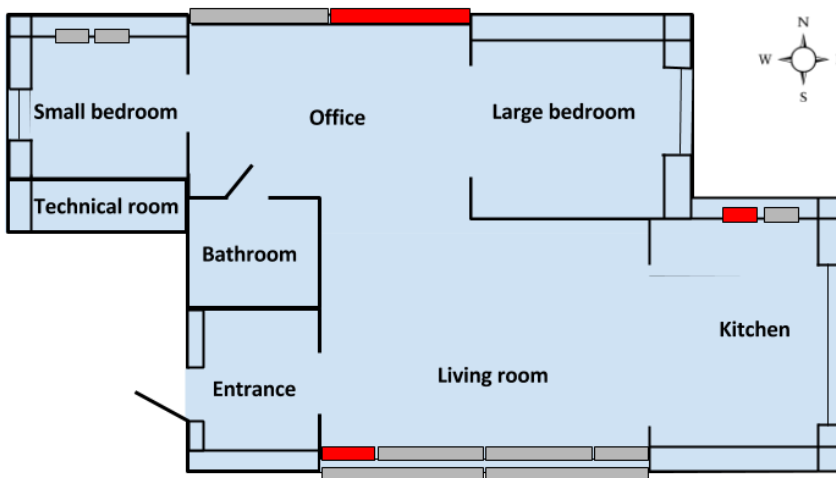


Figure 4.7: Location of the windows used in ventilative cooling measurements

The air velocities and air temperatures were measured with an AirDistSys 5000 from Sensor Electronics. An iButtons from Maxim Integrated Products measured the temperature inside the south window. More information about the measuring equipment can be found in Table A.2 in Appendix A. The measurements were

carried out in March and April 2017, and the sampling periods were set to one minute for each location.

4.2.1 Ventilative cooling with north window

Twenty four points were used to collect velocity- and temperature data at the north window. Figure 4.8 shows the location of these points. The points are also located along the mid-section of the window.

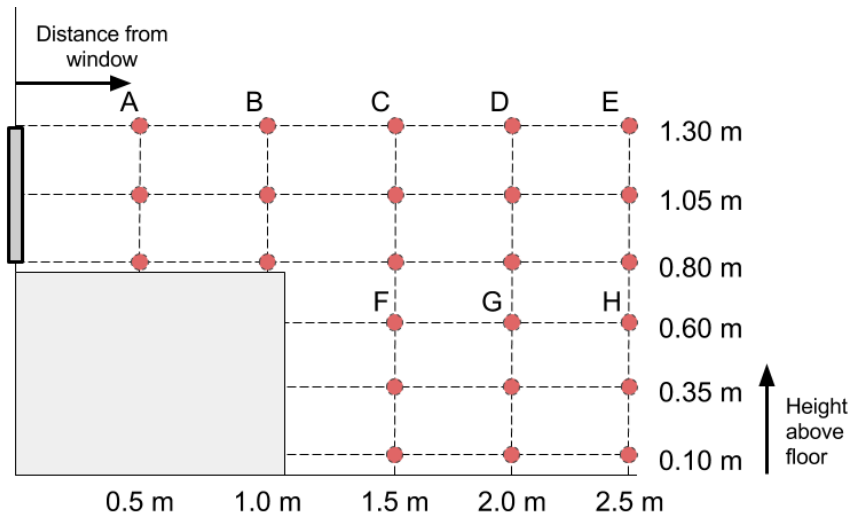


Figure 4.8: Measurement locations for ventilative cooling with north facade windows (from [Blandkjenn, 2017])

4.2.2 Ventilative cooling with south window

The experiments investigating the ventilative cooling effect of the south window measured the temperature and velocity at point locations in front of the open window at different distances and heights. Because of time limitations, none of the data collected from the full-scale measurements from the south window will be used further in this work, although the model that is presented in Chapter 8 can be used to recreate the ventilative opening areas investigated in [Blandkjenn, 2017], and thus the CFD solutions can be validated with full-scale measurements. Investigations on the south window will be suggested in further works.

4.3 The Experiments Used For Validation

Measurements from the full-scale experiment taking place on the 04/25/2017 will be used to validate the CFD model for a window opening surface area of 25% of maximum opening area. Because measurements on the 24 point locations seen in Figure 4.8 were taken during a time period of approximately two hours, only three point locations will be used for the comparison. This is done to reduce the simulation time, as it does take time to setup the simulations and to run them. The measurements chosen to be validated with the experimental data are points B1 (h=0.8m), B2 (h=1.05m) and B3 (h=1.3m), located one meter from the window. The temperature and velocity data for these locations were collected between 03:00:14pm and 03:01:12pm, with data saved every two seconds. From the Living Lab database, relevant data for this day and time have been collected, and will be used in the CFD setup of Case 4 to ensure that the outdoor and indoor conditions for the simulation and the full-scale experiment are alike. These are given in Table 4.6.

Table 4.6: Data from Living Lab Database (04/25/2017 at 03:00:01pm)

Air Temperatures Outside	
Weather station (on roof)	7.9°C
North facade	6.45°C
South facade	18.26°C
Air Temperatures Inside (Average)	
Office (6 sensors)	15.7°C
Living room (6 sensors)	17.0°C
Kitchen (2 sensors)	17.8°C
Bedroom west (2 sensors)	17.05°C
Bedroom east (2 sensors)	16.5°C
Bathroom (2 sensors)	16.7°C
Other Data from Weather Station	
Solar radiation	593 W/m ²
Mean wind speed	1.51 m/s
Mean wind direction*	329.5°

* 180°wind direction is wind from south

Because the measurements were collected during early spring, a time without an actual cooling need, [Blandkjenn, 2017] reduced the indoor temperature to simulate a warmer outdoor environment. The floor heating was therefore turned off during the experiment and the supply temperature from the mechanical ventilation was reduced to 10°C. The air flow rates remained constant.

4.3.1 Sources of error for the experimental data

After the measurements were collected, it was discovered by [Blandkjenn, 2017] that there was some damage on three of the AirDistSys 5000 anemometers. Because the time of when the damage occurred was unknown, the collected measurements might or might not be affected by this. It was also mentioned by [Blandkjenn, 2017] that neither the sensors in ZEB Living Lab or the AirDistSys 5000 rig were calibrated during the experiments. It may therefore be some systematic errors present in the measurements. Finally, the risk of human error that tend to be present during analysis and experiments was disclosed.

The Method

In the next chapters (Chapter 6-8), the created CFD models and the setup for the different simulated cases are presented. During the work on this master thesis, the complexity of the simulation setup did reveal itself to cause larger problems to the progress of the thesis than was anticipated in the beginning of the work. It was therefore decided to break down the simulations, to investigate how the CFD models were influenced and solved when setting up the simulations and applying different boundary conditions, by starting with overly simplified models and gradually running more complex simulations. The benefit of using this type of step-by-step approach has to do with the opportunity it gives to verify that each of the simulations are solved correctly, with the given setup and boundary conditions. In Chapter 3 the literature study revealed that the accuracy of the simulation result are highly dependent on a large number of things, such as the number of cell elements, and the quality of these cells, the type of solvers used to discretize the fundamental equations, the choice of turbulence models, and the model size domain with the boundary conditions defined at the CFD model's outer domain. Especially the latter, discussed in Section 3.10, will be carefully considered, as it has been highlighted by studies [Allocca et al., 2003, Li and Nielsen, 2011] to be a dominant source of error when used inappropriately for the CFD simulations.

5.1 Introducing the CFD Model Geometry

The CFD model geometries were designed with the Workbench DesignModeler task module. The building dimensions are based on the floor plan and sectional drawings found in the appendix of *Ventilative cooling in Living Lab* by [Kirkøen, 2015]. Simplifications have been made to reduce the computational cost of the simulations, and will be clearly stated for the different models.

The goal of this thesis is to create a CFD model that can replace the need for running experiments, where the model can be used for thermal comfort analysis by predicting the air flow and temperature distribution accurately in the building. Simplifications to the geometry usually introduce uncertainty. Therefore, a CFD model that is a replica of the real facility will avoid these uncertainties. However, the limitation of available computer capacity and time restrictions calls for making simplifications to the CFD model. It is therefore not possible to consider a CFD model that is an accurate reproduction of the original facility, as it is too large and expensive to simulate. This thesis will comment on how certain assumptions and simplifications made to the model might affect the end result of the simulations, and use this information to conclude if the model is solved appropriately.

Model A

The first CFD model created and investigated, defined as Model A, is characterized as overly simplified. This model considers only the indoor fluid domain (i.e. no solid walls and windows, no air gap in the double skinned south window, and no external outdoor domain). The inlets and outlets for the balanced mechanical ventilation have been included, to make it possible to run cases where the mechanical ventilation is studied. Model A is illustrated in Figure 6.1.

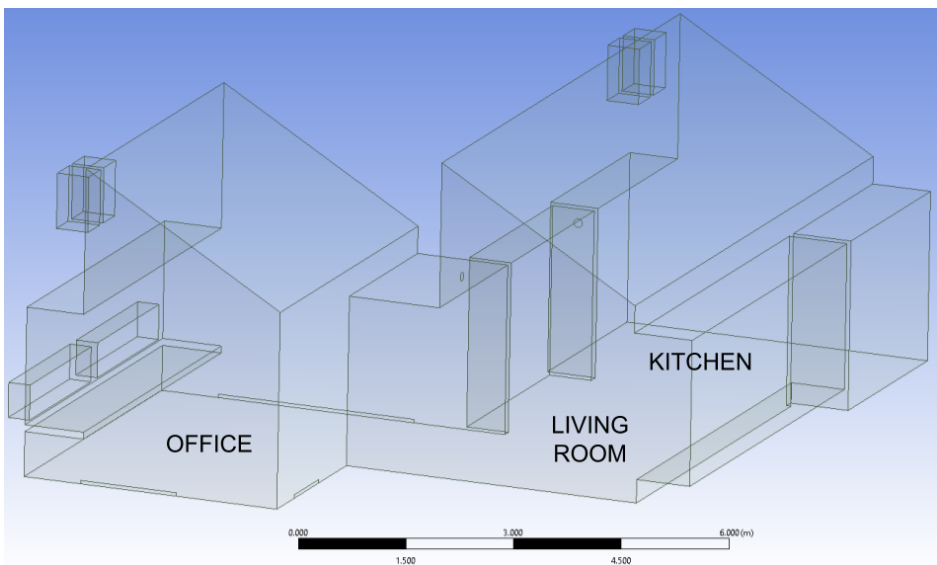


Figure 6.1: Model A geometry

6.1 General Info About the Model

The total surface of the floor area is approximately 55 m^2 . From Subsection 4.1.3 the facility's floor area was given as 100 m^2 . This reduction is due to geometrical simplifications made to the building envelope, by choosing to only investigate the open living areas consisting of the office, living room and kitchen. The dimensions of the floor of the CFD model is given in Figure 6.2. Figure 6.4 depict the dimensions of the model seen from the side.

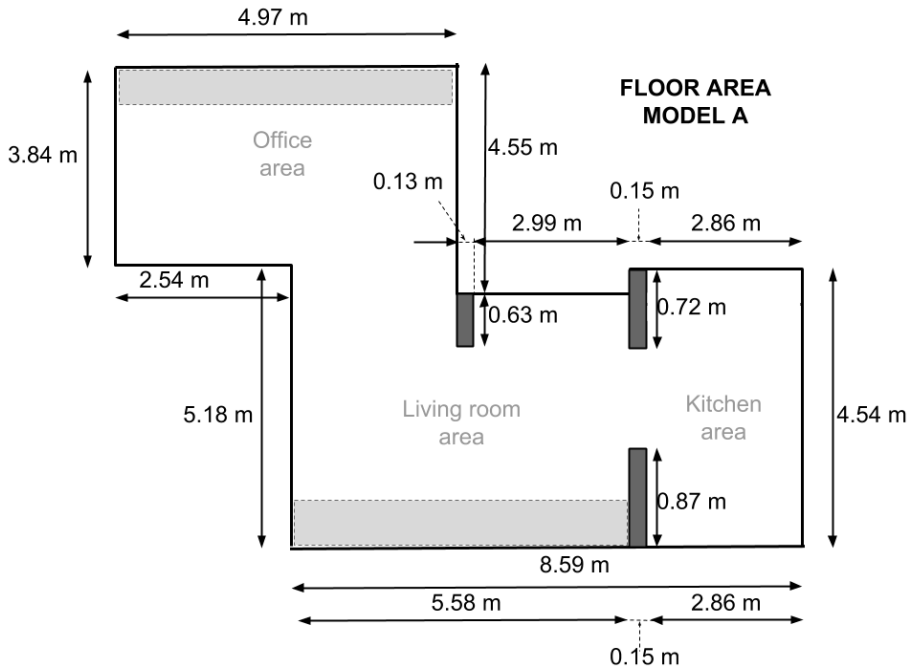
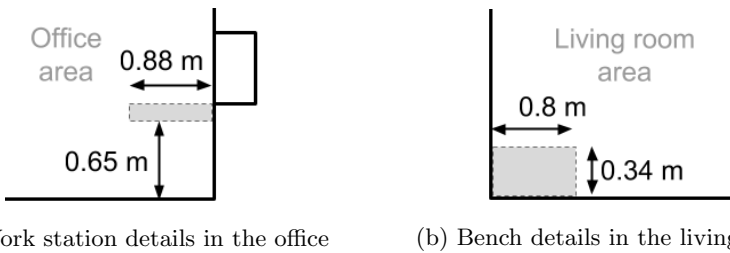


Figure 6.2: Floor dimensions of Model A, given in meters



(a) Work station details in the office

(b) Bench details in the living room

Figure 6.3: Details and dimensions of important geometries in the CFD model

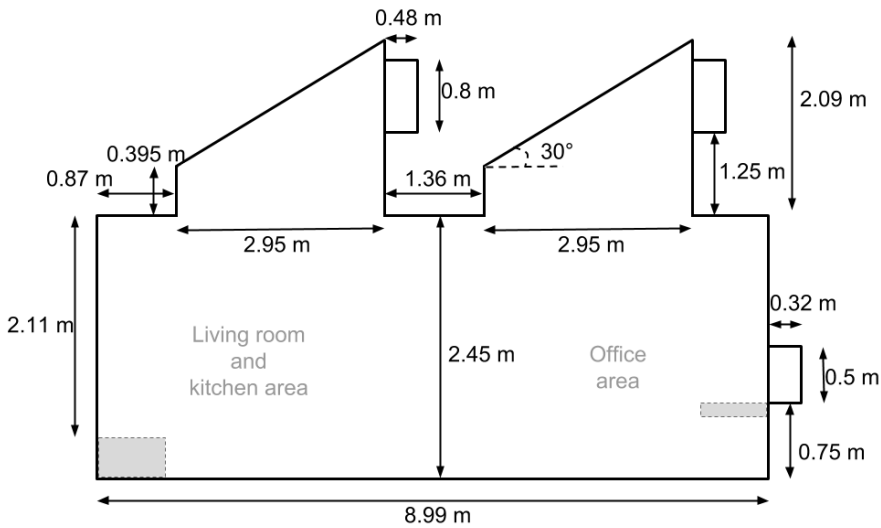


Figure 6.4: Cross section dimensions of Model A, given in meters

The light grey areas represent the work station in the office area, and the bench along the south window in the living room. The work station has a length equivalent to the room length of 4.97 m (seen in Figure 6.2), and a height of 0.1 m. The south window bench is 5.58 m long. The height, width and location of these geometries are given in Figure 6.3. These geometries are expected to influence the airflow inside the building, especially when ventilative cooling is investigated. In addition, they are not complex in a geometrical point of view and are thus included in the CFD model. The dark grey areas in Figure 6.2 represent wall surfaces inside the building.

Although Model A does not include any solid windows or walls in the geometry, the model does include imprinted areas where the outer domain of the fluid model and the windows or walls are connected. In ANSYS Fluent, it is possible to assign surfaces of the fluid model solid material properties while not including the actual geometries in the CFD model, as long as the surfaces are located at the outer domain. This allows the simulations to investigate material characteristics, such as heat transfer through radiation, conduction and convection at and through surfaces, as well as solar load effects.

Figure 6.5 shows the location of the two windows located at the north wall (office), 0.75 m above the floor, and the inner layer of the double-skin south window (living room), located 0.4 m above the floor. The height of the north windows are 0.5 m, while the height of the south windows are 1.91 m. This is illustrated in Figure 6.6. The length of the frame between the two middle windows at the south facade is 0.055 m, and between the middle windows and the two side windows, the distance is 0.11 m.

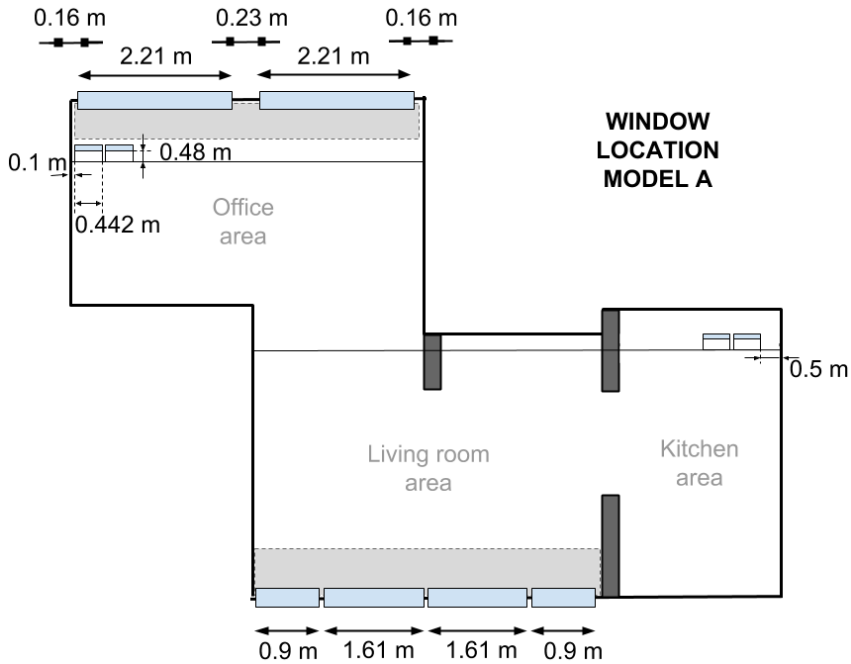


Figure 6.5: Location and dimensions of north and south windows in Model A

There are four skylight windows in the facility, two located in the kitchen and two in the mezzanine. As a result of the geometrical simplification of excluding the mezzanine, the two windows located there are moved to the east in the CFD model, placing them at the north wall of the office area, above the workstation windows. All four windows have the same dimensions (0.8 m · 0.422 m), and are placed at a 0.12 m distance from each other, see Figure 6.6.

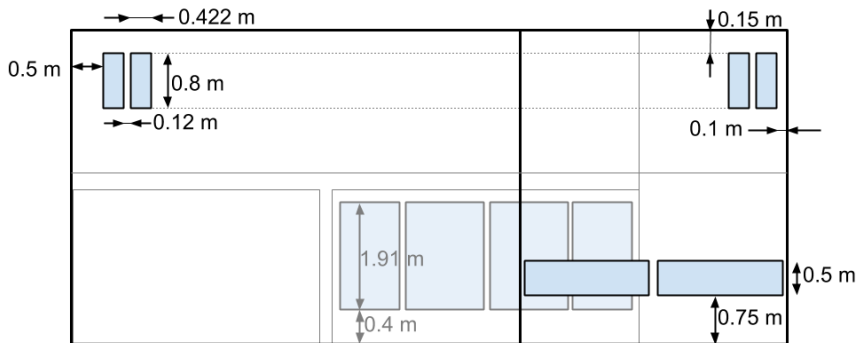


Figure 6.6: Location and dimensions of skylight windows in Model A

Another area that require location alterations are the extracts and supply vents for the mechanical ventilation system. There are three air supply vents in the facility. These are located in the living room, and each of the bedrooms. Because the bedrooms are not modeled, the vent inlets to these rooms had to be moved. In the CFD model, these inlets have been located on the walls, along the floor, in the office area, mimicking the actual flow that will travel under the closed bedroom doors in a real situation. The same assumption have been made for the air extraction that takes place in the bathroom. This is illustrated in Figure 6.7.

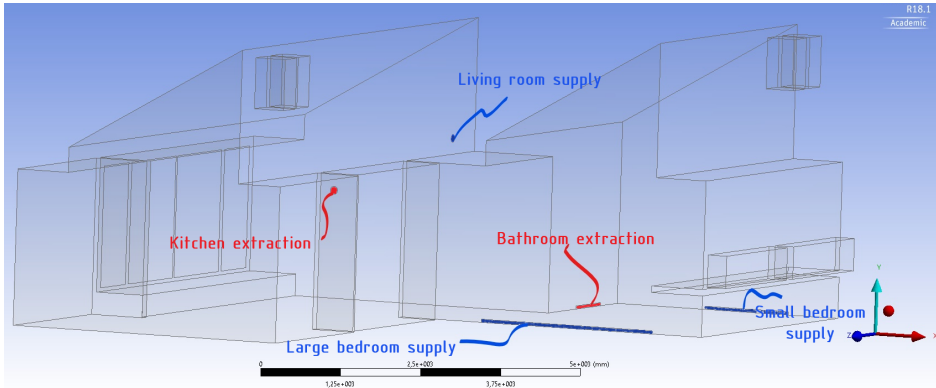


Figure 6.7: Locations of air supply and extraction in the CFD model

The vent supply and extraction characteristics and dimensions are presented in Table 6.1. W, H, and D defines the width, height and diameter of the inlet and outlet areas, respectively. It is assumed that the doors to the two bedrooms and the bathroom are closed and that the air will pass through the surface area between the closed doors and the floor. Positive values for the supply/extraction rate indicates air supplied, while negative flow rate indicates extraction of air.

Table 6.1: Vent characteristics

Name	Dimension (m)			Supply/ extract rate (m^3/h)	B.C. values	
	W	H	D		velocity (m/s)	mass flow (kg/s)
Large bedroom	2.95	0.05	-	52	0.09793	-
Small bedroom	1.44	0.05	-	52	0.20060	-
Living room	-	-	0.125	26	0.58700	-
Kitchen	-	-	0.125	-52	-	0.01790
Bathroom	0.89	0.05	-	-78	-	0.02706

6.2 Additional Simplifications and Comments to Model A

This section will give a brief comment on the geometry elements that have been changed or removed from the original layout and how they are expected to affect the simulation results. The simplifications to the model geometry design revolves mainly around reduction of mesh elements.

- **Simplifying the building envelope:** The building envelope of the CFD model have a floor area of 55 m^2 , and an internal air volume of 195 m^3 , i.e. the floor area is reduced to 55 % of original size and air volume is reduced to 39 % of original size. This reduction is a result of not including the bathroom, bedrooms, entry and mezzanine. By assuming that the doors to the bathroom and bedrooms are closed (which is a possibility in the building), the simulated flow pattern should be representative for an actual flow in real life. During the full-scale measurements, the door positions were not mentioned. The bedrooms were most likely open while the bathroom door was closed. It is uncertain how much this might affect the end result of the simulation.
- **Location of air supply and extraction vents:** The velocity and air temperature will most likely be a little bit different (temperature would be higher, due to heating in floor, and solar radiation through windows, occupants and electrical equipment present in the rooms, etc.). The airflow rate however, we can assume to be correct, as the system is balanced and overflow of supplied air is expected to enter the office from the bedrooms. All in all, the design is assumed acceptable, and the error that follows from this simplification will result in higher velocities at the floor level with lower temperatures, i.e. the need for ventilative cooling will be lower than in real life.
- **The solid materials:** The walls and windows are not included in Model A. Although they are not modeled, some of the simulations will use Fluent's option of giving fluid surfaces a solid material property (in this case wood and glass). By defining the walls, roof and floor as wood, and all the windows as glass, heat transfer calculations over the surfaces can be included in the simulations. What is not a part of the calculations when including material properties, are the heat losses due to infiltration.
- **Windows:** The CFD model have simplified the window geometry to reduce computational costs. This include the actual design of the windows (e.g. no frame details), as well as the opening mechanism for the window (see Appendix C). This is done to avoid complicated details that will lead to the requirement of more cell elements. These simplifications are assumed to have little effect on the end results, and thus assumed acceptable.
- **Skylight windows:** The two skylight windows that are located in the mezzanine in the experimental facility have been moved. The new location for these windows are now at the north wall in the office area, above the two

north windows. The surface area of each of the windows has been reduced from 0.584 m^2 to 0.338 m^2 . The reason for this is explained in more detail in Appendix C.1. The height placement of the windows have not been altered. As long as the height location of the windows are not altered, it is assumed that the stack effects in the building will be intact and the air flow will only be slightly affected by the change. It is therefore concluded that this simplification is acceptable, until new information says otherwise.

- **Doors and other windows:** For the time being, all doors and the rest of the windows in the experimental facility are not included in the CFD model. This may affect the end result of the simulations (temperature distribution and the air flow pattern inside the building), since these are the areas where one would expect the largest heat transfer to occur between the cold and warm environment. A consequence of these simplifications are that the calculated temperature of the air close to the east wall of the kitchen (because of window) and the west wall of of the living room (because of outer door) will differ from real life, depending on the weather outside. For this project, these errors are acceptable. For a more accurate CFD model, it is worth to consider including these geometries to get more accurate simulations.
- **No furniture:** The CFD model have only included the work space in the office and the bench along the south window. Including more furniture and other details will complicate the model geometry, and most likely result in poor quality grid that needs to be fixed. This also means that internal heat loads, such as lighting and other electrical equipment are excluded.
- **No outer environment:** Including an outer environment to the CFD models, will results in more accurate simulation solutions, as defining boundary conditions at these surfaces are easier, compared to setting boundary conditions at the window opening surfaces. This was mentioned by literature in Section 3.10. However, this additional geometry require a large amount of cell elements to obtain an acceptable grid quality, making the computational cost really large.

6.3 Grid

A mesh was created for Model A, with the Mesh modul in Workbench. By choosing and defining different parameters under the sizing tab (information given in Table 6.2) the mesh achieved an acceptable quality, while keeping the mesh elements at a low number.

Table 6.2: Grid operations - Model A

Parameter	Alteration
Size function	Proximity and Curvature
Relevance center	Fine
Proximity Size Function Sources	Faces and Edges Max Face Size 0.25 m Max Tet Size 0.5 m
Minimum Edge Length	5e-02 m

All other operations kept default settings. This produces the mesh illustrated in Figure 6.8 and Figure 6.9. The grid consist only of a tetrahedron cell structure. From the figures, the finer cell elements are located close to areas with either defined inlets and outlets (the supply and extraction vent areas), around the imprinted surfaces (south window area) or where the detailed geometry are close in proximity (like the skylight windows).

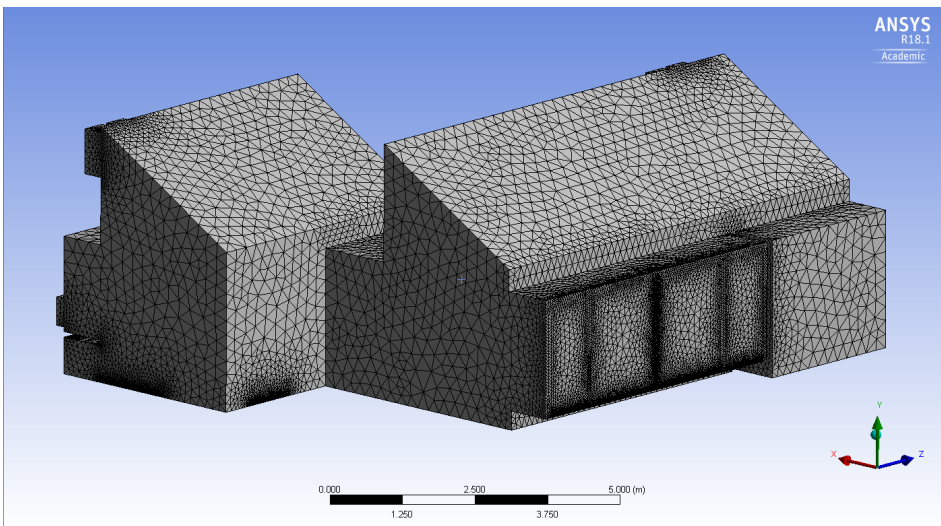


Figure 6.8: Mesh of Model A, viewed from south-west

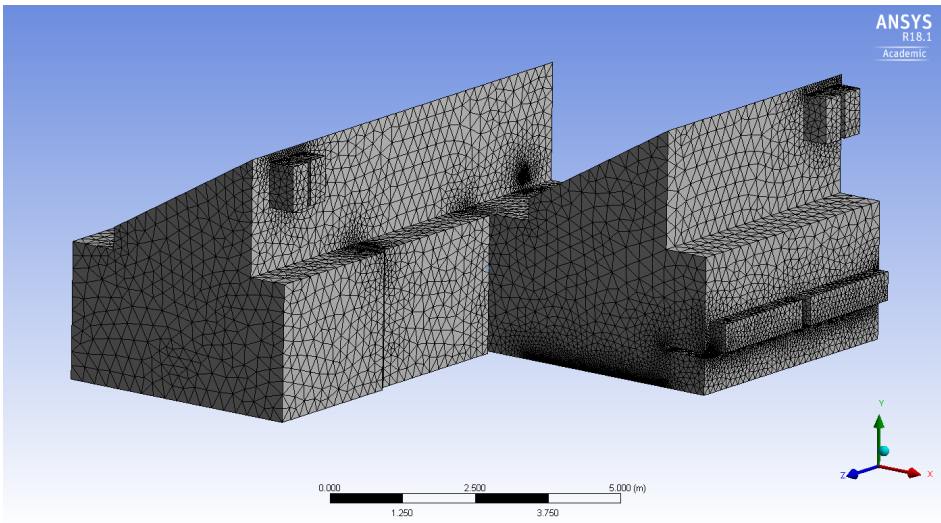


Figure 6.9: Mesh of Model A, viewed from north-east

The mesh statistics are given in Table 6.3.

Table 6.3: Mesh statistics - Model A

Statistics	Value	Comment
Elements	706549	The number of elements is quite low, considering the domain size of Model A, i.e. the computational cost is relatively low.
Aspect ratio	Min. 1.1631 Max. 11.926 Avg. 1.8592	The mesh quality is good in regard to aspect ratio.
Skewness	Min. 3.1491e-4 Max. 0.84772 Avg. 0.23559	Maximum skewness is well below the value of 1, and most of the cells are only slightly skewed. The quality is good in regard to skewness.
Orthogonal quality	Min. 0.15228 Max. 0.99511 Avg. 0.7631	Minimum value is well above the value of 0, and most of the cells are of good orthogonal quality. The quality is good in regard to orthogonal quality.

From the mesh statistics, the simulation should be able to run quite quickly (based on the low number of mesh elements present) and the mesh quality should be good enough for the simulation to calculate sufficiently detailed results.

6.4 CASE 1: Air Flow Investigation

A simple case, investigating the characteristics of the flow as a result of the applied mechanical ventilation in Model A, was performed to ensure that the correct boundary conditions were set to achieve conservation of mass inside the simulation domain. Case 1 is simulated steady, with only the viscous model activated. The settings that will be used in Case 1 and remain constant for all the following cases (unless stated otherwise) are listed in Table 6.4.

Table 6.4: Fixed setup settings for all the simulation cases

These constants are	Pressure-Based Solver Coupled Scheme Method Absolute Velocity Gravitational Acceleration On $Y=-9.81 \text{ m/s}^2$ RNG \bar{k} - ϵ Turbulence Model Standard Wall Function Full Buoyancy Effects
Other constant	Spatial Discretization Least Square Cell Based (Gradient) PRESTO! (Pressure) First and Second Order Upwind (Momentum, Kinetic energy, Dissipation rate, Energy) Temporal Discretization Steady-state: Pseudo Transient On Transient: First Order Implicit (Time Stepping Method: Adaptive)

For Case 1, a steady state simulation will be sufficient to check the flow pattern of the air inside the CFD model and if conservation of mass is achieved. This will reduce the simulation cost, compared to a transient simulation, that requires longer simulation time and greater computer capacity.

6.4.1 Input values for Case 1

Material properties

Only the viscous model is used in Case 1, i.e. no energy calculations will take place. Therefore, the default values for the fluid material air is kept for the simulation.

Boundary conditions

The supply vents at the bedrooms and in the living room are set as velocity inlets, using the calculated velocities from Table 6.1. The extraction vents at the bathroom

and kitchen are first simulated as outflow. Table 6.1 gives a flow rate weighting for the kitchen and bathroom to be 0.39813 and 0.60187, respectively. This type of boundary condition is good to use when all inflow and/or outflow are known. This is the case when only the mechanical ventilation system is used. This boundary condition will not work in situations when ventilative cooling is carried out, because an unknown amount of air enters and exits the fluid domain making it impossible to define flow rate weighting for the outlets. The outflow boundary condition will be used to confirm which other outlet boundary condition that can be used for cases where ventilative cooling is investigated.

Method

The solution method is the same as listed in Table 6.4, with a pseudo time step set to 1e-05s. This is done to accelerate the convergence of the simulation solution. The solution initialization is done with hybrid initialization.

6.4.2 The simulation result for Case 1

The simulation stopped when all the residuals reached the chosen convergence criteria of 1e-05 for the continuity residual, velocity (x, y, z) residuals and the turbulence (\bar{k} , ϵ) residuals.

Conservation of mass - outflow B.C.s at the extraction vents

A monitor reporting the sum of the inlet mass flow rates and outlet mass flow rates were set up. The solution showed that the inlet mass flow rate sum stabilized itself on the value of 4.3348e-02 kg/s, while the outlet mass flow rate sum reported the same value, only with a negative sign, e.i. -4.3348e-02 kg/s. With this information, the mass conservation in this simulation is conserved with outflow boundary conditions, since

$$\text{Sum inlets} + \text{Sum outlets} = 4.3348\text{e-}02 \text{ kg/s} + -4.3348\text{e-}02 \text{ kg/s} = 0 \quad (6.1)$$

Conservation of mass - other B.C.s at the extraction vents

With mass flow outlets as boundary conditions to the extraction vents, using the calculated values from Table 6.1, the conservation of mass is not achieved, as

$$\text{Sum inlets} + \text{Sum outlets} = 4.3348\text{e-}02 \text{ kg/s} + -4.496\text{e-}02 \text{ kg/s} = -0.1612\text{kg/s} \quad (6.2)$$

The difference is caused by round off errors when calculating the velocity magnitudes and mass flow rate for the supply and extraction vents. To achieve conservation of mass, new boundary conditions values for the extraction vents are changed from the values listed in Table 6.1 and set to 0.017259 kg/s for the kitchen outlet boundary condition and 0.026089 kg/s for the bathroom outlet boundary condition. The calculations are shown in Table 6.5.

Table 6.5: Extraction outlet B.C. calculations - new mass flow rates

Inlet mass flow	0.043348 kg/s	
Flow rate weighting		
Kitchen	0.39813	
Bathroom	0.60187	
Calculating new outlet mass flow (kg/s)		
Kitchen	0.39813*0.043348	
Bathroom	0.60187*0.043348	
	Kitchen	Bathroom
Old mass flow rate (kg/s)	0.01790	0.02706
New mass flow rate (kg/s)	0.017259	0.026089
Difference (old-new) (kg/s)	6.41e-04	9.71e-04

Air flow pattern

Figure 6.10 illustrates the stream lines of the air that enters the fluid domain of Model A at the velocity inlets. From the figure, it is possible to conclude that the air will enter at the inlets and exit at the defined outlets in the simulation. This is further illustrated in Figure 6.11, where the streamlines have been separated and given its own color, so that the stream lines from the different inlets are easily distinguished.

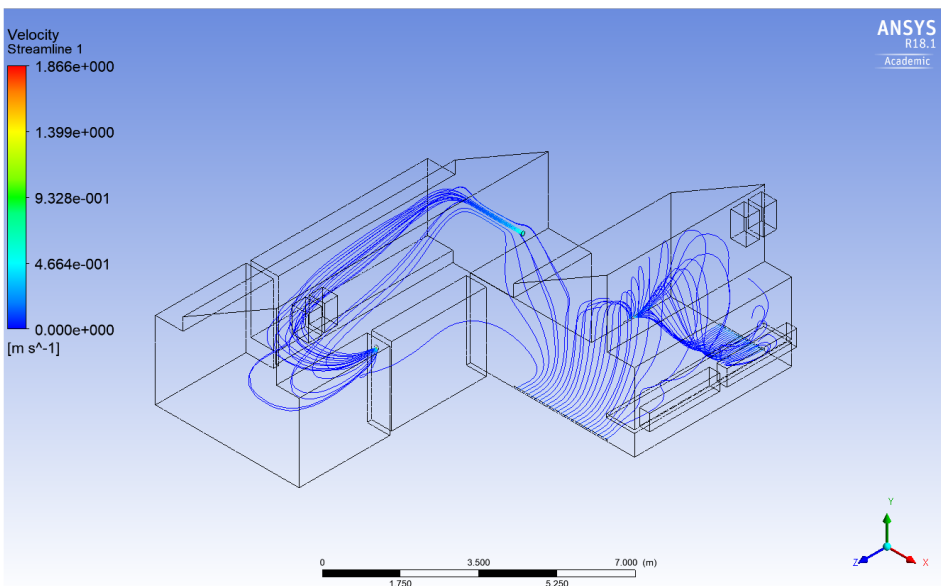
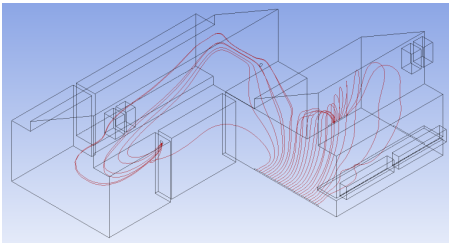
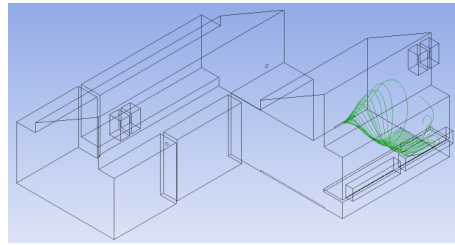


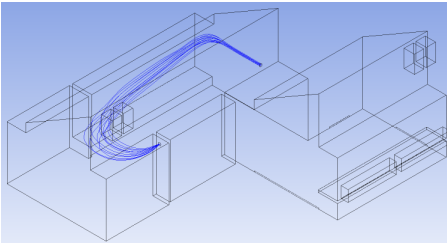
Figure 6.10: Case 1 - Velocity streamlines, starting from the inlets



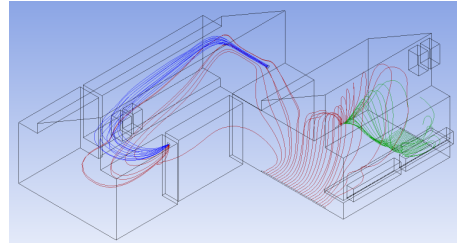
(a) Streamlines from the large bedroom



(b) Streamlines from the small bedroom



(c) Streamlines from the living room



(d) All streamlines included

Figure 6.11: Case 1 - Streamline distribution for the supply vents

6.4.3 Case 1 Comment on the presented results

The change in colors of the streamlines in Figure 6.10 shows that the air experiences the largest velocities at the defined inlets and outlets, i.e. the supply and extraction vents. Around these areas, the streamlines have mostly a lighter blue color, compared with the rest of the streamlines inside the room, having a dark blue color representing a velocity close to zero. From Figure 6.11, the air flow pattern from the different inlets are illustrated. Figure 6.11b shows the air entering the office from the small bedroom side is most likely to be extracted from the bathroom outlet. The air entering the living room, see Figure 6.11c will most likely be extracted by the kitchen outlet, while the supplied air from the large bedroom, Figure 6.11a, are spread between the two outlets.

From the figures, the simulation is assumed to have solved the problem correctly, taking into account the simplifications and assumptions made to the model and setup.

To ensure that the mass is conserved for simulations that do investigate ventilative cooling, a mass flow outlet boundary condition should be defined, with values given in Table 6.5.

6.5 CASE 2: Energy Calculation Effects

Now that setup and boundary conditions for the mechanical system have been verified, the next step is to include heat calculations. In Case 2, studies on the different thermal boundary conditions for the solid materials will be performed, by using contour temperature plots and heat balance information. The operational temperature is determined to be $T_{indoor}=20^{\circ}\text{C}$ and the outdoor air is set to $T_{outdoor}=0^{\circ}\text{C}$.

6.5.1 Input values for Case 2

Material properties

In addition to the viscous model, the energy calculations are included and turned on for the investigations involving Case 2. The fluid material properties of air are determined by assuming an operation temperature of about 20°C . The air properties are listed in Appendix B, in Table B.1 for $T=20^{\circ}\text{C}$. For the solid materials used in Case 2, the properties are listed in Table 6.6

Table 6.6: Case 2 - Solid material properties

Solid	Density	Specific heat capacity	Thermal conductivity
Wood	700 kg/m ³	2310 J/kg-K	0.055 W/m-K
Glass	2500 kg/m ³	800 J/kg-K	0.06 W/m-K

Boundary conditions

Floor heating set to 20 W/m^2 . This number is taken from the IDA ICE simulation setup performed on ZEB Living Laboratory by [Blandkjenn, 2017]. No other heat sources will be placed inside the room. In real life, heat loads from electrical equipment and other installations will be present. It is therefore expected that the simulated results will produce some errors related to this.

The supply vents at the bedrooms and in the living room are set as velocity inlets, using the calculated velocities from Table 6.1. The air supply temperature for the mechanical ventilation is also taken from the IDA ICE simulation setup from [Blandkjenn, 2017], and is set to 19°C for cold conditions and 22°C for warm conditions. The extraction vents at the bathroom and kitchen are set as outflow. Table 6.1 gives a flow rate weighting for the kitchen and bathroom (e.i. 0.39813 and 0.60187, respectively).

The windows are applied a thickness of 0.03 m. The external and internal emissivity for glass are set to 0.9 [Incropera et al., 2013]. The walls are applied a thickness of 0.5 m, and the external and internal emissivity are given the value of 0.82 [Incropera et al., 2013].

When convection boundary conditions are applied, the heat transfer coefficient is set to 25 W/m-K and 7.69231 W/m-K [VVS, 1969], the first value being appropriate for walls facing the outdoor environment and the other value being appropriate for walls facing other internal rooms. The wall boundaries in Case 2 consist of wall surface areas that both face the indoor and outdoor environment. The walls facing the indoor environment are the shared walls of the office and the bedrooms and bathroom, the living room and the entrance, bathroom and the large bedroom, and the kitchen and the large bedroom. The walls facing the outdoor environment includes the remaining walls, in addition to the roof. A small study on the effect of convection coefficient will be performed for Case 2.

The free stream temperature is 0°C. When radiation boundary conditions are included, the external radiation temperature is also set to 0°C.

Method

The solution method is the same as listed in Table 6.4, and the simulations performed with Case 2 are all steady with a pseudo time step set to 1e-05s. The solution initialization was done with hybrid initialization. The simulations were stopped when the energy residual reached a stable value beneath 1e-08 and the remaining residuals reached a stable value beneath 1e-05.

6.5.2 Data extraction

Planes

Three planes were created in the post-processing module in Workbench to compare results from Case 2.1 and Case 2.2. In Table 6.7, the necessary information required to make these planes are listed.

Table 6.7: Case 2 - Plane locations for post-processing

Plane	Type	Coordinate		
		x	y	z
1	XY	-	-	3.705 m
2	YZ	-3 m	-	-
3	YZ	2 m	-	-

Plane 1 connects the south and north wall of the building, and can include heat characteristics over one of the windows on the south facade and on one of the windows on the north facade. Plane 2 connects the east wall of the kitchen and the west wall of the living room, while Plane 3 reaches from one bedroom wall to the other bedroom wall, through the office.

The planes are illustrated in Figure 6.12.

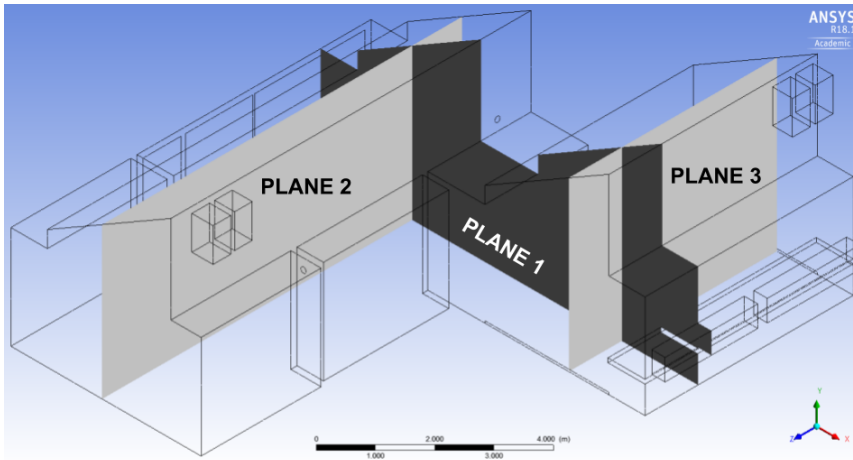


Figure 6.12: Case 2 - Location of the planes used to evaluate the results

Graphics

Temperature contour plots are used to investigate the air temperature distribution inside the building, and for comparing different simulated results.

Flux reports

The fluxes of mass and heat will be presented. The conservation of mass will be confirmed or disputed. For the heat fluxes, the heat transfer rate balance will be investigated. The magnitude of surplus heat for the different sub-cases will be compared and briefly commented.

6.5.3 Case 2.1 Setup and Results

Case 2.1 investigate the heat calculation when only convection is included at the boundary surfaces of the windows and walls of the CFD model.

Case 2.1.1 v.s. Case 2.1.2

In Case 2.1.1, the heat transfer coefficient for the wall surfaces is set to $h = 7.69231$ W/m-K, while the heat transfer coefficient for the windows is $h = 25$ W/m-K.

In Case 2.1.2 the heat transfer coefficient for the walls is set to $h = 25$ W/m-K. The same value is used for convection calculations over the glass surfaces.

Temperature contours

The two simulated cases, presented in Figure 6.13 and Figure 6.14, look seemingly similar at a first glance.

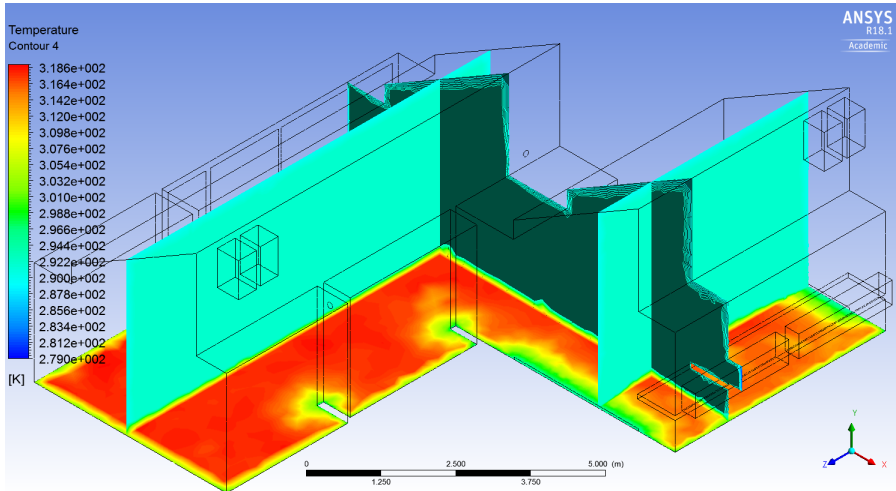


Figure 6.13: Case 2.1.1 - Temperature contours (Wall heat transfer coefficient, $h=7.69231$ W/m-K)

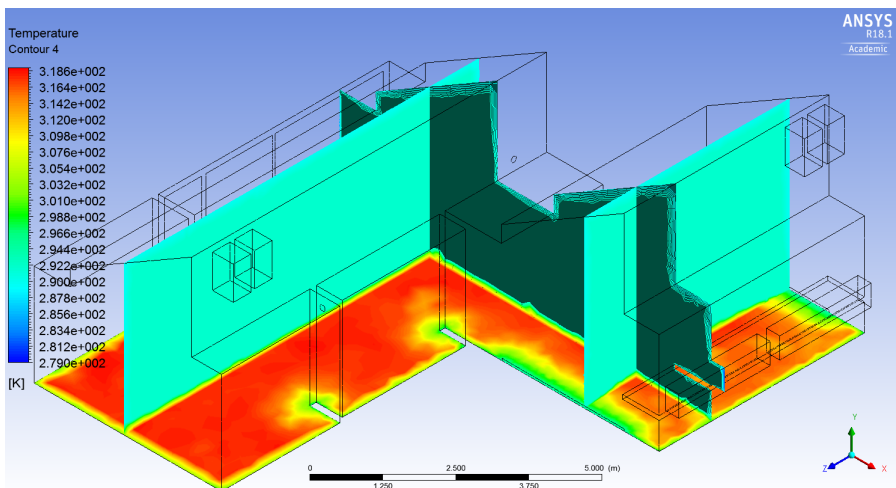


Figure 6.14: Case 2.1.2 - Temperature contours (Wall heat transfer coefficient, $h=25$ W/m-K)

From the contour plots, the indoor air temperature remains fairly constant, with a

value of around $T_{indoor}=292$ K for both heat transfer coefficients. This is the same temperature as the set supply temperature (T_{supply}) of the mechanical ventilation. The floor temperature is much higher than the indoor air temperature, with the highest value in the middle of the floor, $T_{floor,max}=318.6$ K (for both cases). Closer to the walls, the trend for both cases show that the floor temperature is reduced.

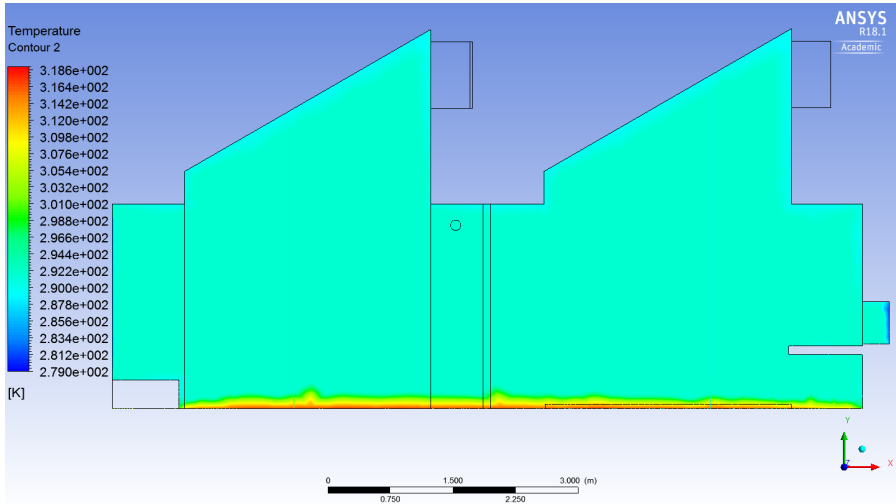


Figure 6.15: Case 2.1.1 - Temperature contour, plane 1 (Wall heat transfer coefficient, $h=7.69231$ W/m-K)

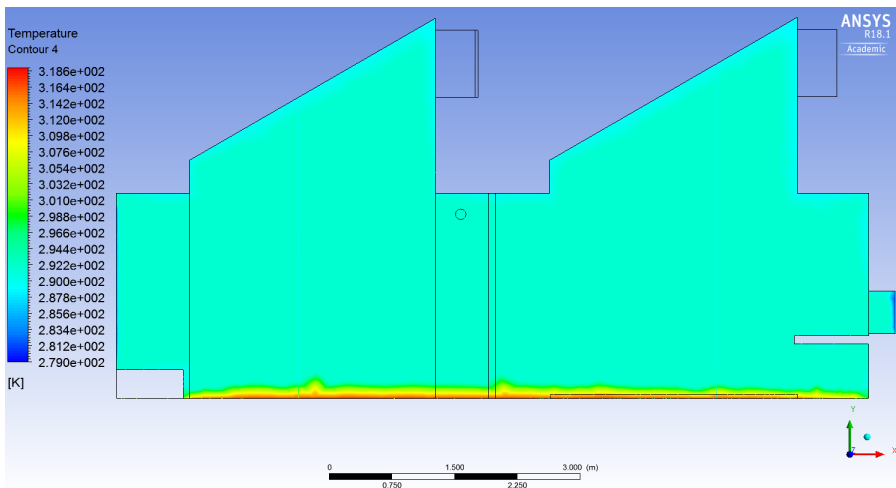


Figure 6.16: Case 2.1.2: Temperature contour, plane 1 (Wall heat transfer coefficient, $h=25$ W/m-K)

The contour plots in Figure 6.15 and Figure 6.16 substantiates the simulation result similarities further. The contour plots show that the coldest areas on the model are located at the surfaces of the windows, with a temperature of $T_{window}=279$ K. Close to the roof the temperature ranges from $T_{roof}=289.5-291$ K depending on distance from the wall surface, where the lowest temperature is the wall surface temperature. Despite the large temperatures close to the floor, only the air closest to the floor is heated up. This indicates that the choice of convection only as a boundary condition for the CFD simulation should be reconsidered.

Flux reports

The mass flux reported for Case 2.1.1 and Case 2.1.2 are given in Figure 6.17. Although the net mass flux for both cases are not absolute zero, the discrepancies are assumed to be so small that the mass in the simulations are accepted as conserved.

"Flux Report"		"Flux Report"	
Mass Flow Rate	(kg/s)	Mass Flow Rate	(kg/s)
-----		-----	
floor	-0	floor	-0
inlet_large_bedroom	0.017405833	inlet_large_bedroom	0.017405833
inlet_livingroom	0.0085380951	inlet_livingroom	0.0085380951
inlet_small_bedroom	0.017404056	inlet_small_bedroom	0.017404056
interior-fluidindoor	0.041757772	interior-fluidindoor	0.023681193
outlet_bathroom	-0.035562882	outlet_bathroom	-0.037633725
outlet_kitchen	-0.020631259	outlet_kitchen	-0.018761827
walls	-0	walls	-0
windows	-0	windows	-0
-----		-----	
Net	-0.012846157	Net	-0.013047567

(a) Case 2.1.1 - Mass flow rate (b) Case 2.1.2 - Mass flow rate

Figure 6.17: Case 2.1 - Flux Report, Mass flow rate

The total heat transfer rate reported for Case 2.1.1 and Case 2.1.2 are given in Figure 6.18. For both of the cases, a heat surplus will occur. Case 2.1.1 obtain an excess heat transfer rate of 525.98 W, while Case 2.1.2 obtain an excess heat transfer rate of 523.47 W. With $h=25$ W/m-K (Case 2.1.2), a smaller heat surplus is simulated, which is expected when $h_{Case2.1.2} > h_{Case2.1.1}$. The larger the convective heat transfer coefficient is, the more heat is transferred by convection. However, the surplus heat transfer rate difference between the two simulations is so small that Case 2.1 is concluded to be independent of the choice of heat transfer coefficient of either 7.69231 W/m-K or 25 W/m-K.

"Flux Report"		"Flux Report"	
Total Heat Transfer Rate	(w)	Total Heat Transfer Rate	(w)
floor	1089.129	floor	1089.129
inlet_large_bedroom	-107.46599	inlet_large_bedroom	-107.46061
inlet_livingroom	-52.771324	inlet_livingroom	-52.77108
inlet_small_bedroom	-107.54757	inlet_small_bedroom	-107.54506
outlet_bathroom	219.79734	outlet_bathroom	232.60772
outlet_kitchen	127.51651	outlet_kitchen	115.9619
walls	-424.76857	walls	-428.51929
windows	-217.91241	windows	-217.92857
Net	525.97703	Net	523.47406

(a) Case 2.1.1 - Heat transfer rate

(b) Case 2.1.2 - Heat transfer rate

Figure 6.18: Case 2.1 - Flux Report, Heat transfer rate

6.5.4 Case 2.2 Setup and Results

In Case 2.2, the viscous-, energy- and radiation models are used, and it is the Surface-to-Surface radiation model that is included in the setup for Case 2.2. The boundary conditions for the window- and wall surfaces are set to mixed thermal boundary conditions, where both convective and radiative heat transfer are included in the simulation calculations. The heat transfer coefficient is set to 25 W/m-K for the walls and the windows.

Temperature contours

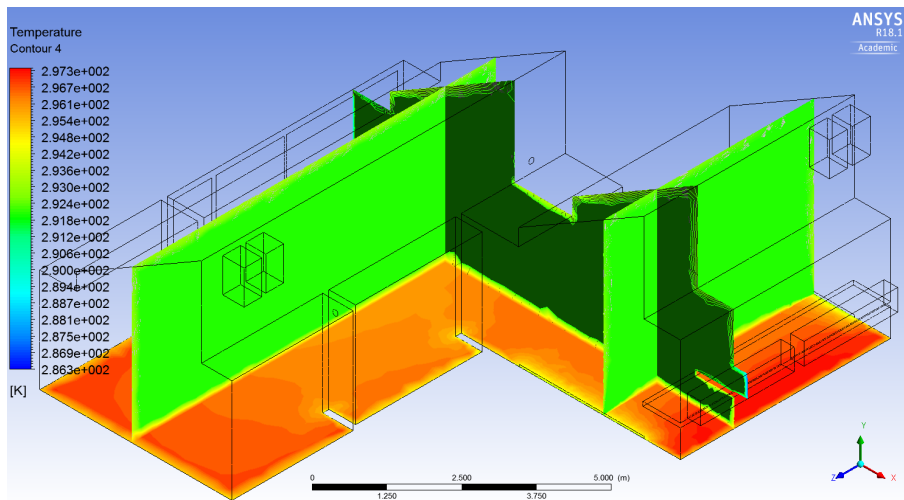


Figure 6.19: Case 2.2 - Temperature contours

The temperature contours (Figure 6.19-6.21) for Case 2.2 shows that including radiative boundary conditions on the walls and windows will result in a quite different temperature distribution inside the room, compared with the simulated results in Case 2.1.

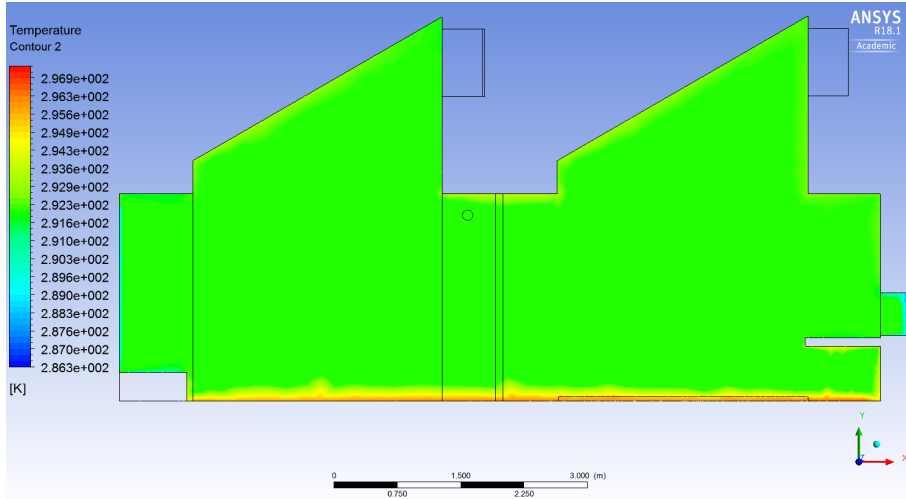


Figure 6.20: Case 2.2 - Temperature contour, plane 1

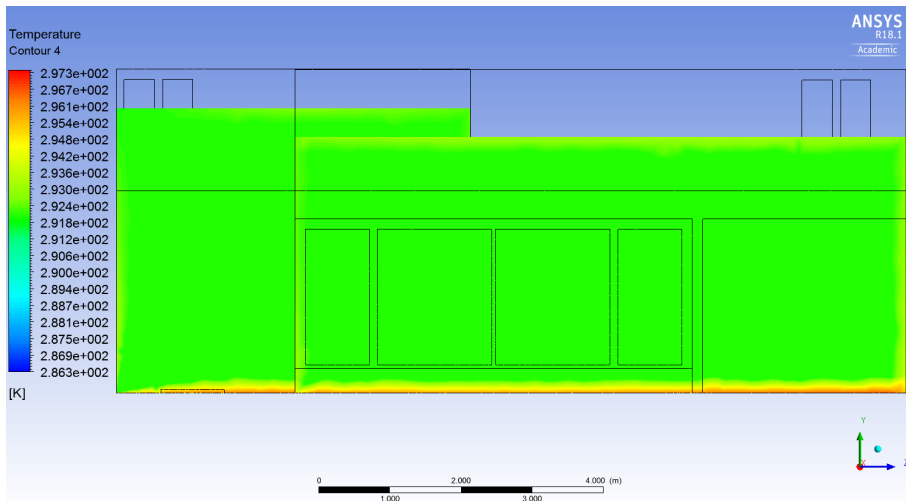


Figure 6.21: Case 2.2 - Temperature contours, viewed from the south

There are some similarities, such as constant indoor air temperature of $T_{indoor}=292$ K, that the temperature along the windows and walls are lower, that the temper-

ature close to the floor is high, compared to the rest of the room, and that despite the larger temperature at the floor, only the air closet to the floor is heated up. The main differences are that the calculated temperatures in Case 2.1 are more extreme compared to the ones calculated in Case 2.2. The highest temperatures in Case 2.2 are found at the floor surface, with a maximum temperature of $T_{floor}=296.9$ K. In other words, by including a radiation model in the simulation, the floor surface temperature is reduce by 21.7 K. The roof surface temperatures range from $T_{roof}=291.5-293.5$ K (cooler temperature around the skylight windows). This is higher than for Case 2.1. The surface temperature of the windows are also at a higher temperature magnitude compared to Case 2.1. For Case 2.2 the coldest window surface temperature is $T_{window}=286.3$ K, that is 7.3 K higher than for simulations that only considers the convective heat transfer.

Flux reports

Mass flow rate sufficiently low that the conservation of mass is accepted. The total heat transfer rate for Case 2.2 is under half of what was reported for both situations in Case 2.1. From a thermal point of view does Case 2.2 predict the flow better than Case 2.1, which means that radiation effects should be included in future simulations.

"Flux Report"		"Flux Report"	
Mass Flow Rate	(kg/s)	Total Heat Transfer Rate	(w)
-----		-----	
floor	-0	floor	1089.129
inlet_large_bedroom	0.017405833	inlet_large_bedroom	-108.88345
inlet_livingroom	0.0085380951	inlet_livingroom	-52.809791
inlet_small_bedroom	0.017404056	inlet_small_bedroom	-108.24567
interior-fluidindoor	-0.0049620805	outlet_bathroom	160.88116
outlet_bathroom	-0.026089851	outlet_kitchen	106.57108
outlet_kitchen	-0.017258133	walls	-494.06637
walls	-0	windows	-369.92537
windows	-0	-----	
Net	3.469447e-18	Net	222.65063

(a) Case 2.2 - Mass Flow Rate

(b) Case 2.2 - Total Heat Transfer Rate

Figure 6.22: Case 2.2 - Flux Report, Mass Flow Rate & Total Heat Transfer Rate

6.5.5 Case 2 Comment on the presented results

A simplification was made when the model's boundaries were divided up and given names during the mesh process, to make the setup easier. All the walls, and roof were grouped together and called "Wall". This is why only one heat transfer coefficient was defined for the entire wall in Case 2.1.1 and Case 2.1.2. The heat transfer coefficient should be 7.69231 W/m-K for the internal walls, i.e. the east, west and south walls of the office area (walls that separate the bedrooms, bathroom and office), and the west wall of the living room (entrance area) and part of the north wall of the living room/kitchen (large bedroom). The walls that have heat

transfer coefficient equal to $25 \text{ W/m}^2\text{-K}$ are the remaining walls and roof. In addition to the assumption of only one heat transfer coefficient, the grouped wall will also result in wrong definitions of the external temperatures (i.e. the free stream temperature and external radiation temperature) for some of the surfaces. For the internal wall surfaces, the free stream temperature and the radiation temperature are not equal to the outdoor environment temperatures ($T=0^\circ\text{C}$), but rather to indoor temperatures ($T=20^\circ\text{C}$). By not dividing up the wall surfaces properly, and thus not including both heat transfer coefficients in the simulation, the energy calculations in the simulation will give some errors to the temperature distribution and reported heat transfer rates, when compared with the actual building.

A smaller heat transfer coefficient means less heat transfer along the walls. So, by choosing a heat transfer rate of $25 \text{ W/m}^2\text{-K}$, the result can be expected to produce lower temperatures in the building that might occur in the actual building. The simplification in regards to the temperature will enhance the temperature error further. The lower temperatures set as boundary conditions will act as larger heat sinks than if room temperatures had been applied.

The high floor temperature reported in Case 2.1 is most likely a result of wrong B.C. setup. From Case 2.2 it can clearly be seen that the heat transfer from the floor to the external fluid (air) acts in a more correct way. In Case 2.1 the simulation under-predicts the heat transfer causing a higher floor temperature, while Case 2.2 manage to reduce this temperature by quite a lot. Case 2.2 also show tendencies in regards to the room being heated up, as the temperatures along the walls and roof experience an increase. For the continued simulations, combined convective and radiative heat transfer rate calculations should be included.

The thermal mass of the building have not been considered when defining the material. The walls, roof and floor consist of more layers of different materials, not just one wood material. These layers create a unique quality that have the ability to store heat. The ability is not incorporated into the CFD model, because of simplifications. This might be another reason for why the simulation is not able to accurately predict the flow inside the building. However, for the purpose and the investigations performed in this master thesis, it is assumed that this error is acceptable.

The positive total heat transfer rates indicate that there might be a risk of overheating in the building. This will be further investigated in Case 3, with a new model presented in the next chapter.

Model B

Most of the geometry of Model B is the same as the CFD geometry of Model A (introduced in Chapter 6). However, Model B also includes the four skylight windows, the two north windows in the office and the four windows of the inner layer of the double-skin window at the south facade. The windows are easily seen in Figure 7.1, given the color of yellow to emphasize their location. A solar load study will be performed with the model. The focus will be on setting up the problem, the application of the boundary conditions, placing the model correctly in regards to the sun direction, and investigate the risk of overheating inside the building.

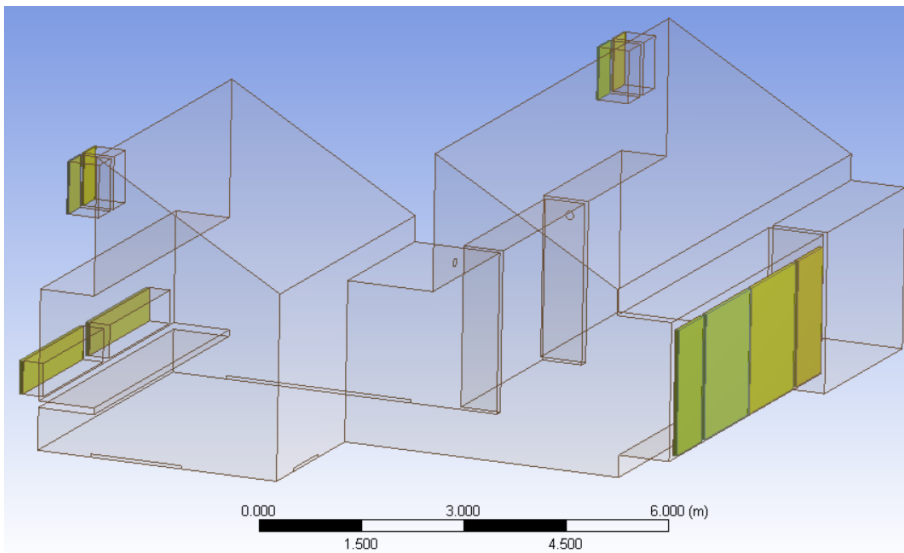


Figure 7.1: Model B geometry

7.1 General Info About the Model

From the U-values listed in Table 4.2, the thickness and thermal conductivity of the different window glasses were calculated. These are presented in Table 7.1.

Table 7.1: Window thickness

Window type	Thickness (mm)	Thermal conductivity (W/m-K)
South window (outer)	30	0.0585*/0.0621**
South window (inner)	60	
North window	60	0.0582
Skylight windows	30	0.03

*,** Depending on air flow rate

Model B will be used to study the contribution of solar load. The windows will be defined as semi-transparent materials, so that the solar radiation may travel through the glass surfaces and heat up the internal walls of the CFD model. From the simulations performed with Model A, it was made clear that a heat surplus exists inside the CFD domain, i.e. the indoor environment will gradually become warmer, unless some form of method is applied to the CFD domain that might remove the excess heat (e.g using ventilative cooling). Applying a solar load on the CFD model will presumably increase the risk of overheating. An investigation into whether the CFD model experiences overheating or not will verify if the model setup is correct. All windows will be closed during Model B simulations.

7.2 Grid

A mesh was created for Model B, with the Mesh modul in Workbench. By choosing and defining different parameters under the sizing tab (information given in Table 7.2) the mesh achieved an acceptable quality, while keeping the mesh elements at a low number.

Table 7.2: Grid operations - Model B

Parameter	Alteration
Size function	Proximity and Curvature
Relevance center	Fine
Proximity Size Function Sources	Faces and Edges Max Face Size 0.25 m Max Tet Size 0.5 m
Minimum Edge Length	3e-02 m

All other operations kept default settings.

This produces the mesh illustrated in Figure 7.2-7.4.

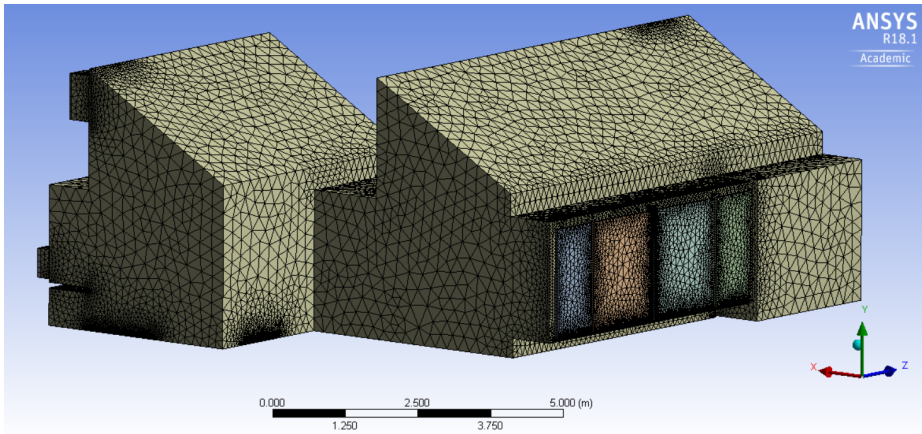


Figure 7.2: Mesh of Model B, viewed from south-west

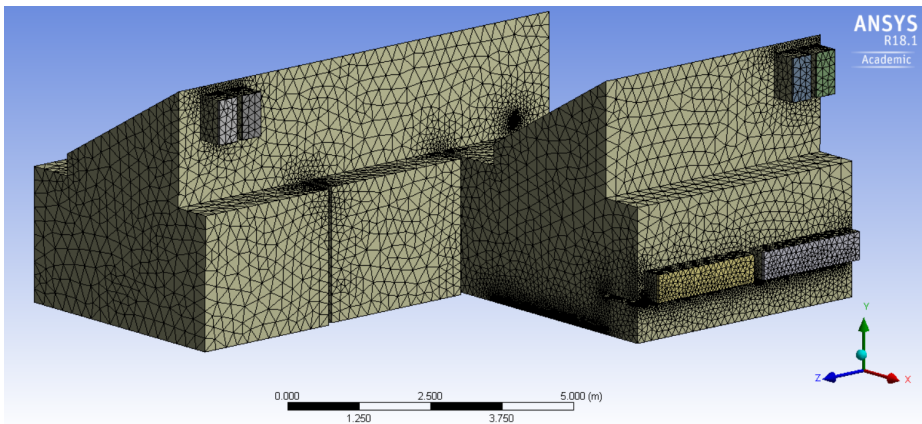


Figure 7.3: Mesh of Model B, viewed from north-east

The grid consist mostly of tetrahedron cell structures, and some wedge cell structures around the solid window geometries. From the figures, the finer cell elements are located close to areas where the defined inlets and outlets are (the supply and extraction vent areas), around the windows and where the detailed geometry are close in proximity (like wall corners).

Figure 7.4 shows how the cell elements are finest close to the walls and increase in size as the cells move toward the center of the model. The fine mesh area showing

vertically down at the north wall of the living room are due to a wall edge, while the area showing horizontally along the floor of the office are due to the defined inlet for the mechanical ventilation from the large bedroom (the east bedroom).

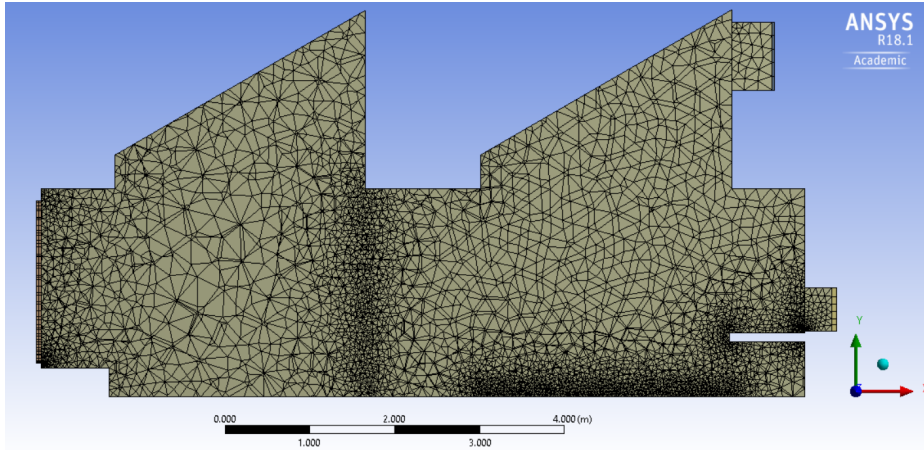


Figure 7.4: Mesh of Model B, cross-section

The mesh statistics are given in Table 7.3.

Table 7.3: Mesh statistics - Model B

Statistics	Value	Comment
Elements	715477	The number of elements is quite low, considering the domain size of Model B, i.e. the computational cost is relatively low.
Aspect ratio	Min. 1.1681 Max. 13.8822 Avg. 1.8725	The mesh quality is good in regard to aspect ratio.
Skewness	Min. 6.0386e-4 Max. 0.84962 Avg. 0.23451	Maximum skewness is well below the value of 1, and most of the cells are only slightly skewed. The quality is good in regard to skewness.
Orthogonal quality	Min. 0.15038 Max. 0.99688 Avg. 0.76421	Minimum value is well above the value of 0, and most of the cells are of good orthogonal quality. The quality is good in regard to orthogonal quality.

From the mesh statistics, the simulation should be able to run quite quickly, based on the low number of mesh elements present (that are only slightly higher than in Model A), and the mesh quality should be good enough for the simulation to calculate sufficiently detailed results.

7.3 CASE 3: Effect of Solar Load

Two cases will be investigated. The first one, Case 3.1, will be treated as a steady state case, while the second simulation, Case 3.2 will be performed as a transient case. The outdoor conditions represents the weather during the autumn season, with outdoor temperature set to about $T_{outdoor}=14^{\circ}\text{C}$. High solar load effects are assumed, and used to study the risk level for overheating during slightly cooler weather (not summer conditions).

7.3.1 Input values for Case 3

All three models (viscous, energy and radiation) are included in the simulations, and the settings listed in Table 6.4 are used. The S2S radiation model is the chosen radiation model.

Material properties

The material properties for both the solids and the fluid are found in Table B.1. An operational temperature of $T=20^{\circ}\text{C}$ determines the air properties. The south window thermal conductivity set to 0.0621 W/m-K . The wood wall thickness is set to 0.5 m , when defining the boundary conditions.

Boundary conditions

The window surfaces that are adjacent to the indoor fluid uses a coupled boundary condition. The same goes for the surfaces' shadow walls. The internal emissivity specified for this boundary condition is listed in Table 7.4. The window surfaces that are adjacent to the outer domain are given mixed thermal boundary conditions where the B.C. specifications are given in Table 7.4. Mixed thermal boundary conditions are also defined for the walls.

Table 7.4: Case 3 - Thermal condition specifications

Specification	Value
Heat Transfer Coefficient	25 W/m-K
Free Stream Temperature	287 K
External Emissivity	
Glass	0.9
Wood	0.82
External Radiation Temperature	287 K
Internal Emissivity	
Glass	0.9
Wood	0.82

The floor heating is set to 20 W/m^2 . The supply vent boundary conditions to the bedrooms and the living room are given in Table 6.1. The supply temperature is set to 19°C . The extraction vents at the bathroom and kitchen are set as outflow. The flow rate weighting being 0.60187 and 0.39813, respectively.

The solar load model uses solar ray tracing, and the input values selected in the solar calculator for Case 3 are listed Table 7.5. The sun direction vector, and the direct and diffuse solar irradiation parameters are computed from the solar calculator.

Table 7.5: Case 3 - Input values for the solar load model

Solar calculator		
Global position	Long. (deg)	10.422
	Lat.(deg)	63.449
	Timezone (+GMT)	1
Mesh orientation	North	(1,0,0)
	East	(0,0,1)
Solar irradiation method	Fair weather conditions	
Sunshine factor	1	
Starting date and time	Day of year	21.09
	Time of day	13.00

Method

The solution method used for Case 3 is given in Table 6.4. Both a steady state and a transient run will be investigated. For the steady state, a pseudo time step of $1\text{e-}05 \text{ s}$ will be defined at the beginning of the simulation run. For the transient simulation, an adaptive time step of $1\text{e-}05 \text{ s}$ is set. The parameters are updated every 25 time step. The maximum number of iterations per time step is defined as 20, and a new time step calculation is automatically started when the previous iteration reach a convergence criteria of $1\text{e-}03$ for the continuity residual, velocity residuals and turbulence residuals, and $1\text{e-}06$ for the energy residual.

7.3.2 Data extraction

The planes introduced in Table 6.7 for Case 2.2 will also be used in Case 3. Temperature contour plots are used to investigate the air temperature distribution inside the building, and it will be used to compare the simulated cases.

7.3.3 Case 3 The simulation results

Case 3.1 - Temperature contours

A steady state was assumed for Case 3.1. The case was simulated until the residuals of the simulation reached a stable solution. Figure 7.5-7.7 shows the temperature distribution inside the building for the steady-state simulation, when solar load model is included in the setup and simulation.

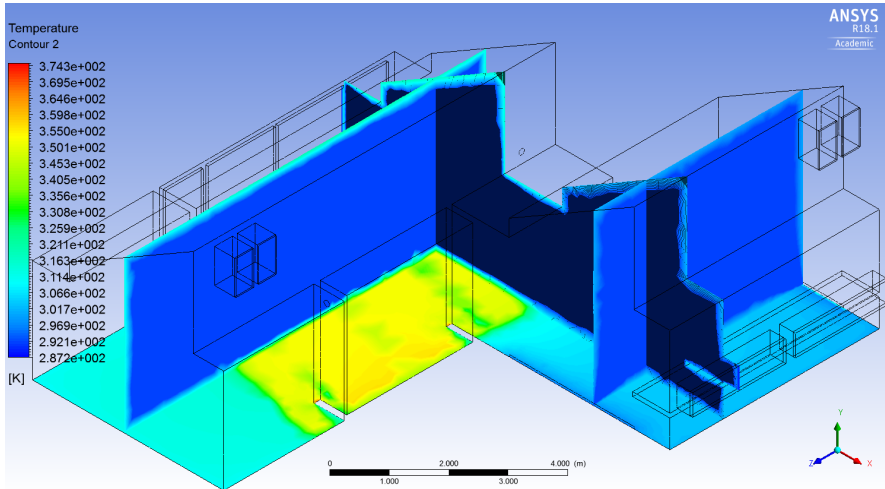


Figure 7.5: Case 3.1 - Temperature contours (steady state)

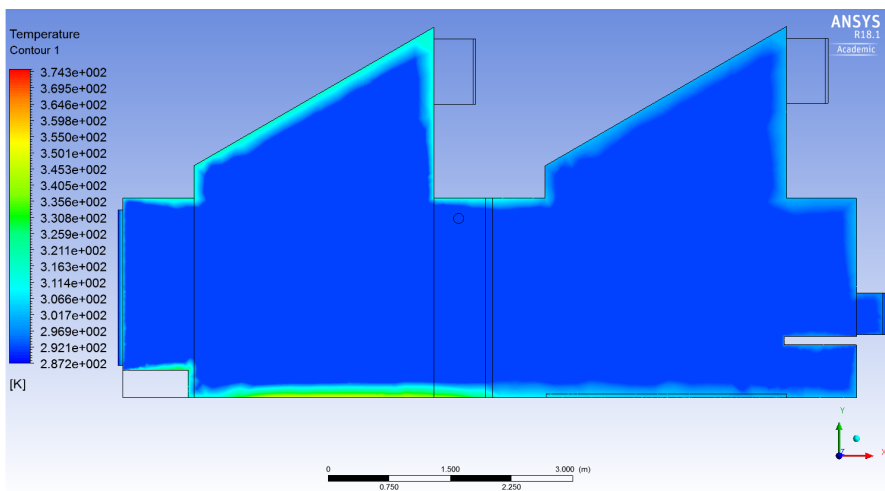


Figure 7.6: Case 3.1 - Temperature contour, plane 1 (steady state)

The high temperatures (in Figure 7.5) located on the living room floor are a result of solar radiation that enters the CFD model through the south windows.

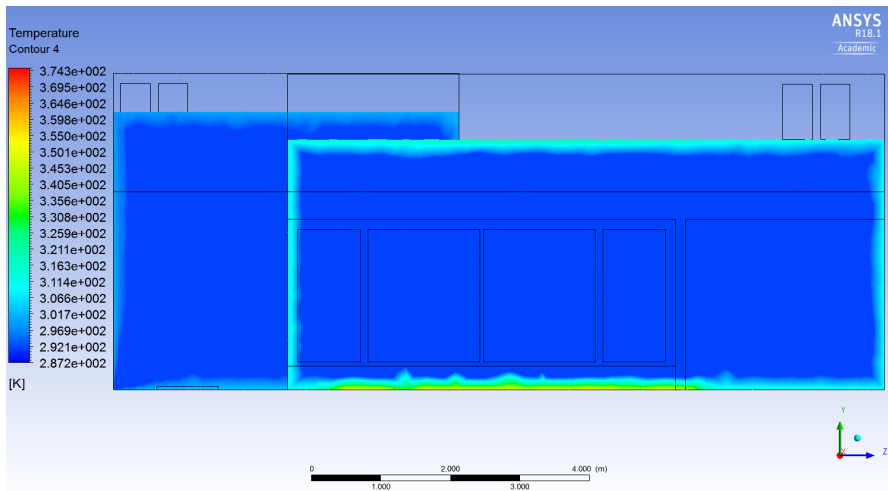


Figure 7.7: Case 3.1 - Temperature contours, viewed from the south (steady state)

In Figure 7.6 and Figure 7.7, the temperature distribution inside the building are more easily described. Most of the air maintain a temperature of 292 K. However, there seems to be a larger accumulation of warmer air close to the ceiling and along the walls, compared with the solutions in Case 2. The lowest temperatures are found at the outer window surfaces, with a temperature equivalent to the free stream temperature $T=287$ K. The conductive heat transfer over the windows at the south and north facade of Case 3.1 are illustrated in Figure 7.8.

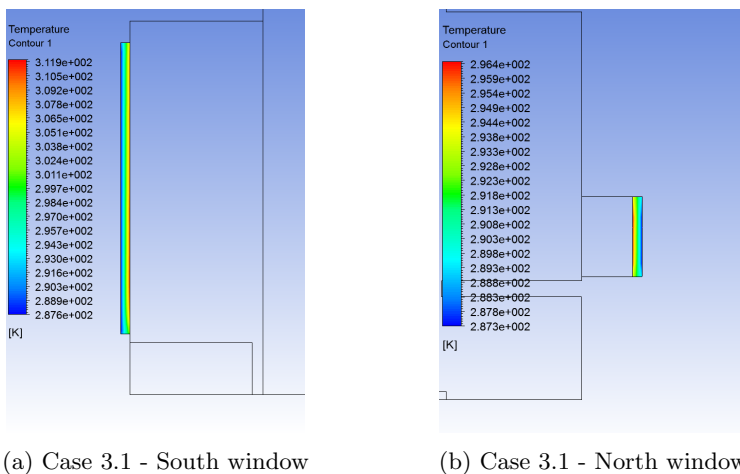


Figure 7.8: Case 3.1 - Heat conduction over the solid windows

Case 3.2 - Temperature contours

In Case 3.2, a transient simulation was performed. The simulation was stopped after the solution had reached a time of 21 s. A transient simulation was performed to see how much the simulated solution is affected by a steady-state assumption. Temperature contours of two different times ($t_1=10.4471$ s and $t_2=20.4761$ s) will be used to compare the development of the air temperature and flow inside the building for the transient simulation. Figure 7.9-7.11 shows the temperature distribution of these two simulated times.

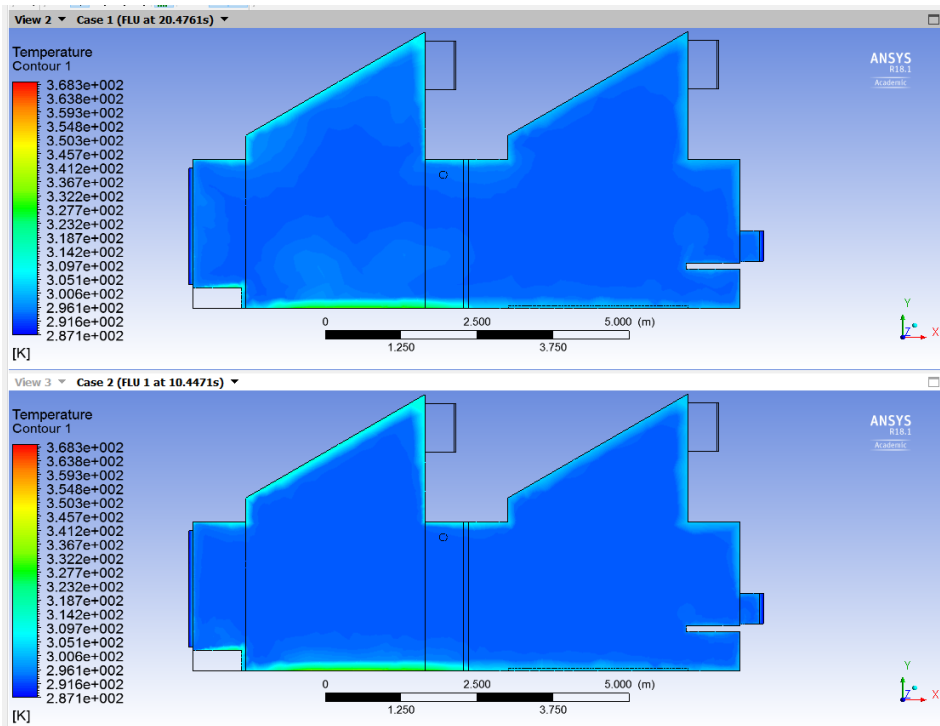


Figure 7.9: Case 3.2 - Temperature contours, plane 1 (transient, $t_1=10.4471$ s and $t_2=20.4761$ s)

From the contour plots shown in Figure 7.9 and Figure 7.10, it can be seen that the air temperature distribution inside the building is dependent on time. Already at $t=10.4471$ s (the illustrations at the bottom of both Figure 7.9 and Figure 7.10), the temperature of the indoor air increases as a result to the solar radiation. The air around the living room floor is heated up to a much larger degree than what is the case for the steady-state simulation performed for Case 3.1. This is depicted as the lighter blue colors that gradually moves upwards in the room. At $t=20.4761$ s, the air temperature has continued to increase. The temperature distribution shows that there are multiple locations where, at a height of 1 m above the floor,

the temperature has reaches the an indoor air temperature of up to 294.5 K. The transient simulation gave solutions for more than just the presented times in Figure 7.9-7.11. For the total transient simulation time of 21 s, the solution trend showed that the indoor air temperatures increased for each new time. If the transient simulation was allowed to continue for a longer period of time (longer than 21 s), based on the solution trend, it is assumed that the risk of experiencing overheating inside the building would be high.

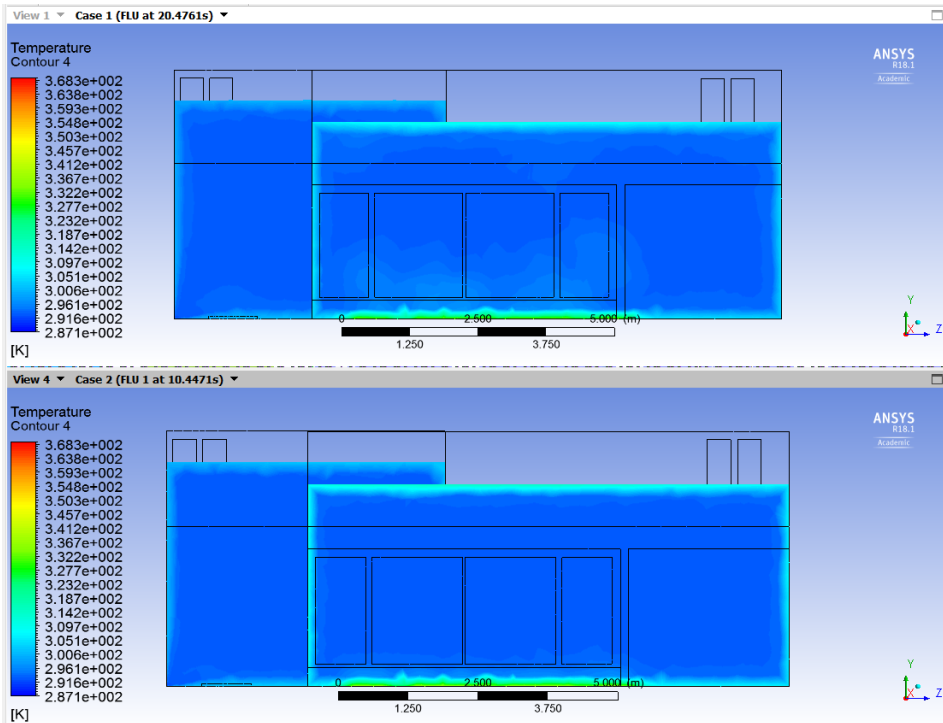


Figure 7.10: Case 3.2 - Temperature contours, viewed from south (transient, $t_1=10.4471s$ and $t_2=20.4761s$)

In Figure 7.11, the two bottom contours illustrates the temperature distribution for $t=10.4471s$ and the two top contours represent the temperature distribution in the building at $t=20.4761s$. Similar to the steady case, the air close to the ceiling and along the walls experience an temperature increase. This is made more clearly in Figure 7.9 and Figure 7.10. The contribution of solar radiation heat transfer is visible on the living room floor, presented with a yellow-green color.

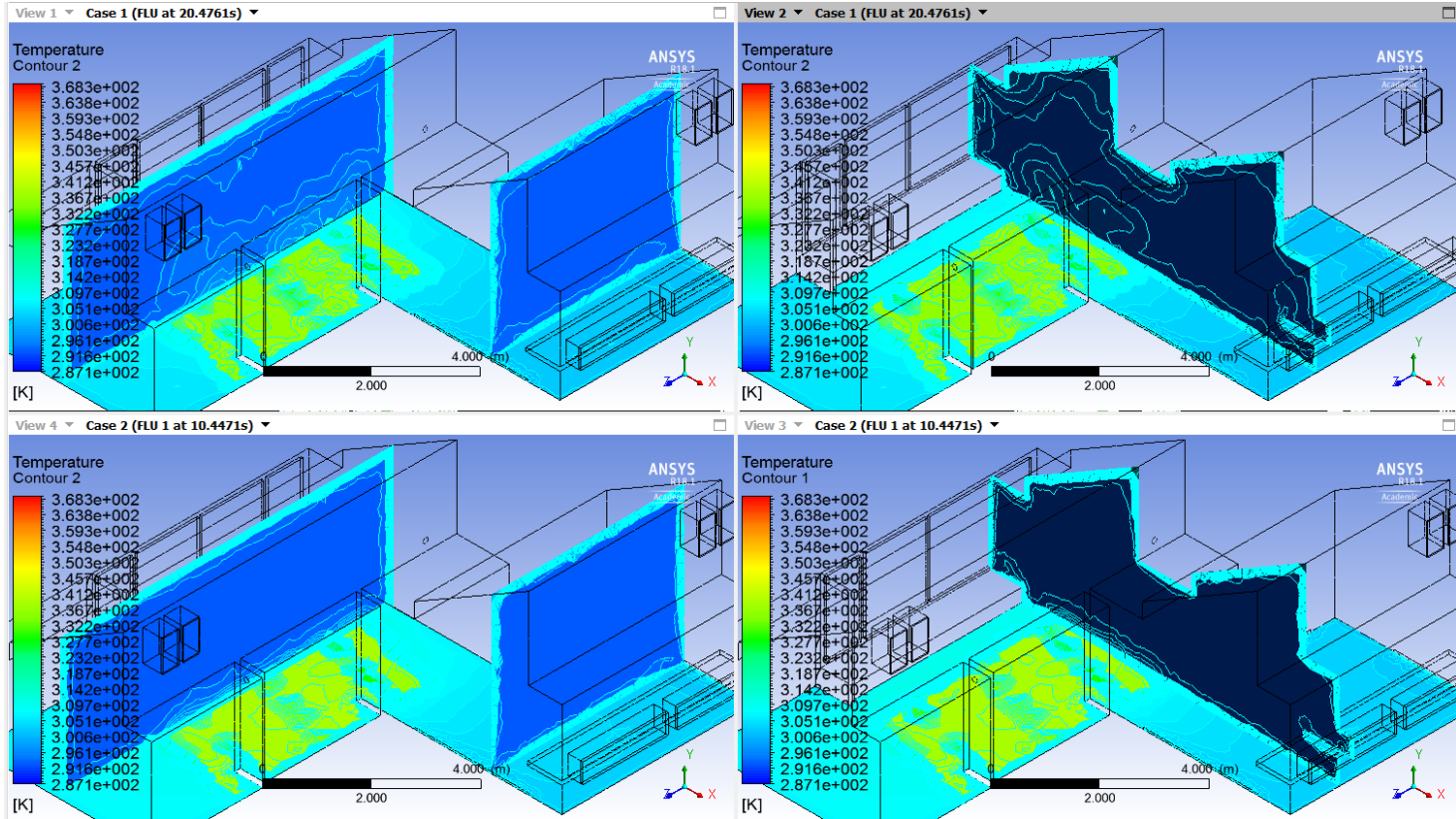


Figure 7.11: Case 3.2 - Temperature contours (transient, $t_1=10.4471s$ and $t_2=20.4761s$)

Flux reports

The mass balance for both the steady-state simulation and the transient simulation is conserved. Figure 7.12 gives the flux report for the mass flow rate.

"Flux Report"		"Flux Report"	
Mass Flow Rate	(kg/s)	Mass Flow Rate	(kg/s)
inlet_large_bedroom	0.017405833	inlet_large_bedroom	0.017405833
inlet_livingroom	0.0085380951	inlet_livingroom	0.0085380951
inlet_small_bedroom	0.017404056	inlet_small_bedroom	0.017404056
interior-indoor_fluid	0.0019067934	interior-indoor_fluid	-0.71577225
outlet_bathroom	-0.026089851	outlet_bathroom	-0.026089851
outlet_kitchen	-0.017258133	outlet_kitchen	-0.017258133
Net	0	Net	1.0408341e-17

(a) Case 3.1 (Steady-state)

(b) Case 3.2 (Transient)

Figure 7.12: Case 3 - Flux Reports, Mass Flow Rate

Both of the cases report a heat surplus, which is in accordance with previous simulations, and confirm the presence of overheating risks in the building.

7.3.4 Case 3 Comment on the presented results

The addition of a solar load to the simulations, shows that the indoor air increases in temperature, compared with for example Case 2.2. The transient simulation shows that there is a risk for overheating, even when the weather outside is not that warm. The different outcomes for Case 3.1 and Case 3.2 shows that a steady-state assumption will not be appropriate to use when validating the CFD model with full-scale experimental results, because the simulation does not indicate any risk of overheating and the measurements that shall be compared with the full-scale data should be time-dependent. When ventilative cooling is used, it is of interest to know what the temperature and velocity of the air inside the room is at different times, so that optimal control solutions may be put into place, while keeping the thermal comfort of the occupants a priority.

A steady state assumption might be used to investigate risk of thermal discomfort for cases where really small window openings are used to supply the building with cool air (the equivalent amount to the heat surplus), so that the indoor air maintains a stable temperature.

Model C

Model C is the final model used to carry out simulations. The model is a continuation of Model A and B, where the geometry of the double-skin south window is included. The design of the double-skin window is meant to reduce heat loss from inside the building, avoid condensation on both sides on the exterior glass, and be a part of the building's cooling strategy [Woods and Samdal, 2017]. Model C will run simulations, investigating flow situations where ventilative cooling is carried out, and the solutions will be compared with experimental measurements obtained from [Blandkjenn, 2017]. The model is illustrated in Figure 8.1.

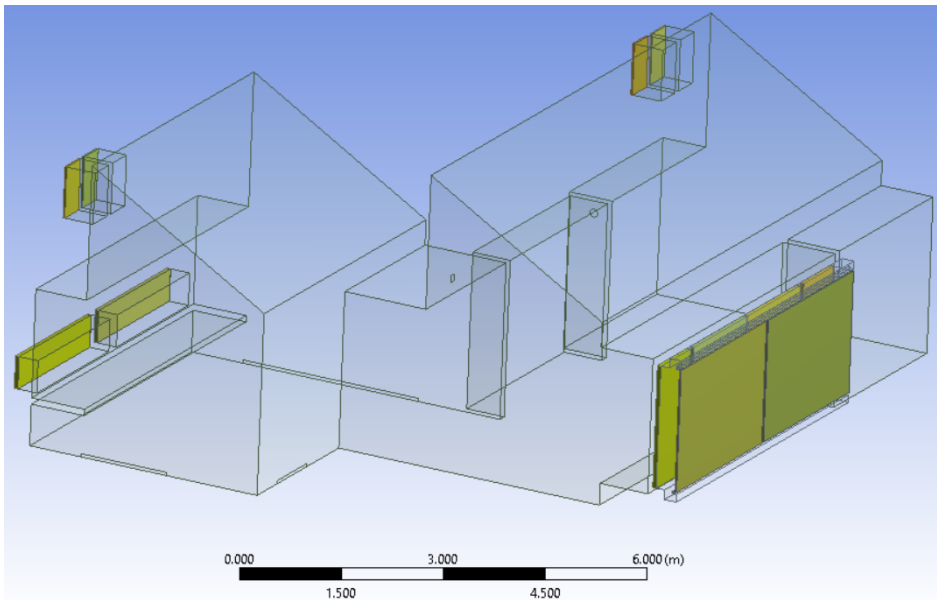


Figure 8.1: Model C geometry

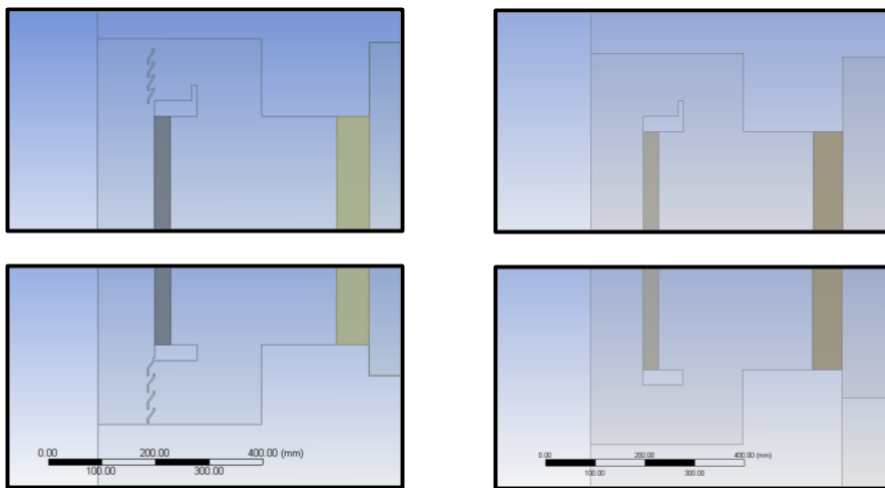
8.1 General Info About the Model

Because of time constraints, only ventilative cooling with the north window will be investigated.

8.1.1 South window

The double-skin window located on the south facade of the facility have been specially designed for the Living Lab building. The low U-value for the window depends on the airflow between the outer and inner surfaces, ranging from 0.65-0.69 $\text{W}/\text{m}^2\text{-K}$ (see Table 4.2). The ventilation rate is affected by the geometry of the inlet and outlet grills (illustrated in Figure 8.2a). The design of the grills, however, increases the required number of mesh elements around the inlets and outlets of the window.

It is assumed that making simplifications to the grill-design will have minimal effect on the flow calculations when ventilative cooling is carried out with the north windows and the skylight windows. The simplified design is shown in Figure 8.2b. For ventilative cooling with the south window, special consideration to the inlet boundary condition might be necessary (i.e. setting slightly lower velocity magnitudes at the inlet to compensate for the removed grills that would cause flow resistance). Figure 8.2 shows the simplification made to the CFD model.



(a) Grill design of the south window from the side (b) Simplified south window from the side

Figure 8.2: South window cross section. The two illustrations at the bottom show the inlet geometry, as the air will enter at the bottom of the window, heat up and exit through the top opening (the two top illustrations).

8.1.2 Skylight windows

The simplified geometry of the skylight windows mentioned in Section 6.2 is still valid for Model C. The surface area of the skylight windows have been reduced from 0.584 m^2 to 0.338 m^2 . The reason for doing this, is connected to another simplification made to the windows - the windows opening method. The opening method for all the skylight windows have been simplified. When the windows are used for ventilative cooling, they are opened to their maximum capacity. This was measured to be 0.338 m^2 opening area [Blandkjenn, 2017]. Instead of rotating the windows to achieve this opening area, the CFD model have been simplified so that each of the skylight windows have a surface area of 0.338 m^2 . Therefore, when one of the skylight windows will be open, the glass will simply be removed from the model and the surface that originally was the outer window surface will act as an outlet with a defined boundary condition. This is discussed further in Appendix C.1. The simplification reduces the required number of elements greatly, avoiding sharp angles with the open windows and the walls, which will happen with an open pivot window.

8.1.3 North windows

The simplifications done to the north windows include geometry simplifications (e.g. ignoring frame details) and opening mechanism simplifications (to reduce the occurrence of small angles). A top hung windows will normally allow air to pass through both under and over the open window. This is illustrated in Figure C.2 in Appendix C. For the CFD model, when one of the windows are opened, the air will only be allowed to enter the indoor environment through the sides and under the window (see Figure C.3). The opening areas used in the experiments of [Blandkjenn, 2017] for the north windows were 25% and 50% of the maximum opening surface area of 0.786 m^2 [Blandkjenn, 2017]. The angles the windows will need to rotate to obtain surface areas of 25% and 50% of maximum opening area have been calculated in Appendix C and are given in Table C.1.

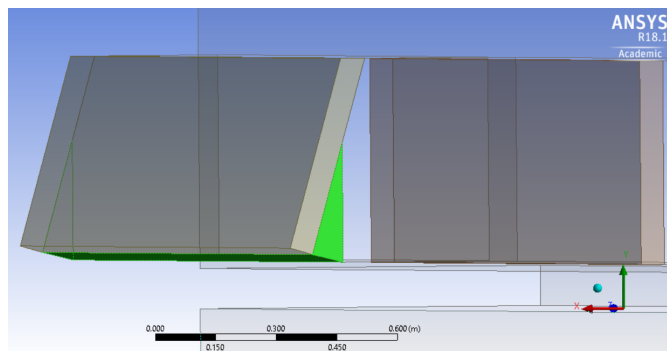


Figure 8.3: North window open - New boundary surfaces

As the window is rotated, new boundary surfaces are created so that cooler outdoor air may enter the office area in the CFD domain. These surfaces are highlighted in green in Figure 8.3, and require appropriately defined boundary conditions to recreate and match the flow pattern inside the building facility.

The thickness and thermal conductivity properties for the windows are the same as for Model B (see Table 7.1).

8.2 CASE 4: Ventilative Cooling with the North Window

The CFD simulation is set up, so that the solution may be compared with measurements obtained from full-scale experiments. For Case 4, the kitchen skylight window (east) will be 100% open and the north office window (east) will be 25% open. From Table C.1, this means that the north window must be rotated with an angle of 16°. Due to the window rotation, three new surfaces are created, where boundary conditions must be defined (illustrated in Figure 8.3).

8.2.1 Grid

A mesh was created for Model C, when the north window to the east is opened 25%, with the Mesh modul in Workbench. By choosing and defining different parameters under the sizing tab (information given in Table 8.1) the mesh achieved an acceptable quality, while keeping the mesh elements at a low number.

Table 8.1: Case 4 - Grid operations - Model C

Parameter	Alteration
Size function	Proximity and Curvature
Relevance center	Fine
Span Angle Center	Medium
	Curvature Normal Angle 78.30°
	Num Cells Across Gap 2
Proximity Size Function Sources	Faces and Edges
	Min Size 4e-03 m
	Proximiy Min Size 4e-03 m
	Max Face Size 0.25 m
	Max Tet Size 0.5 m
Minimum Edge Length	1e-02 m

All other operations kept the default settings. This produces the mesh illustrated in Figure 8.4-8.7.

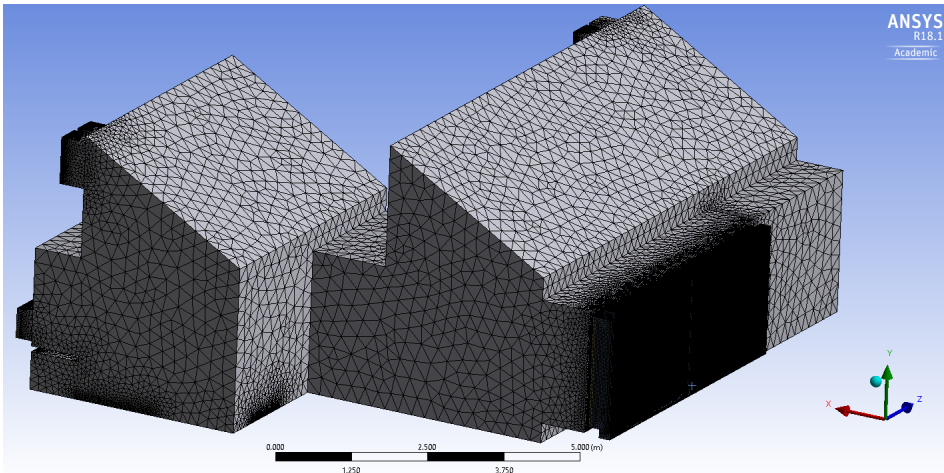


Figure 8.4: Mesh of Model C, north window 25%, viewed from south-west

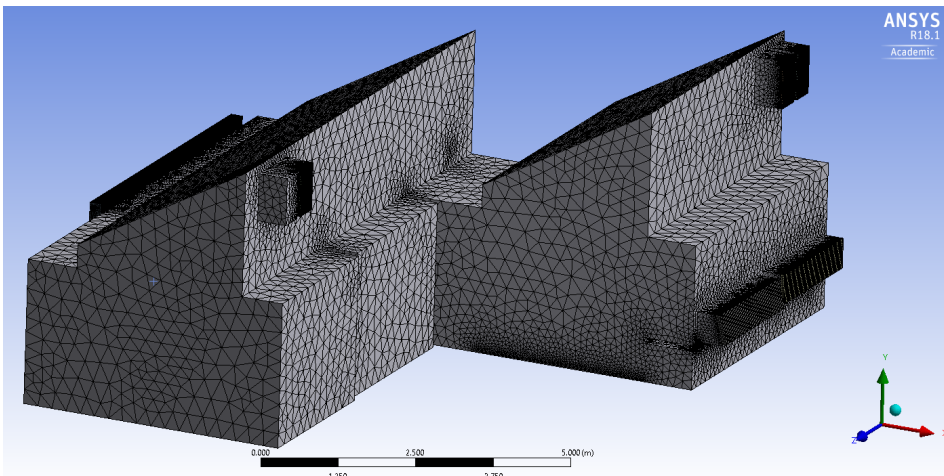


Figure 8.5: Mesh of Model C, north window 25%, viewed from north-east

The grid consist mostly of tetrahedron (fluid indoor) and hexahedron (solids and air gap) cell structures, with a few wedge cell structures (in the air gap of the double-skin window) and some pyramid cell structures (mainly around and on the window surfaces).

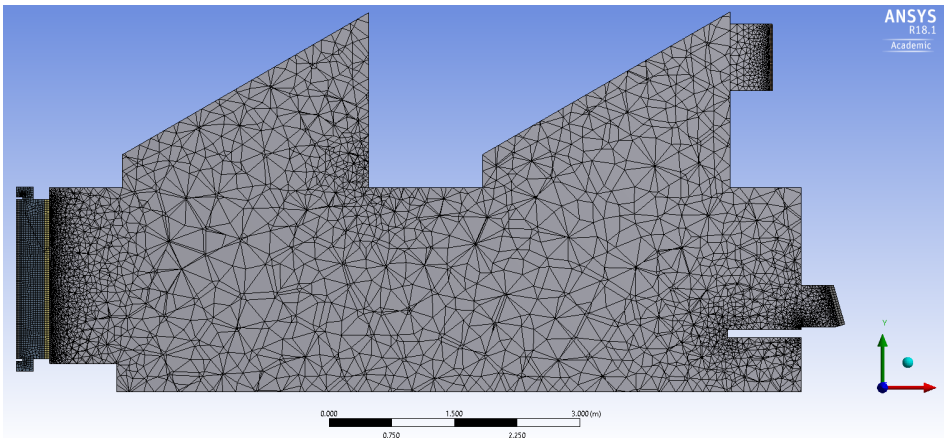


Figure 8.6: Mesh of Model C, north window 25%, cross-section

From the figures, the finer cell elements are located close to areas where the solid material are, where inlets and outlets are defined (the supply and extraction vent areas), and where the detailed geometry are close in proximity (like wall corners). Figure 8.6 shows how the cell elements are finest close to the walls and increase in size as the cells move toward the center of the model. Figure 8.7 gives a closer look at the mesh around the open north window.

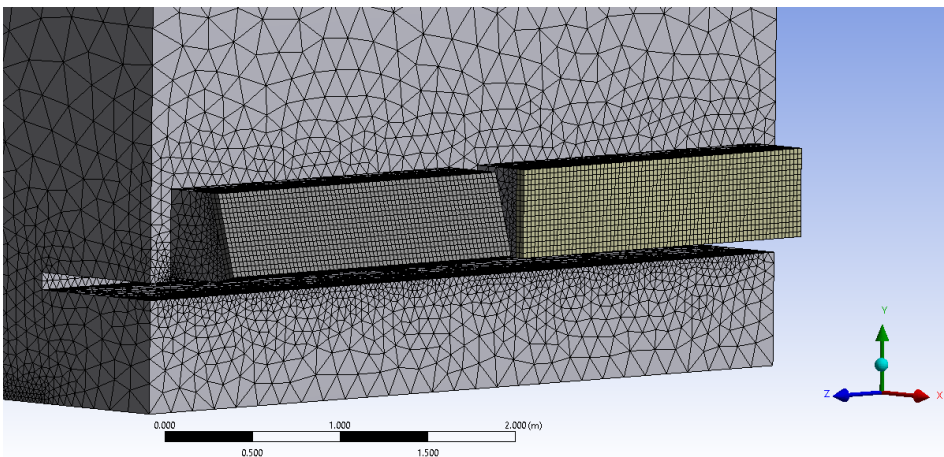


Figure 8.7: Mesh of Model C, north window 25%, details of the north window

The mesh statistics are given in Table 8.2.

Table 8.2: Case 4 - Mesh statistics - Model C

Statistics	Value	Comment
Elements	1611324	The number of elements for the model is neither particularly low or high. It is higher than for both Model A and B. The computational cost is medium low.
Aspect ratio	Min. 1.0003 Max. 9.6773 Avg. 1.7481	The mesh quality is good in regard to aspect ratio.
Skewness	Min. 1.2717e-5 Max. 0.83913 Avg. 0.1918	Maximum skewness is well below the value of 1, and most of the cells are only slightly skewed. The quality is good in regard to skewness.
Orthogonal quality	Min. 0.16087 Max. 1 Avg. 0.82282	Minimum value is well above the value of 0, and most of the cells are of good orthogonal quality. The quality is good in regard to orthogonal quality.

From the mesh statistics, the simulation should be able to run quite quickly, although the number of elements are over double the elements for Model A and Model B. Due to the increase in mesh elements, the aspect ratio, skewness and orthogonal quality in Model C (Case 4) is better than the meshes created for Model A and B. The mesh quality should be good enough for the simulation to calculate sufficiently detailed results

8.2.2 Input values for Case 4

The case is set up to match the conditions for when full-scale measurements were collected for ventilative cooling with 25% of the north window maximum opening area, on April 25th 2017 at 3pm. The outdoor and indoor conditions are measured with sensors and obtained from the Living Lab database. These are listed in Table 4.6. All three models (viscous, energy and radiation) are used in the simulation and the settings are listed in Table 6.4. The S2S radiation model is the chosen radiation model. Solar load effects are included and the solar calculator is used to define solar ray tracing properties.

The outdoor temperature at the north window was 6.45°C. Because of the slightly higher temperature measured at the weather station, an outdoor temperature of 7.85°C (281 K) is chosen as the free stream temperature and external radiation temperature for the simulation. The indoor temperature is taken as the average of all the temperatures measured in the office (six sensors), living room (six sensors) and kitchen (two sensors), and is calculated to be 16.8°C. The free stream

temperature and external radiation temperature set to the surfaces that share a wall with another room, are calculated by taking the average of the temperatures measured in the bedrooms (two sensors each) and bathroom (two sensors). The heat in the floor is off in the experiment. In the CFD simulation a small load is supplied (calculated to represent the internal heat loads such as technical equipment and lighting). The temperature of the supplied air from the mechanical ventilation system is set to 10°C. The global solar irradiance measured at 3pm was 593W/m², and the wind was blowing from the north west.

Material properties

Operational temperature is 10°C. Air properties are given by the operational temperature and are found in Table B.1. The properties for the south, north and skylight windows and the walls, floor and roof are also listed in Table B.1. The south windows are assumed to have a thermal conductivity of 0.0621 W/m-K. Because the thermal conductivity of the floor, walls and roof are so similar, and because of simplifications made to the CFD model in regards to *NameSelections* of the boundaries, only one wood material is created with thermal conductivity of $k=0.0525$ W/m-K.

Boundary conditions

The window surfaces that are adjacent to the indoor fluids uses a coupled boundary condition. The same goes for the surfaces' shadow walls. The internal emissivity specified for this boundary condition is listed in Table 8.3. The window surfaces and walls that are meant to be adjacent to the outer environment are given mixed thermal boundary conditions where the B.C. specifications are given in Table 8.3 (external surfaces values). Mixed thermal boundary conditions are also defined for the internal walls, i.e. walls that will experience heat transfer between two areas inside the building (internal surfaces values). The walls that the office and living room are sharing with the two bedrooms, the bathroom, and the entry are included in the internal surface definition.

The external walls are given a thickness of 0.5 m. The internal walls are given a thickness of 0.15 m.

The floor heating is set to 2.3 W/m². The actual floor heating is set to zero. The value of 2.3 W/m² is the sum of the constant heat loads listed in Table 4.3 and the divided by the total floor area.

$$\frac{[20\text{W (office)} + 90\text{W (kitchen)} + 15\text{W (living room)}]}{55\text{m}^2(\text{floor area CFD model})} = 2.3\text{W/m}^2$$

The supply vent boundary conditions to the bedrooms and the living room are given in Table 6.1. The supply temperature is set to 10°C. The extraction vents at the bathroom and kitchen are set as mass flow rate. The mass flow rates are given in Table 6.5.

Table 8.3: Case 4 - Thermal condition specifications

Specification	Value	Unit
Heat Transfer Coefficient		
External surfaces	25	W/m-K
Internal surfaces	7.69231	W/m-K
Free Stream Temperature		
External surfaces	281	K
Internal surfaces	289.9	K
External Emissivity		
Glass	0.9	-
Wood	0.82	-
External Radiation Temperature		
External surfaces	281	K
Internal surfaces	289.9	K
Internal Emissivity		
Glass	0.9	-
Wood	0.82	-

The solar load model uses solar ray tracing, and the input values selected in the solar calculator for Case 4 are listed in Table 8.4. The sun direction vector, and the direct and diffuse solar irradiation parameters are computed from the solar calculator. The sunshine factor is set to give a solar irradiation close to the measured value from the Living Lab Database, listed in Table 4.6. The GMT is set to +2, because of summer time.

Table 8.4: Case 4 - Input values for the solar load model

Solar calculator		
Global position	Long. (deg)	10.422
	Lat.(deg)	63.449
	Timezone (+GMT)	2
Mesh orientation	North	(1,0,0)
	East	(0,0,1)
Solar irradiation method	Fair weather conditions	
Sunshine factor	0.7	
Starting date and time	Day of year	25.04
	Time of day	15.00

The inlet at the south window is defined as a velocity inlet, where the velocity is set to 0.1 m/s and the temperature is the outdoor temperature of 281 K. The outlet for the south window is defined as a zero pressure outlet with back flow temperature

set to 281 K. The kitchen skylight outlet is also set to zero pressure outlet with back flow temperature set to 281 K. For the north window inlets, the two surfaces on each side are defined as zero static pressure inlets with a total temperature set to 281 K. For the bottom inlet surface, both pressure inlet and velocity inlet boundary conditions are defined. Most of the literature studying CFD problems where wind is present, usually include an outer flow domain to account for the generated pressure and velocity distributions around the building facility. Due to wind effects, the simplifications made to the geometry of Model C makes defining the correct boundary condition for the inlet at the north window really difficult. Different inlets are therefore compared with each other and the experimental data to see how the defined inlet parameters affect the flow calculations. Table 8.5 gives an overview of the inlet types and computational parameters set for this boundary.

Table 8.5: Case 4 - Boundary conditions for the north window

Case 4.	Boundary Condition	Parameters
1	Pressure Inlet	Total Pressure 0 Pa Total Temperature 281 K
2	Velocity Inlet	Components $x = -0.05$ m/s $y = 0.07$ m/s Temperature 281 K
3	Pressure Inlet	Total Pressure 0 Pa Total Temperature 281 K
4*	Pressure Inlet	Total Pressure 0 Pa Total Temperature 287 K
5	Velocity Inlet	Components $x = -0.1$ m/s $y = 0.14$ m/s Temperature 281 K
6**	Pressure Inlet	Total Pressure 0 Pa Total Temperature 281 K
7	Velocity Inlet	Components $x = -0.075$ m/s $y = 0.105$ m/s Temperature 281 K

* Case 4.4 simulates for a case where indoor temperatures exceeds 24°C.

** Case 4.6 operates with an indoor air temperature of 288.5 K (not 290K)

Case 4.4 simulates for a real situation when the indoor temperature exceeds 24°C (the critical temperature found in [Kirkøen, 2015], see Section 2.4), and cooling is required. The floor heating is on (20W/m²-K), and the supply air temperature is set to 19°C. Following the conclusion of [Blandkjenn, 2017], the temperature difference between indoor and outdoor should not exceed $\Delta T < 10^\circ\text{C}$, for window openings equal to 25% of maximum opening area. The outdoor temperature is set to 290 K, the indoor start temperature set to 297 K and for the mixed conditions of the internal walls, the temperatures are equal to 295 K. The rest of the setup

is identical to the other cases. In Case 4.6, a slightly lower indoor air temperature (288.5 K) was used in the simulation, to see whether the indoor air temperature collected and calculated with data from the Living Lab was done correctly.

Method

The solution method used for Case 4 is given in Table 6.4. A transient run will be investigated. An adaptive time step starting on 1e-04 s is set. The parameters are updated every 16 time step, with a maximum time step size of 0.125 s to ensure updates every two seconds. The maximum number of iterations per time step is defined as 20, and a new time step calculation is automatically started when the previous iteration reach a convergence criteria of 1e-03 for the continuity residual, velocity residuals and turbulence residuals, and 1e-06 for the energy residual.

8.2.3 Data extraction

Measurement locations for the simulation

In Section 4.2 it was explained that the simulation solution will mainly be compare with data obtained from three points, located at a distance of approximately one meter from the window, at three different heights. These three points are found in Table 8.6. The other locations where temperature and velocities were measured in the full-scale experiment are found in Table B.2, in Appendix B. Table 8.6 gives the coordinates of the points used to compare the CFD model with full-scale measurements, while Table B.2 gives the coordinates for all the locations the full-scale experiments collected data from at the north window.

Table 8.6: Case 4 - North window measurement points (in coordinates)

Point location		Coordinates		
		x (m)	y (m)	z (m)
B	1	3.138	0.800	3.705
	2	3.138	1.050	3.705
	3	3.138	1.300	3.705

The temperatures and velocities will be placed into plots, to be compared with the experimental data. When comparing experimental results with Case 4.4, the temperature difference between the indoor and outdoor environment will be subtracted from the temperatures predicted in Case 4.4. It is the temperature difference that is the main force that drives the air flow, which makes this assumption fine to use. The simulated velocity require no form of adaptation to be compared with the other simulated solutions and full-scale experiments.

8.2.4 Case 4: The simulation results

The simulation results are presented for each of the point locations. The obtained data are placed into plots, and the results of the different boundary conditions are briefly discussed for each point. A more thorough discussion of the results is found in Chapter 9.

Collected data from point B1

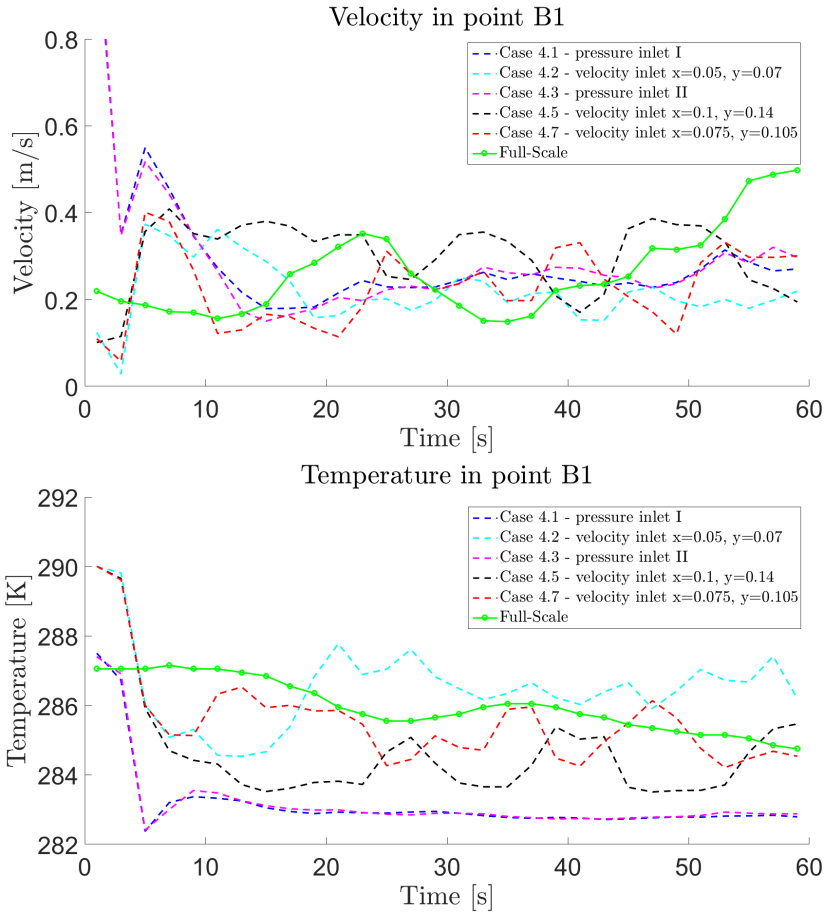


Figure 8.8: Plots of velocity and temperature data over 60 seconds at point B1

Figure 8.8 shows the simulated results for Case 4.1-4.3, 4.5 and 4.7 compared to the experimental data (light green color) measured in point B1. From the velocity profiles, all the simulated cases show similar trends in magnitude, after almost 20 seconds. The velocity inlet cases behaves in a more similar manner to the full-scale measurements, with an oscillating pattern. This is especially the case for Case 4.5

and 4.7. The pressure inlet cases keeps a more stable pattern. The temperature plot indicates that velocity inlet boundary conditions gives more similar solutions to the full-scale measurements, compared to the cases with pressure inlet boundary conditions. With the pressure inlet cases, the measured temperatures in point B1 experience, after a few seconds, a large drop in the temperature and it remains stable over the entire sampling period of 60 seconds.

For the two cases that simulated for different set up conditions, Case 4.4 and Case 4.6, the results are presented in Figure 8.9 for point B1. To compare the results from Case 4.4, the obtained temperatures from the simulation will be subtracted by the temperature difference between the outdoor and indoor environment.

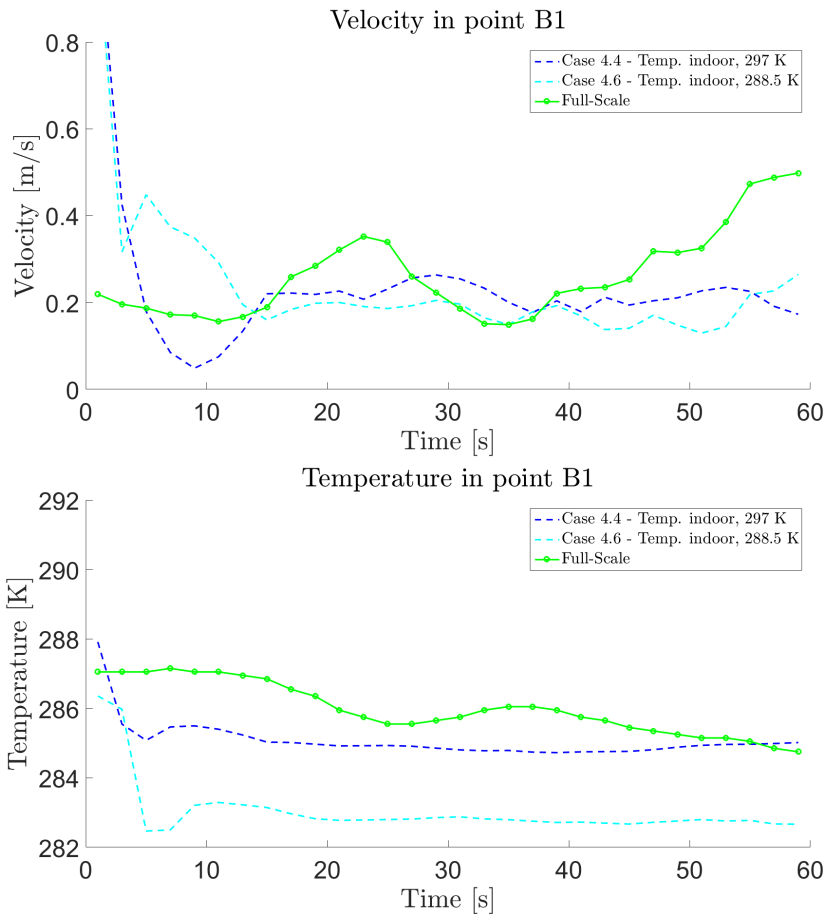


Figure 8.9: Plots of velocity and temperature data over 60 seconds at point B1

The plots show that both cases give quite good predictions for the flow in point B1.

Case 4.4 match the temperature profile really well, when compared with full-scale measurements. The cases that predicted the flow best in point B1 are Case 4.2, Case 4.4, Case 4.5 and Case 4.7.

Collected data from point B2

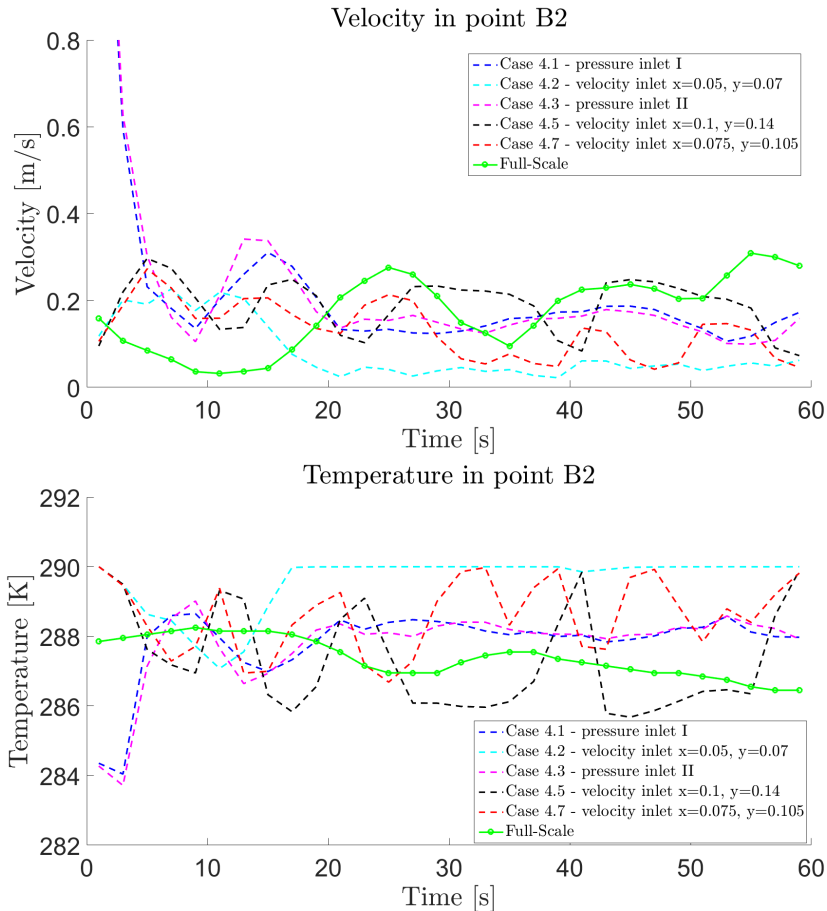


Figure 8.10: Plots of velocity and temperature data over 60 seconds at point B2

Figure 8.10 shows the simulated results for Case 4.1-4.3, 4.5 and 4.7 compared to the experimental data measured in point B2. From the velocity profiles, all the simulated cases do again show similar trends in magnitude, after almost 20 seconds. This time however, it is Case 4.2 that predicts the flow pattern with the largest deviation to the measured full-scale data. The velocity profile of Case 4.5 can be said to follow the flow pattern of the full-scale data better than the pressure inlet cases, but the solutions from Case 4.1 and 4.3 are not bad. Case 4.7 predicts velocities that are a little low. The temperature profiles substantiate that Case 4.2

has a problem with predicting the flow at point B2. The two pressure inlet cases are able to predict the temperature pattern fairly well, while Case 4.5 oscillates around the full-scale temperature data. Case 4.7 predicts the temperature well in the first sampling period (up to 25 sec) and then maintains a slightly higher temperature than the full-scale measurements for the remaining time period.

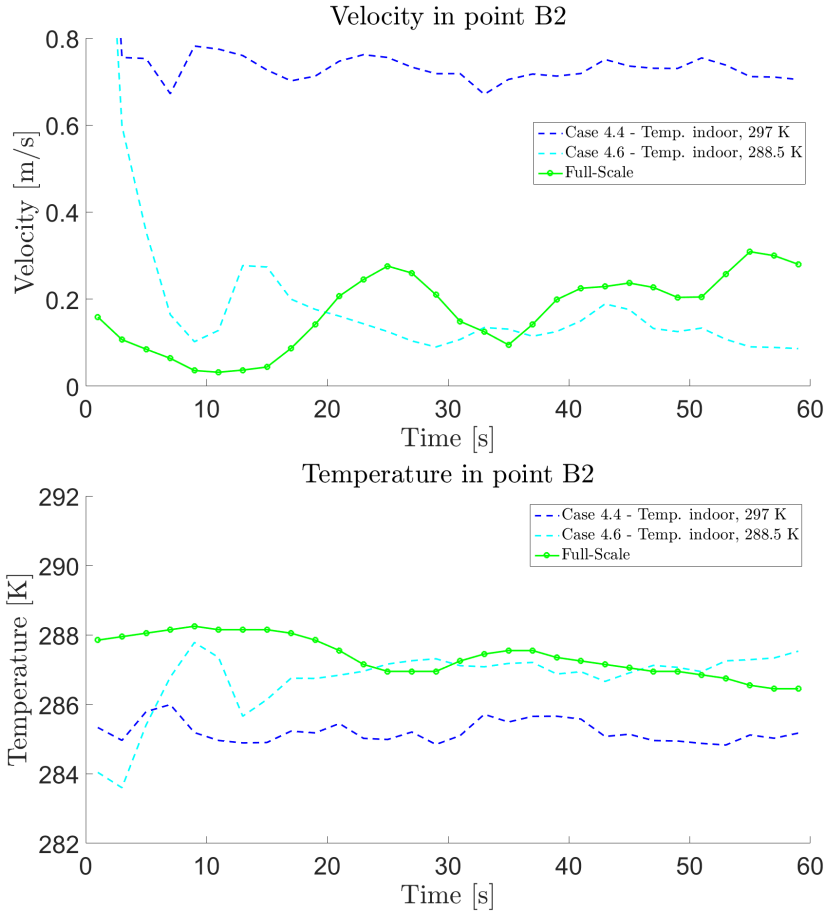


Figure 8.11: Plots of velocity and temperature data over 60 seconds at point B2

Figure 8.11 shows that Case 4.4 have trouble with predicting the velocity at point B2. The temperature data from Case 4.4 are also a little lower in this location, compared with full-scale measurements obtained during the sampling period. Case 4.6 manage to predict the flow well at point B2. The cases that predicted the flow best at point B2 are Case 4.1, Case 4.3, Case 4.5, and Case 4.6.

Collected data from point B3

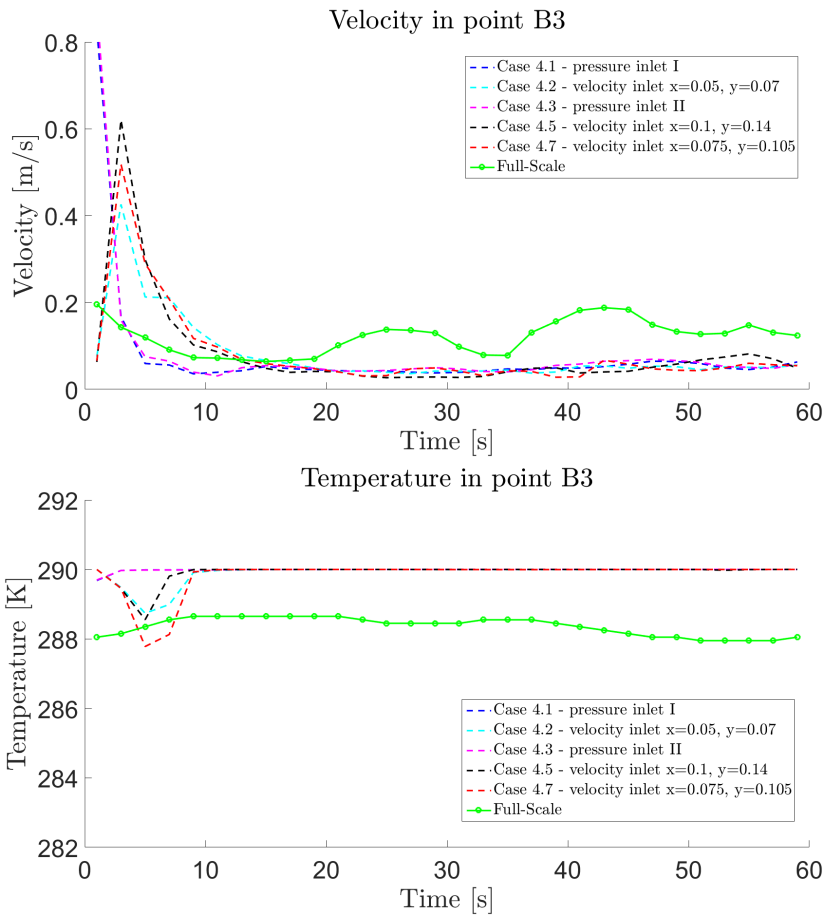


Figure 8.12: Plots of velocity and temperature data over 60 seconds at point B3

Figure 8.12 shows the simulated results for Case 4.1-4.3, 4.5 and 4.7 compared to the experimental data measured in point B3. In both of the plots, the simulated cases are similarly good at predicting the flow pattern of velocity and temperature, when compared to the full-scale data. The velocity profile of the simulations are not completely incorrect, although all the cases demonstrate quite high velocities in the first seconds and slightly lower velocities compared to the full-scale after approximately 15 seconds. The velocity inlet cases are the ones that are closest to correctly predict the temperature profile of the full-scale in point B3, with the short drop in temperature in the beginning of the sampling period. After this drop, all the simulations give the same flow predictions.

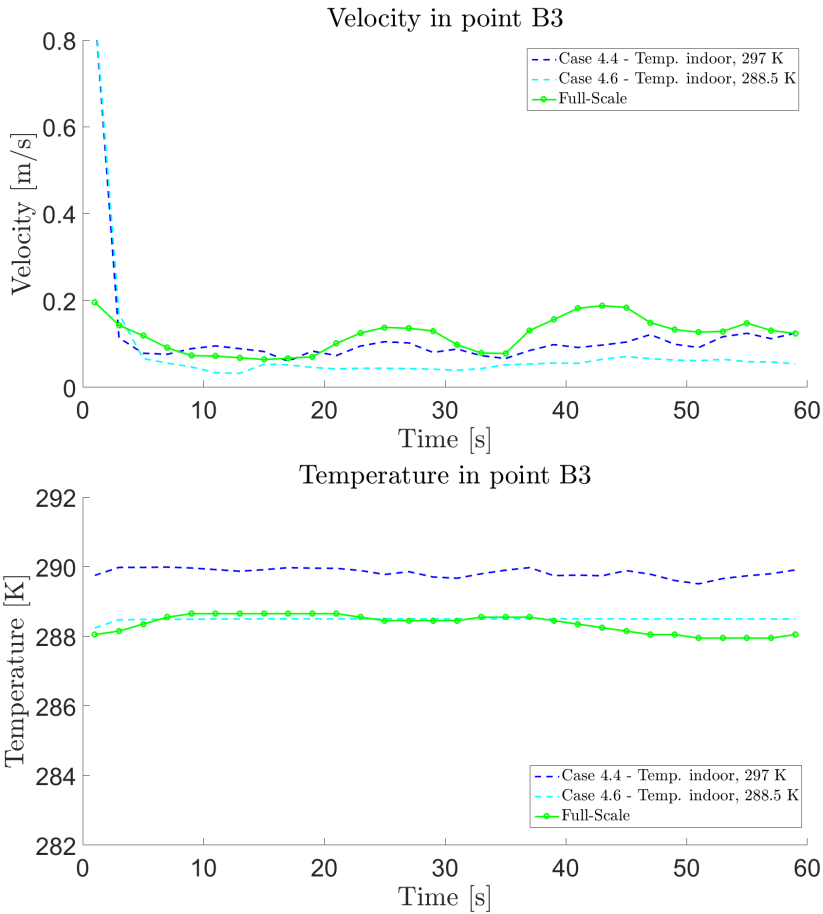


Figure 8.13: Plots of velocity and temperature data over 60 seconds at point B3

Figure 8.13 show that Case 4.4 and Case 4.6 are able to predict the flow well at point B3. Case 4.4 are closest of all the simulations to predict the velocity profile of the full-scale measurements. The velocity profile for Case 4.6 is quite similar to the simulations in Figure 8.12. Case 4.6 predicts the temperature really well at point B3, while Case 4.4 gives a slightly higher temperature compared with the full-scale. However, the temperature profile is similar to the other simulations. At point B3, all the cases predicts the flow pattern well, but the best might be Case 4.6.

8.2.5 Comment on the results

For point B1 it was generally the velocity inlet cases that performed best, although Case 4.4 did predict the flow well too. The pressure inlet cases varied only little for the velocity plot, but gave too low temperatures at point B1. At point B2, the solutions of Case 4.2 and Case 4.4 deviated by quite a lot, while the other cases differed only a little from the full-scale data. Case 4.5 and the three pressure inlet cases 4.1, 4.3 and 4.6 predicted the flow really well for B2. At the final point, B3, all the cases were again able to get solutions close to the experimental data. The velocity profile were extremely similar for most of the simulations, with the exception of Case 4.4 that predicted the flow better. Case 4.6 managed to predict the temperature profile best at point B3.

When considering all the presented results from the different cases, it is Case 4.5 that is able to predict the flow pattern most similar to the full-scale data. Although the simulation does not give exact results, it is the only case that avoid large deviations from the full-scale experiment at all the points for both the velocity profile and the temperature profile. Case 4.7 is also generally good at predicting the flow, but experience a larger discrepancy in the results at point B2, compared to Case 4.5.

The velocity inlets seems to perform better than the pressure inlets, which indicates that the wind direction and velocity affected the flow during the full-scale measurements, and should be considered for the CFD model. From Table 4.6 the wind velocity is given as 1.51 m/s, while the wind direction is given as 329.5° . This means that the wind is coming from the north-west, and generated pressure on the north facade will most likely increase the natural ventilation through the north window.

Discussion of the Model Simulations and Results

9.1 The CFD Investigations

9.1.1 Case 1

From Chapter 6, in Case 1 the mechanical ventilation system was simulated, and the setup used for the simulation was verified for further investigations. The velocity inlet and outflow boundary conditions worked well for the CFD simulation where conservation of mass was achieved for the setup. For the simulation that used mass flow as outlet boundary conditions, the conservation of mass was not achieved due to round off errors during the calculations of the boundary conditions of the mechanical system in Table 6.1. It was concluded that the outflow boundary condition worked well for the cases where the CFD domain was only subjected to the mechanical ventilation, while mass flow boundary conditions should be used at the extraction vents when ventilative cooling is investigated.

9.1.2 Case 2

The simplified model, in Chapter 6, continued the study by looking into the effects of temperature and radiation in Case 2. First an investigation on how the simulation results are affected by the choice of heat transfer coefficients was performed, where the results for two different values of heat transfer coefficients; one assuming that the wall boundary surfaces are coupled with the indoor environment, $h=7.69231 \text{ W/m}^2\text{-K}$, and one assuming that the wall boundary surfaces are coupled with the outdoor environment, $h=25 \text{ W/m}^2\text{-K}$. Both the simulated cases gave results without large differences. A comment was made on how the defined free stream temperature may cause wrong estimates on the heat transfer over the wall surfaces, being that the free stream temperature was defined as the outdoor

temperature, when certain walls should have operated with free stream temperatures equal to the inside environment. This will be discussed more in Section 9.2. The conclusion of the case was that both heat transfer coefficients could be used for future simulations, and give satisfying results, when considering the existing simplifications made to the model. However, by dividing up the wall surfaces into two groups, one consisting of the internal walls and the other consisting of the external walls, and then give these groups appropriate boundary conditions would be preferred.

Secondly, the choice of thermal boundary conditions for the walls are looked into. The simulations in Case 2.1 were performed with convection boundary conditions for the walls, while Case 2.2 used mixed thermal boundary conditions that include convection and radiation heat transfer over the walls. The radiation model used in Case 2.2 was Surface-to-Surface (S2S). From the temperature contours of Case 2.1 (convection only), really high temperatures could be observed on the floor of the CFD model, reaching a value of 318.6 K. The high temperatures are a result of poor heat transfer from the floor surface to the rest of the room. With the mixed boundary condition for the walls, in Case 2.2, better predictions of the temperature distribution was achieved, as the temperature registered on the floor was substantially lower with a value of 296.9 K. This is a temperature that falls under the recommended floor temperature condition that are perceived as acceptable for people wearing normal footwear [ANSI/ASHRAE, 2010]. Thus, the addition of radiation heat transfer gives a better prediction of the flow for the CFD model compared with only convection, and the mixed thermal boundary condition will be used for the walls in the following simulation setups.

9.1.3 Case 3

By including windows as solid geometries, the solar load effects could be properly investigated in Case 3 with Model B. The glass material was given conductive characteristics and the surfaces of the windows were defined as semi-transparent. All other walls remained opaque. Appropriate emissivities were set for the materials. The case simulated for both steady and transient conditions. Based on the temperature contours, both sub-cases showed tendencies with regards to increased temperatures in the indoor environment of the building. The results did however indicate that the assumption of a transient situation is more suitable for the circumstances investigated in this thesis. From the transient simulation with the solar loads included, it was concluded that the risk of overheating was present in the simulation model.

9.1.4 Case 4

The model in Chapter 8 are used to validate the computational parameters for Case 4. Ventilative cooling with the north window is investigated, where the air enters the building through the north window (25% of maximum opening area) and exits through one of the skylight windows in the kitchen (100% of maximum opening

area), causing a cross-flow ventilation to happen. Different boundary conditions at the north window surface are investigated, due to unknown effects of external wind and temperature differences between the indoor and outdoor environment. The case that was concluded to predict the flow most accurate was using a velocity inlet boundary condition, where the velocity in the x-direction and the y-direction were set to -0.1 m/s and 0.14 m/s, respectively. Based on all the simulated results, it was concluded that the presence of the wind around the building facility most likely have an effect on the flow inside the building. This means that the simplification of reducing the flow domain to only the building facility, will probably give wrong solutions, because understanding the flow field exactly at a boundary subjected to wind, is really difficult.

The CFD model can still be used for flow predictions and thermal comfort calculation, as long as the solution uncertainties connected to the model assumptions and model simplifications are acceptable for the user. Because the consequences of these choices remain unknown, it is difficult to fully commit to the results the simulations give. The appropriate thing to do before deciding upon the validity of the model would be to perform a set of parameter studies, to get a clearer understanding of how much the simulation setup may be affected by different settings. More simulations investigating the other locations (A and C-H) where the measurements were taken should also be carried out before any conclusion is made.

9.2 Sources of Error

For the performed simulations, the simplifications and assumptions made to the geometry, design, and setup of the models results in unknown levels of errors to the CFD predictions. Most of these have already been mentioned in the previous chapters, and they will in this section be discussed in relation to the simulation solutions and the full-scale measurements.

9.2.1 Sources of error that result in under- and over-estimating heat loss in the simulation

For the cases where only one heat transfer coefficient were used for the walls and roof, the free stream and external radiation temperatures were defined as the outdoor temperatures. This assumption caused the simulation to estimate higher heat losses over the solid materials, compared with the the actual building. This was improved in Case 4, when the wall were simulated as both external and internal. In the experimental facility, the mechanical ventilation is supplied in the bedrooms and in the living room. Here the air will be slightly heated up before it overflows to the office area. With the design simplification of moving the supply vents directly to the office in the CFD model, the air supplied to the office will be cooler than than for the facility. The simplification causes the simulation to overestimate the heat loss. Another simplification that overestimates the heat loss is connected to not including additional heat loads that are present in the building. By excluding

lighting and other electrical equipment, the simulation predicts a lower temperature in the indoor environment for the CFD model that is the case for the actual building. In Case 4, these internal heat loads were included, by applying them to the floor. The load used IDA ICE values from previous studies on Living Lab to determine the size. The material used in the CFD model (especially in regards to the walls, roof and floor) are not defined to store heat, and thermal mass is not included in the Fluent program. The properties of the material in ZEB Living Lab works in a way that the walls and other surfaces absorb and store heat energy, that is later released back to the building at night.

By not including other windows than the skylights, south and north windows, the required number of elements for the CFD model is kept low. However, the simplification leads to underestimation of the heat losses with the CFD simulations, because these areas are known to be heat sinks, when large heat transfers occurs between the warm indoor- and cold outdoor environment. When performing simulations in Fluent, air leakage will not be included in the calculations. This factor causes the simulated solution to underestimate the heat loss, compared with what is the situation for the building.

9.2.2 Sources of error related to the simulation setup and solution

From the investigation done in Case 4, in regards to defining appropriate boundary conditions at the north window, it was concluded that the CFD model would perform better if it included an outer domain in the simulation, due to wind-effects that were present during the full-scale experiment. Literature that have studied CFD situations where wind have been a part of the modelling, have usually used a CFD domain that combines the internal (building facade/room) and external (outdoor) environment. The simplification of making the CFD model only consist of the indoor environment was done to reduce the computational cost, because of resource limitations such as computer power and time. In hindsight, the simplification should probably not have been carried out, as the boundary condition investigation in Case 4 struggled to give acceptable simulation solutions that could match the full-scale measurements.

The geometry simplification made to the opening method for the north windows may have contributed to the measured deviations between the simulations and the experiment at location B. In ZEB Living Lab, the outdoor air is able to enter the indoor environment over the north window. From fluid theory, the air flow may either move down to the lower part of the window frame, due to differences in air densities arising from different air temperatures, or it may follow the upper part of the window frame, due to pressure gradients and presence of turbulence [Abu-Ghannam and Shaw, 1980]. If the air flow follows the surface of the upper

window frame, it may explain the discrepancies between the measured velocities and temperatures presented in Chapter 8. All the simulations predicted higher temperatures at point B3 compared with the experiment (except for Case 4.6 that simulated for a lower indoor air temperature). During most of the sampling period, the simulations also predicted lower velocities at this point than the experiment measured. Considering the fact that the CFD model do not offer the flow to pass over the open window, this might be the cause of the error.

To recreate a real life scenario in a simulation, it is crucial to properly understand the thermal conditions and to use this information correctly when the setup for the simulation is specified. The solar load calculator is used to define the applied amount of solar irradiation to the CFD model. The sunshine factor was reduced to achieve an irradiation close to the value given in Living Lab Database. However, it might be more appropriate to not use the solar calculator but rather put in the irradiation directly. The error due to this is unknown, as it might be zero or it might be significant. Other computational parameters that are available for the solar model might also give better modelling of the thermal outdoor conditions. Both the indoor and outdoor air temperatures were approximated for the simulation setup, by using the measured temperatures obtained by the sensors in Living Lab. The method for calculating these temperatures might not give accurate answers, still these possible errors are assumed to be small and acceptable.

In Subsection 4.3.1, uncertainties in regard to the accuracy of the measurements were mentioned, as it was discovered some damage to the measurement equipment. This discovery happened some time after the experiments were carried out, and it was unknown if the damage occurred before, during or after the experiments. The equipment was also not calibrated during the experiments. This may or may not be a reason for the deviation between the CFD results and the full-scale measurements presented in Subsection 8.2.4.

Parameter studies on different computational parameters such as turbulence models, grid independence, choice of solvers and convergence criteria were not performed, mainly due to time limitations. Literature [Ramponi and Blocken, 2012] strongly urge that this is something that should be investigated when trying to validate CFD models, because the solutions may vary greatly when different conditions are considered.

9.2.3 The assumed most dominant sources

Based on the results and the discussed sources of errors, the simulation results are assumed to be most affected by the geometrical simplifications of the domain size and the window opening method for the north window, and by not including appropriate parameter studies on computational parameters, to ensure that the model simulations are carried out with the correct setup.

Chapter 10

Thermal Comfort Investigation

In Chapter 8, Case 4.5 was concluded to give the best predictions of the flow, when the simulation results were compared with the full-scale data. In this chapter, the case will be used to explain how the data from the finished model may give information on the perceived thermal comfort inside the building.

10.1 Contours of Case 4.5

In Section 10.2 the method for calculating the percentage draught rate will be explained, and the risk of thermal discomfort due to this concern will be evaluated. The factors affecting the risk of draught are the local mean air velocity, the local air temperature, and the local turbulence intensity (see Eq.(2.6)). Because neither the local mean air velocity or the local air temperature are included in the CFD simulation results, a correction formula presented by Koskela et al. will be used to estimate for the local mean air velocity (V_o) and the local turbulence intensity (I_o) by utilizing the computed vector velocity (V_V) and turbulence kinetic energy (\bar{k}) [Koskela et al., 2001].

Plane 1 is defined in Table 6.7, and is used to investigate the flow development for Case 4.5 at time 15 s, 29 s, 45 s, and 59 s. Contour plots of the velocity, temperature and turbulent kinetic energy are presented in the following subsections. The combination of these variables determines if the perceived thermal environment is acceptable to the occupants or not. Too high velocities, too low temperatures and high values of turbulence kinetic energy are components that may increase the risk of draught.

10.1.1 Velocity contours at plane 1

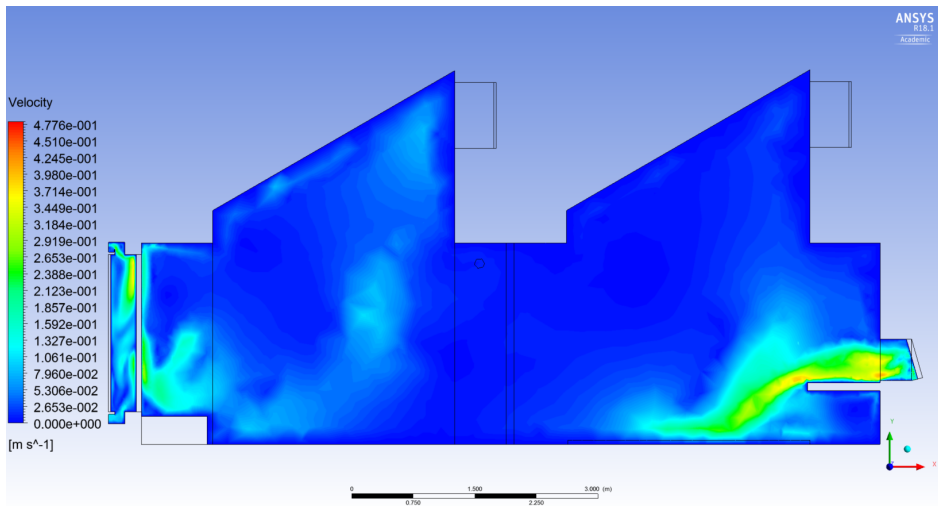


Figure 10.1: Case 4.5 - Velocity profile at t=15 s

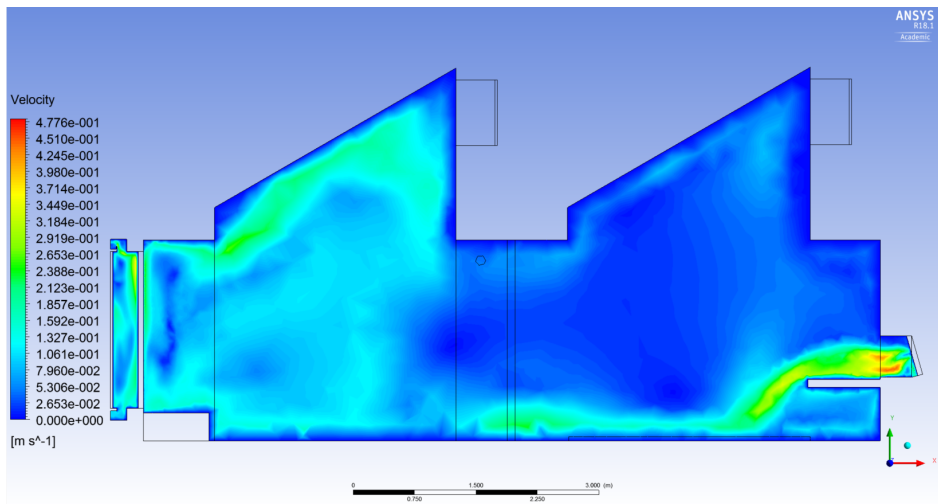


Figure 10.2: Case 4.5 - Velocity profile at t=29 s

The velocity profiles in Figure 10.1-10.4 show that applying ventilative cooling to the building will cause an air flow inside the facility. After 15 seconds (Figure 10.1), the velocity over the work station and around the sitting area of the work station are subjected to air with velocities reaching 0.4 m/s. Based on draught rate theory, these areas are at risk of experiencing thermal discomfort due to high

velocities. The final outcome are then dependent on the temperature difference between the outdoor and indoor environment. In Figure 10.2, after 29 seconds of applying ventilative cooling, the air velocities are reduced some around the edge of the work station. There seems to be more air movement along the floor of the building and in the living room area. The flow in the southern area of the building may be partly due to the solar irradiation that enters through the south window and contributes largely to the temperature increase in the living room.

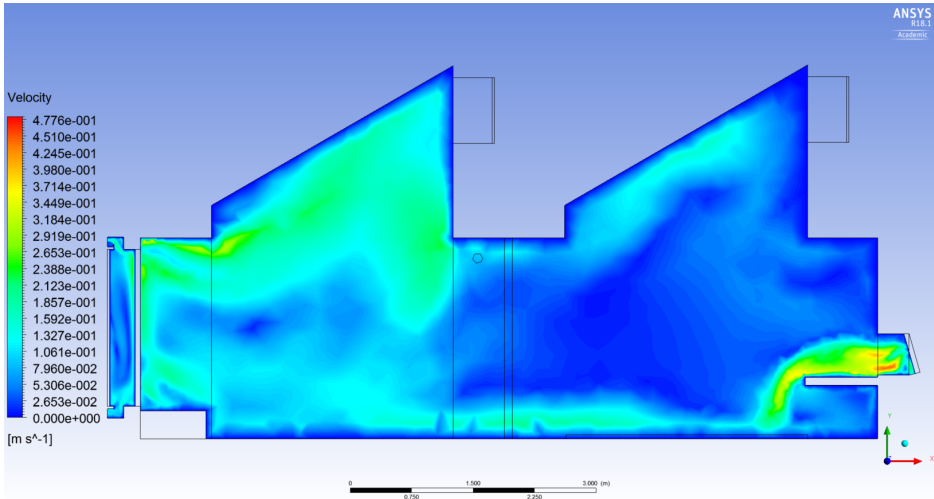


Figure 10.3: Case 4.5 - Velocity profile at t=45 s

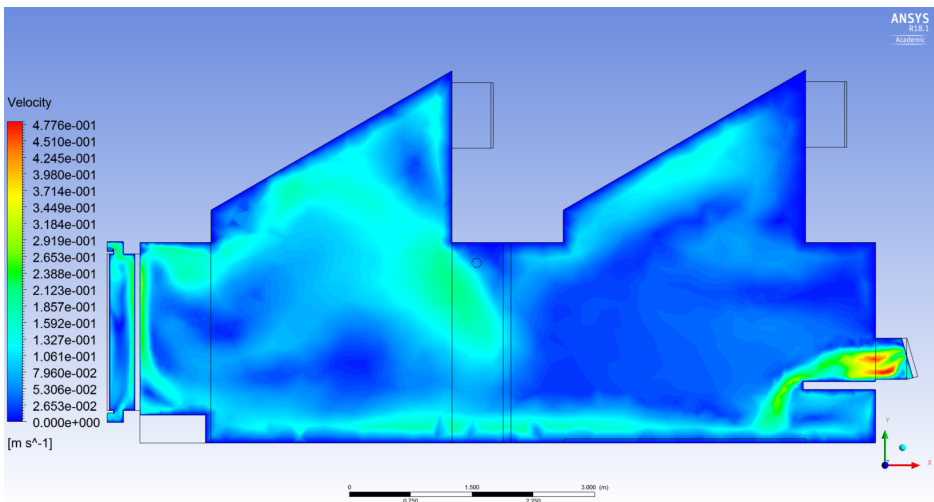


Figure 10.4: Case 4.5 - Velocity profile at t=59 s

In Figure 10.3 the flow is even more distinct, with the flow moving in a rotating motion, from along the floor to rising up over the south window and further up to the living room ceiling. After 59 seconds, the flow velocities seems to be reduced further around the office work station (presumed to be the most critical area for draught risks).

10.1.2 Turbulent kinetic energy contours at plane 1

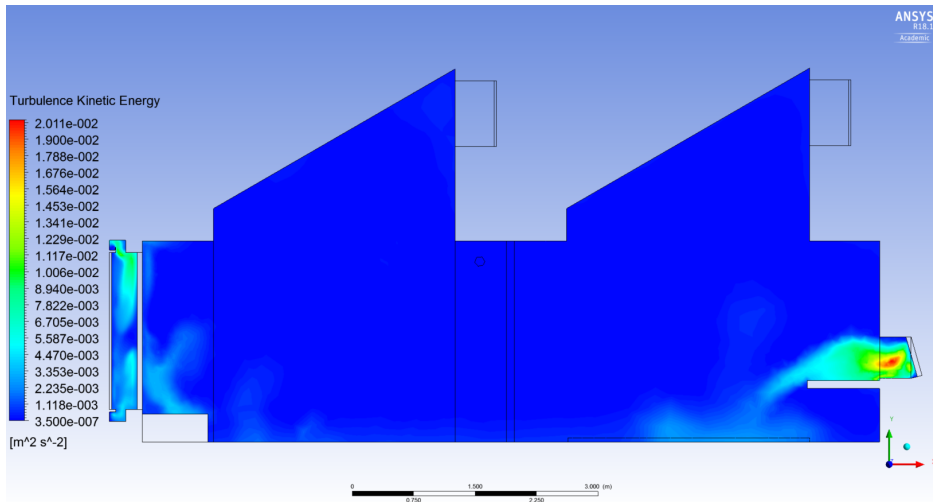


Figure 10.5: Case 4.5 - Turbulent kinetic energy profile at $t=15$ s

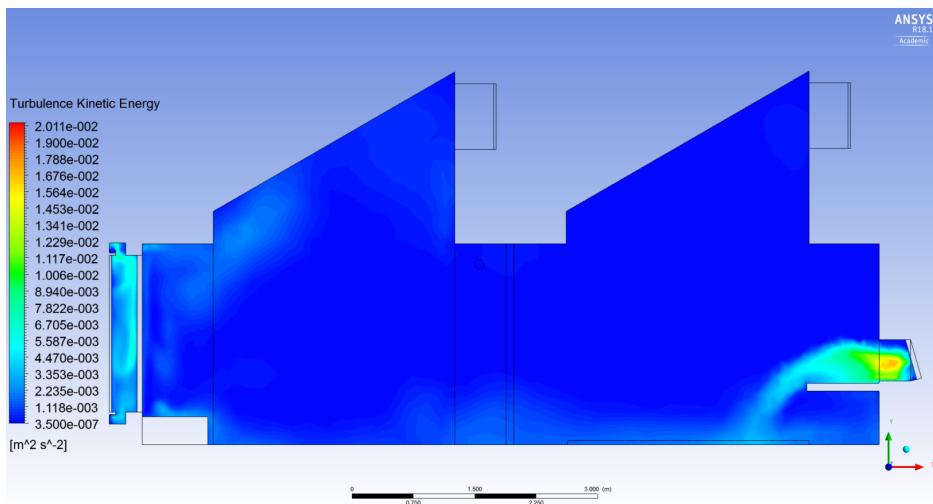
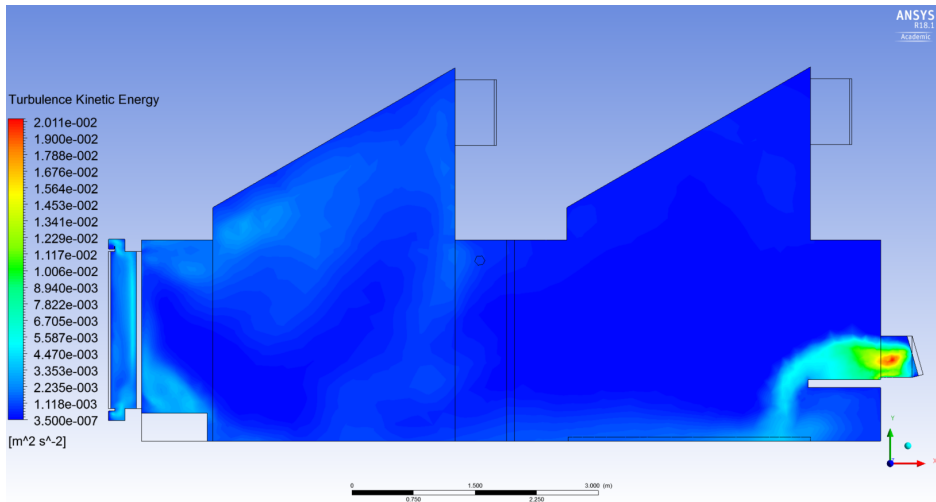
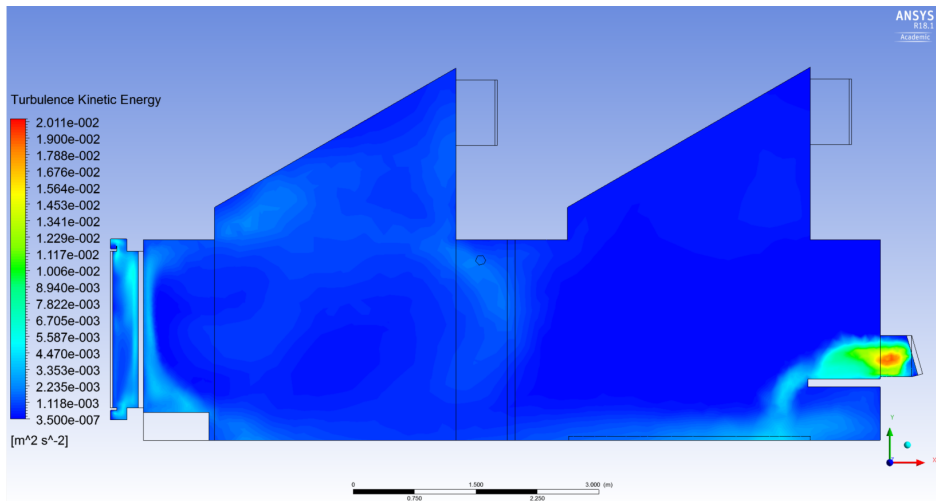


Figure 10.6: Case 4.5 - Turbulent kinetic energy profile at $t=29$ s

Figure 10.7: Case 4.5 - Turbulent kinetic energy profile at $t=45$ sFigure 10.8: Case 4.5 - Turbulent kinetic energy profile at $t=59$ s

The turbulent kinetic energy is dominant around the open window and along the work station, and slightly dominant near the south window, for all the time steps. The presence of turbulence promote re-attachment for flow [Ayad, 1999]. This relationship is visible when comparing the velocity contours with the turbulent kinetic energy contours, seeing increased velocities (in Figure 10.1-10.4) in the same areas where the presence of turbulence (Figure 10.5-10.8) is predicted. The air flow over the work station and up along the inner south window and the living room roof are attached to the surfaces, showing air flow with high speeds.

10.1.3 Temperature contours at plane 1

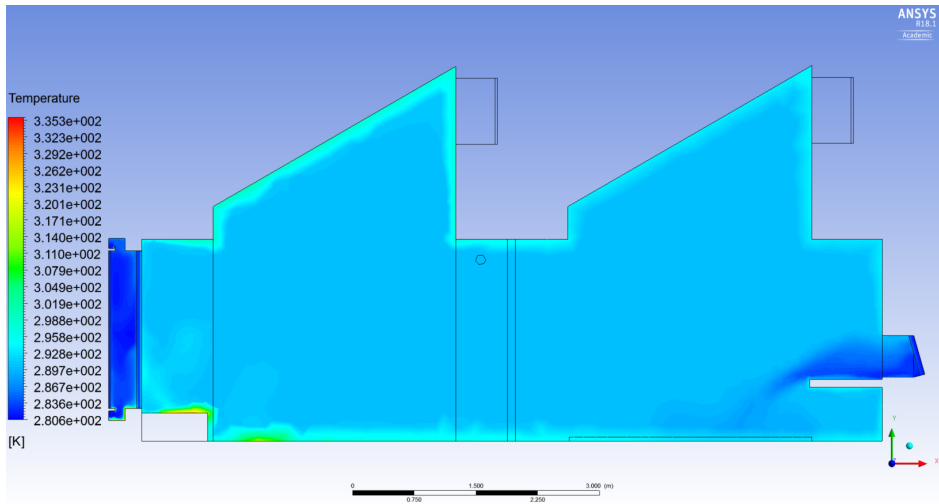


Figure 10.9: Case 4.5 - Temperature profile at $t=15$ s

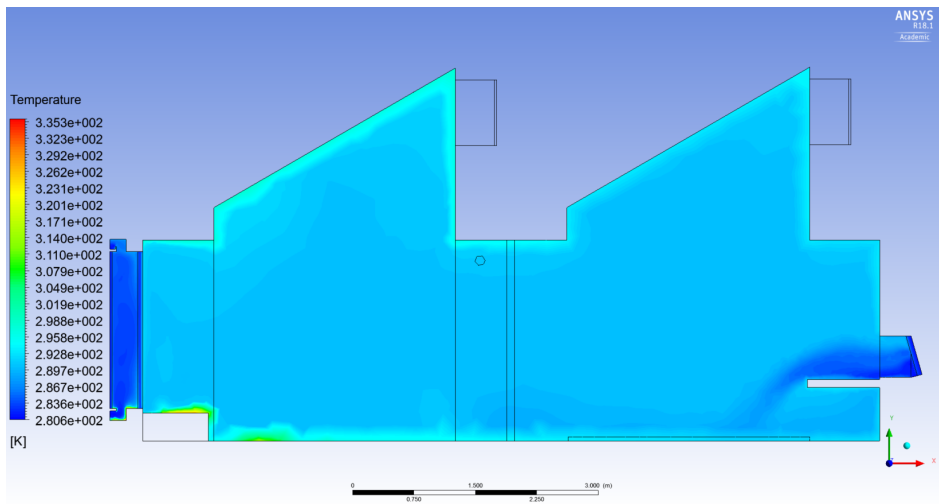


Figure 10.10: Case 4.5 - Temperature profile at $t=29$ s

From Figure 10.9-10.12 it is seen that the open window causes cold air to enter the indoor environment. As the flow develops due to time passing, the cold air progress further into the building, mainly along the floor. The heat loads present in the building, along with the existing temperature differences between the indoor and outdoor environment, causes the air to move inside the room. This is illustrated

both in the temperature contours (Figure 10.9-10.12) and the velocity contours (Figure 10.1-10.4).

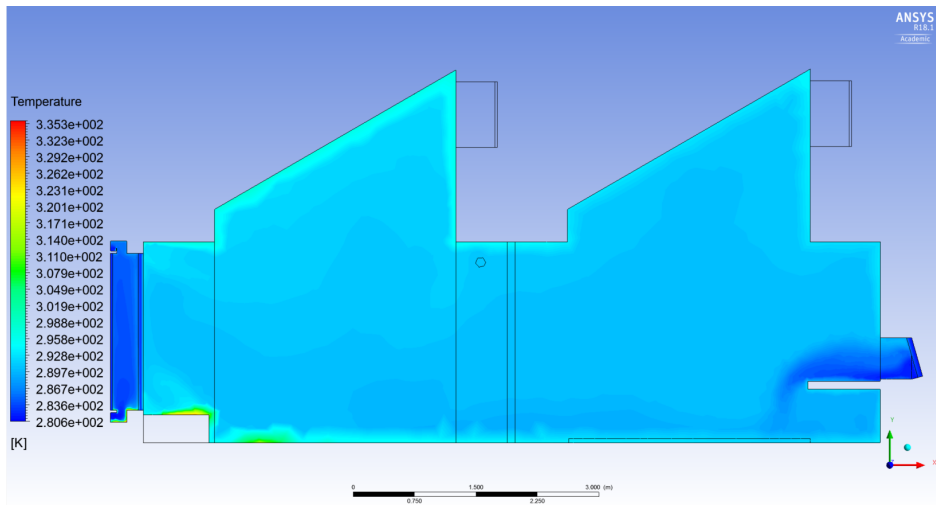


Figure 10.11: Case 4.5 - Temperature profile at t=45 s

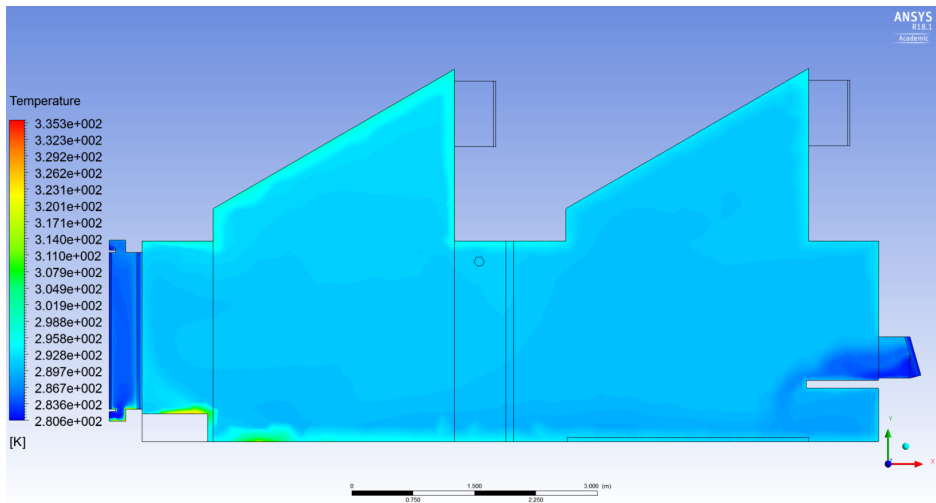


Figure 10.12: Case 4.5 - Temperature profile at t=59 s

Based on the information the contours have supplied, it is concluded that it is the area close to the work station that poses the greatest risk of thermal dissatisfaction due to local discomfort.

10.2 Draught Rate Calculations

The three points associated with location B will be used to compare the mean air velocity and the turbulence intensity with the full-scale data. All the measurement points listed in Table B.2 in Appendix B will be used to investigate the draught rate at the end of the sampling period (at $t=59$ s).

10.2.1 Correction formulas for turbulence intensity I_o and mean air velocity V_o

When the airflow is not dominated by turbulence in the room, it is in many cases fine to use the vector values V_V and I_V for PMV and DR calculations. For turbulent flows the omnidirectional values V_o and I_o should be used, as there might be significant difference between the omnidirectional values and the vector values [Koskela and Heikkinen, 2002]. Both cases will be included in the calculations and compared.

The vector value for the turbulence intensity I_V is defined in Eq.(10.1), and uses the relationship between the mean velocity vector and the turbulent kinetic energy.

$$I_V = \frac{\sqrt{\frac{2}{3}k}}{V_V} \quad (10.1)$$

The correction formula presented by Koskela et al. uses Eq.(10.2) and Eq.(10.3) to estimate the mean air velocity V_o and the turbulence intensity I_o .

$$\begin{aligned} \frac{V_o}{V_V} &= 1 + I_V^2 && \text{for } I_V \leq 0.45 \\ \frac{V_o}{V_V} &= \frac{1.596 \cdot I_V^2 + 0.266 \cdot I_V + 0.308}{0.173 + I_V} && \text{for } I_V > 0.45 \end{aligned} \quad (10.2)$$

$$I_o = \sqrt{(1 + 3 \cdot I_V^2) \frac{V_V^2}{V_o^2}} - 1 \quad (10.3)$$

In Figure 10.13 the directional value of the mean velocity from the CFD model simulation, the omnidirectional value of the mean velocity calculated with correction formulas and the experimental value of the mean velocity from the full-scale measurements are presented.

In Figure 10.14 the directional value of the local turbulence intensity from the CFD model simulation, the omnidirectional value of the local turbulence intensity calculated with correction formulas and the experimental value of the local turbulence intensity from the full-scale measurements are presented.

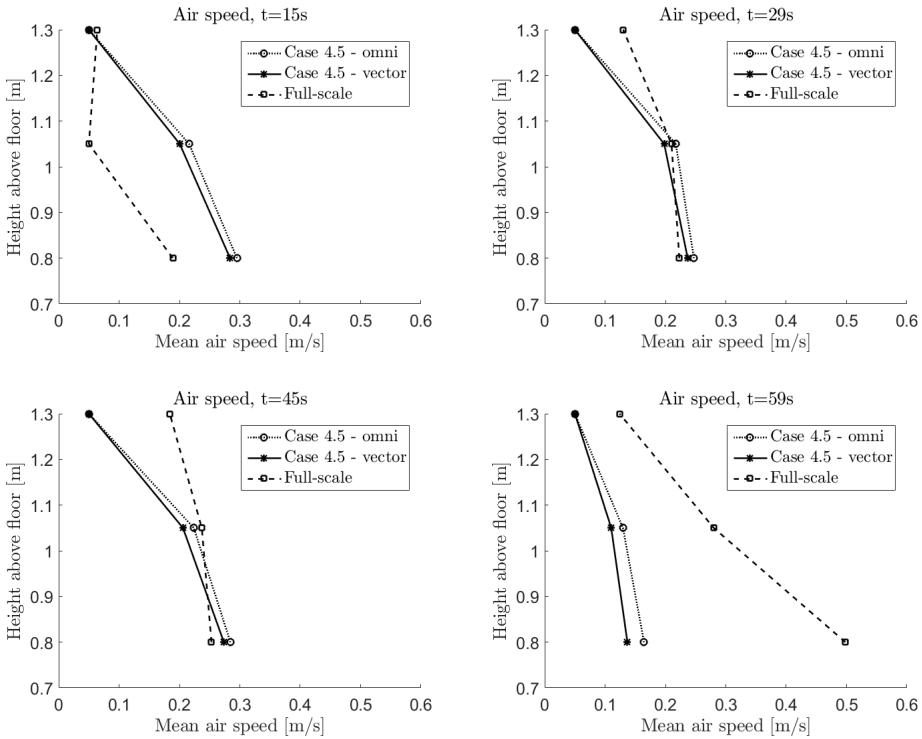


Figure 10.13: Comparison of mean air velocity for Case 4.5 and full-scale data at four different times

The variations between the directional and the omnidirectional velocity are small at all the presented time points, which means that the effects of the turbulence correction for the mean velocity are small. The velocities from Case 4.5 at $t=29$ s and $t=45$ s are predicted well in point B1 and B2, and the velocity at point B3 is predicted well at time $t=15$ s (see Figure 10.13).

The turbulence correction effects for the directional and omnidirectional turbulence intensity are seen in Figure 10.14. The effects are small for the three first time steps. From the final time (plot at $t=59$ s), there is a difference of about 10% between the directional and the omnidirectional turbulence intensity at points B1 and B2, indicating that the turbulence correction should be used.

However, both Figure 10.13 and Figure 10.14 indicate that there is a large discrepancy between the predicted flow obtained from the simulation (Case 4.5) and the full-scale experiment, most likely due to design simplifications and/or wrong setup for the CFD case. The air speeds varied in similarities. The simulation over-predicted the flow velocities at $t=15$ s, while greatly under-predicted the flow at $t=59$ s. For the turbulence intensity, the simulation largely under-predicted the turbulence effects. This might be due to the simplified opening at the north

window, discussed in Subsection 9.2.2.

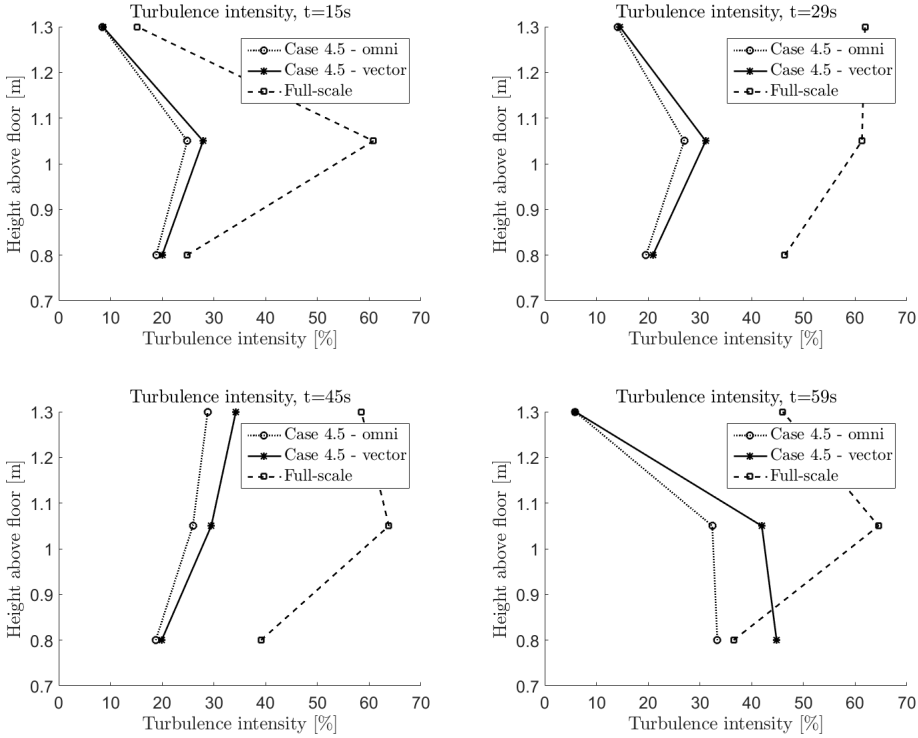


Figure 10.14: Comparison of turbulence intensity for Case 4.5 and full-scale data at four different times

10.2.2 Draught rate comparison

The draught rates are calculated with the formula given in Eq.(2.6). Due to the given requirements set by the formula in regards to temperature range and velocity range, certain assumptions have been carried out. To attain a scenario where an actual need for ventilative cooling existed, the indoor temperatures were manipulated, by reducing the supply air temperature and turning off the heating in the floor. By doing this, all the collected temperature data during the full-scale experiment gave low local air temperatures, i.e. temperatures outside the temperature range for the draught rate formula. For the draught calculations to work, [Blandkjenn, 2017] calculated the DR for a hypothetical scenario where the indoor air temperature was 24°C and the temperature difference for the experiment remained the same. This gave a hypothetical outdoor air temperature equal to

$$T_{out,hyp} = 24^{\circ}\text{C} - T_{in,real} + T_{out,real}$$

The temperature difference is then added to the measured temperatures at the different collection locations. The thermal conditions during the full-scale experiment

measured an indoor temperature of around 17°C and an outdoor temperature of around 8°C, which gives a temperature difference equal to 9°C. The same principle will be used for the air temperatures attained from the CFD simulation. Here, the indoor air was assumed to be 290 K (16.85°C) and the outdoor air was set to 281 K (7.85°C), which also gives a temperature difference equal to 9°C.

For the limitations regarding the magnitude of the velocity, the formula operates with the simplifications that measured velocities under the value of 0.05 m/s, are given the value of 0.05 m/s. This velocity gives predicted percent of people being bothered by draught to zero [NS-EN ISO 7730, 2006]. For values above 0.5 m/s, the equation is no longer usable.

The results can be seen in Figure 10.15, where draught rates are calculated for the directional and omnidirectional values from the simulated Case 4.5 and the full-scale experimental values.

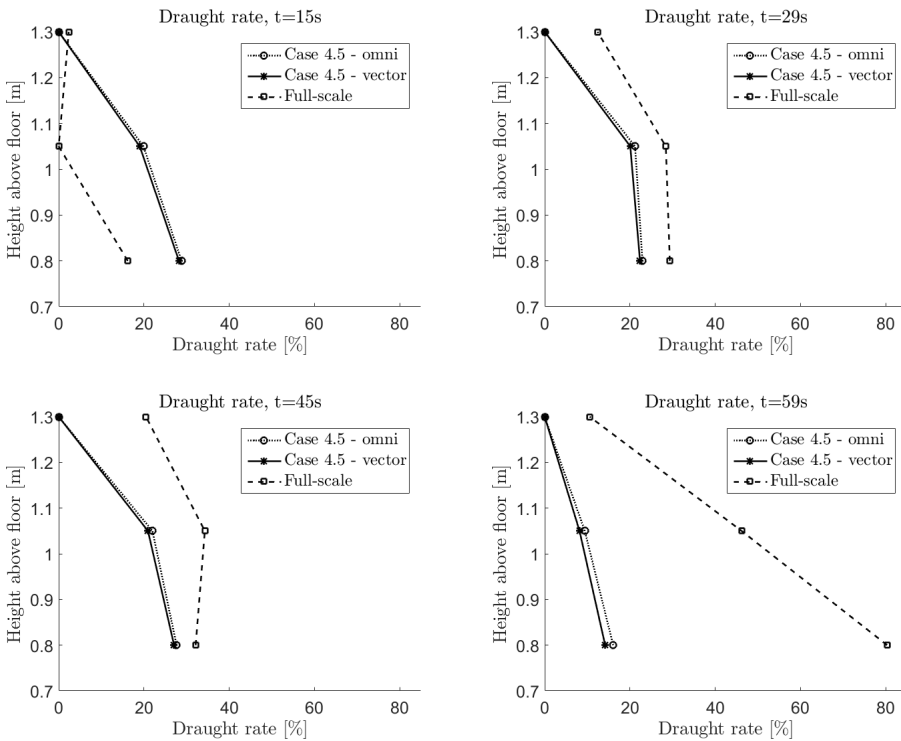


Figure 10.15: Comparison of draught rate for Case 4.5 and full-scale data at four different times

Again, the difference between the omnidirectional and the directional values are small, which is unsurprising when considering the results presented in Figure 10.13 and Figure 10.14. Except for the time step $t=15$ s, the CFD simulation underesti-

mates the DR, when compared with the calculated DR for the experiment. This is especially visible at the final time step, in point B1, where the difference between the simulation and the experiment is over 60%.

Sources of error

The conditions set to the DR equation (Eq.(2.6)), forces the CFD results and the full-scale results to be manipulated, before draught rates can be investigated. It is unknown how much this might affect the outcome, and if the manipulation is even valid to use.

The experiment reported uncertainties in regards to the sensor equipment, not knowing when the damage to the equipment occurred. If the data collected contain large errors, it will of course affect the calculations of the draught rates. This was also discussed in Subsection 9.2.2.

The experimental draught rates have been calculated with unprocessed data given by [Blandkjenn, 2017], and misunderstanding of the data may be a cause of error when the velocities, turbulence intensities and DR calculations (Figures 10.13-10.15) are presented in this paper.

The sources discussed in Section 9.2 are also possible reasons for the deviation between the presented results for the CFD simulation and the experiment.

10.2.3 Local thermal discomfort calculations for Case 4.5

For this subsection, data collected from the points listed in Table B.2 will be used to investigate local thermal discomfort due to draught rate for Case 4.5. The results will be discussed in a way that assumes that the simulation model is validated and that the predicted flow is acceptable (even though this is not the situation for Case 4.5). From the results comparing the vector velocities with the mean air velocities in the previous subsection, it is concluded that the turbulence effects do not need to be included. For the following calculations, it is therefore the vector values V_V and I_V that will be used.

The calculated draught rates for location A, B, C+F, D+G and E+H are presented in Figure 10.16. The plots show that there are high risks of thermal discomfort at location A, with measured draught rates up to 40%. However, this location is placed at the middle of the work station, which means that occupants will not be directly subjected to the discomfort. For the remaining locations, i.e. areas where the occupants may be directly exposed to the draught rates, the calculated maximum values are either close to or less than 20%. These draught rates will be deemed acceptable, when the indoor environment is classified as a Category B (from Table 2.2), when all the other discomfort calculations are assumed to be below the maximum criteria. The use of the north window to supply ventilative

cooling is, from the results presented here, considered to be acceptable and the thermal environment will maintain a pleasant thermal comfort level.

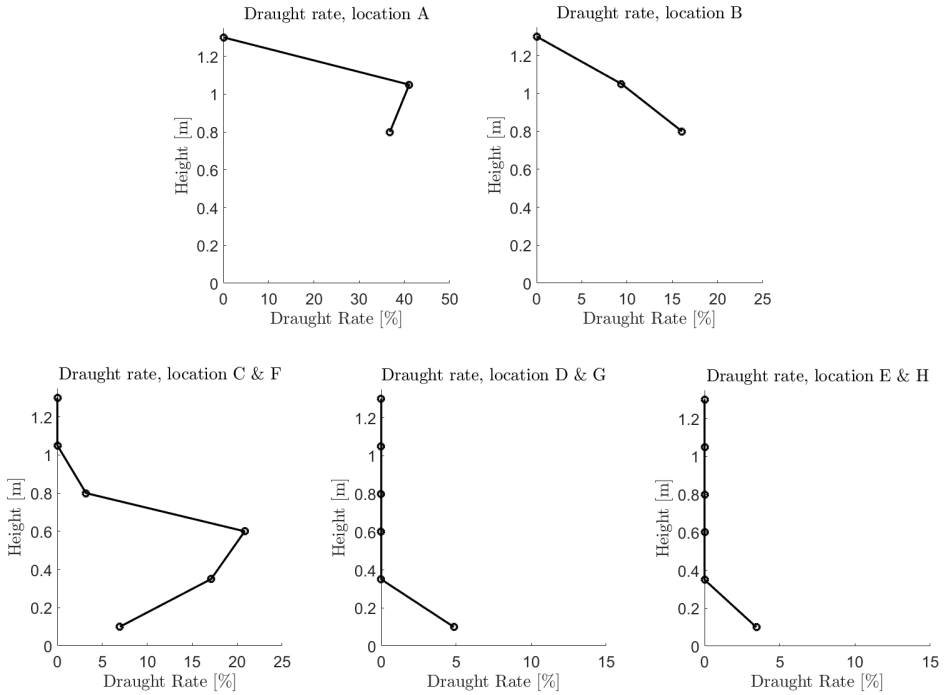


Figure 10.16: Draught rate calculations for Case 4.5 at t=59s at different distances from the north window

Conclusion

11.1 Conclusion

Three models have been established during the work of this master thesis. A set of simplifications to the model geometry and the simulation setup have been carried out, due to limitations in computer capacity and time restrictions. The models have simulated for different setups, and accordingly, the simulations have been verified to solve the fundamental equations correctly for each case.

Model A verified the boundary conditions at the inlets and outlets for the simulated mechanical ventilation system. The supply vents were defined as velocity inlets, while the extraction vents were defined as outflows for cases where all windows were closed and as mass flows when ventilative cooling was investigated. Model A did also verify that mixed boundary conditions, set to the walls and roof in the simulation, were preferred over only convection boundary conditions, since radiation effects are dominant in the simulation.

Model B included solar load effects in the simulation and verified the setup of the solar load, and the setup for the surface material characteristics for the solid walls (set as opaque) and windows (set as semi-transparent). Both steady state and transient conditions were simulated, and the results indicated that the assumption of a transient situation was more suitable, considering the simulation circumstances. The transient simulation with the solar load revealed a risk of thermal discomfort in the building due to overheating.

Model C was used to validate the CFD model geometry and setup with the full-scale experiment. The model simulated for a scenario where ventilative cooling with 25% opening at the north window and 100% opening at the skylight window was carried out. The outdoor and indoor conditions were determined from data collected by sensors at ZEB Living Lab, on April 25th 2017, at 3pm, to ensure

that the thermal conditions for the simulation and for the experiment were alike. The presence of wind during the full-scale measurements resulted in difficulties when estimating and defining the boundary conditions for the open north window inlet. Therefore, a set of different boundary conditions were investigated. The results from the simulations showed that none of the cases managed to accurately re-create the air flow that was measured during the experiment. However, the simulated solutions were not completely wrong and managed to predict the flow fairly well for some of the boundary conditions. Sources of errors that may be the cause for the solution discrepancies were discussed. From the presented results, it was assumed that the most dominant sources of errors were due to geometrical simplifications made to the model, i.e. reducing the domain size to only the building facility and simplifying the opening method for the north window, and due to not including appropriate parameter studies on important computational parameters.

The case that was concluded to predict the air flow best, compared to the experiment, was Case 4.5. This case carried out simulations with a velocity inlet boundary condition, where the x-velocity was set to -0.1 m/s and the y-velocity was set to 0.14 m/s. The simulated solution from this case was used in thermal discomfort investigations. Four time steps were included and plots containing the turbulence intensity, mean air velocity and draught rate of the directional and omnidirectional values of the simulation case, and the full-scale experiment were compared. The results showed that the effects of turbulence in the simulation calculations were small, and that the simulation struggled to estimate values similar to the experiment for the turbulence intensity, mean velocity and draught rate. A final risk assessment on draught was performed for Case 4.5, to investigate the risk of thermal discomfort to the occupants. For this particular situation, it was assumed that the case and model had been validated (even though this is not the situation for Case 4.5 or for Model C). The calculated draught rates were considered acceptable, when the indoor environment was classified as a Category B, and concluded that the use of ventilative cooling with 25% opening area for the north window managed to maintain a pleasant thermal environment.

11.2 Suggestion for Further Works

The goal of this master thesis - *of establishing a model of ZEB Living Lab that can predict air flow characteristics accurately inside the building, to be used for thermal comfort analysis* - have not yet been accomplished. However, the models presented in this thesis have potential for reaching this goal. In regard to further work on the models, the following suggestions are made:

- Carry out more simulations where the results may be compared with the full-scale measurements obtained from [Blandkjenn, 2017]. This include CFD simulations of ventilative cooling with the south window.
- Do parameter studies on different computational parameters such as turbulence models, domain size (CFD domain of building facility v.s. CFD domain

of building facility and outer environment, when wind effects are present), grid quality, choice of solvers, convergence criteria and boundary conditions, and compare them with the each other.

- Investigate how much the geometrical simplifications affect the final results by making a more exact model of the full-scale facility, and perform simulations that may be compared with the simplified model. This include investigation to the north window opening.
- When the CFD model is properly validated, run simulations with ventilative cooling inside the building for different scenarios, where the solutions may be used for thermal comfort investigations.
- Use the CFD model to find optimal window opening areas and window configurations for different outdoor conditions.

Bibliography

- [VVS, 1969] (1969). *Regler for beregning av bygningers varmebehov*. Norsk VVS.
- [Abu-Ghannam and Shaw, 1980] Abu-Ghannam, B. and Shaw, R. (1980). Natural transition of boundary layer—the effects of turbulence, pressure gradient, and flow history. *Journal of Mechanical Engineering Science*, 22(5):213–228.
- [Admin, 2017] Admin, A. (2017). Zeb definitions. <http://zeb.no/index.php/en/about-zeb/zeb-definitions>.
- [Aldawoud, 2017] Aldawoud, A. (2017). Window design for maximum cross-ventilation in buildings. *Advances in Building Energy Research*, 11(1):67–68.
- [Allocca et al., 2003] Allocca, C., Chen, Q., and Glickman, L. R. (2003). Design analysis of single-sided natural ventilation. *Energy and buildings*, 35(8):785–795.
- [Anderson et al., 2014] Anderson, T., Gillen, J., and Norris, S. E. (2014). Natural convection heat loss from an open room.
- [Andersson et al., 2011] Andersson, B., Andersson, R., Håkansson, L., Mortensen, M., Sudiyo, R., and van Wachem, B. (2011). *Computational fluid dynamics for engineers*. Cambridge University Press.
- [ANSI/ASHRAE, 2010] ANSI/ASHRAE (2010). Standard 55-2010: Thermal environmental conditions for human occupancy. 2010. *American Society of heating, Refrigerating and Airconditioning Engineers: Atlanta*.
- [ANSYS, a] ANSYS, I. Fluent documentation. https://www.sharcnet.ca/Software/Ansys/16.2.3/en-us/help/ai_sinfo/flu_intro.html.
- [ANSYS, b] ANSYS, I. Workbench documentation. https://www.sharcnet.ca/Software/Ansys/16.2.3/en-us/help/ai_sinfo/wb_intro.html.
- [ANSYS, 2006] ANSYS, I. (2006). Ansys fluent 6.3 user’s guide. https://www.sharcnet.ca/Software/Fluent6/html/ug/main_pre.htm.

- [ANSYS, 2009] ANSYS, I. (2009). Ansys fluent 12.0 theory guide. http://www.afs.enea.it/project/neptunius/docs/fluent/html/th/main_pre.htm.
- [ANSYS, 2012] ANSYS, I. (2012). Lecture 4 solver settings.
- [ANSYS, 2015] ANSYS, I. (2015). Fluent intro course.
- [Awbi, 2010] Awbi, H. (2010). Basic concepts for natural ventilation of buildings. In *CIBSE BSG Seminar: Natural and Mixed-Mode Ventilation Modelling*.
- [Ayad, 1999] Ayad, S. A. (1999). Computational study of natural ventilation. *Journal of Wind Engineering and Industrial Aerodynamics*, 82(1):49–68.
- [Bazilchuk, 2017] Bazilchuk, N. (2017). Living with zero-emission technology. <http://zeb.no/index.php/en/about-zeb/zeb-definitions>.
- [Blandkjenn, 2017] Blandkjenn, S. (2017). Ventilative cooling of zero emission buildings *zeb(. Master’s thesis, Norges teknisk-naturvitenskaplige universitet, Trondheim.
- [Böhler, 2017] Böhler, K. H. (2017). Study of window ventilation in cold climates.
- [Carlos and Corvacho, 2013] Carlos, J. S. and Corvacho, H. (2013). Ventilated double window for the preheating of the ventilation air comparison of its performance in a northern and a southern european climate. *Journal of Renewable Energy*, 2013.
- [Chen, 2009] Chen, Q. (2009). Ventilation performance prediction for buildings: A method overview and recent applications. *Building and environment*, 44(4):848–858.
- [Delta OHM, 2007] Delta OHM (2007). Lp pyra 03 pyranometers. http://www.deltaohm.com/ver2012/index.php?main_page=product_info&products_id=212.
- [Delta OHM, 2018] Delta OHM (2018). Hd52.3d. http://deltaohm.com/ver2012/index.php?main_page=product_info&cPath=1_17&products_id=106.
- [Direktoratet for Byggkvalitet, 2011] Direktoratet for Byggkvalitet (2011). *Veiledning til forskrift om tekniske krav til byggverk (TEK10)*, 2.utg. edition.
- [Evola and Popov, 2006] Evola, G. and Popov, V. (2006). Computational analysis of wind driven natural ventilation in buildings. *Energy and buildings*, 38(5):491–501.
- [Finocchiaro et al., 2016] Finocchiaro, L., Georges, L., and Hestnes, A. (2016). Passive solar space heating 6. *Advances in Solar Heating and Cooling*, page 95.
- [Foucquier et al., 2013] Foucquier, A., Robert, S., Suard, F., Stéphan, L., and Jay, A. (2013). State of the art in building modelling and energy performances prediction: A review. *Renewable and Sustainable Energy Reviews*, 23:272–288.

- [Gaspar et al., 2003] Gaspar, P. D., Barroca, R. F., and Pitarma, R. (2003). Performance evaluation of cfd codes in building energy and environmental analysis. *Building Simulation 2003*.
- [Gilani et al., 2016] Gilani, S., Montazeri, H., and Blocken, B. (2016). Cfd simulation of stratified indoor environment in displacement ventilation: Validation and sensitivity analysis. *Building and Environment*, 95:299–313.
- [Goia et al., 2015] Goia, F., Finocchiaro, L., and Gustavsen, A. (2015). The zeb living laboratory at the norwegian university of science and technology: a zero emission house for engineering and social science experiments. In *Passivhus Norden Conference, Sustainable Cities and Buildings, Copenhagen, Denmark*.
- [Griffiths and Boysan, 1996] Griffiths, W. and Boysan, F. (1996). Computational fluid dynamics (cfd) and empirical modelling of the performance of a number of cyclone samplers. *Journal of Aerosol Science*, 27(2):281–304.
- [Hilgenstock and Ernst, 1996] Hilgenstock, A. and Ernst, R. (1996). Analysis of installation effects by means of computational fluid dynamics cfd vs experiments? *Flow measurement and instrumentation*, 7(3-4):161–171.
- [Hulme, 2005] Hulme, P. E. (2005). Adapting to climate change: is there scope for ecological management in the face of a global threat? *Journal of Applied ecology*, 42(5):784–794.
- [Inc., 2005] Inc., A. (2005). Ansys workbench documentation.
- [Incropera et al., 2013] Incropera, F. P., Dewitt, D. P., Bergman, T. L., and Lavine, A. S. (2013). *Principles of Heat and Mass Transfer*. John Wiley & Sons, Inc., 7 edition.
- [Intergovernmental Panel on Climate Change, 2015] Intergovernmental Panel on Climate Change (2015). *Climate change 2014: mitigation of climate change*, volume 3. Cambridge University Press. Chapter 9.
- [International Energy Agency, 2013] International Energy Agency (2013). Transition to sustainable buildings - strategies and opportunities to 2050. <https://www.iea.org/Textbase/npsum/building2013SUM.pdf>.
- [Janson, 2010] Janson, U. (2010). *Passive Houses in Sweden. From Design to Evaluation of Four Demonstration Projects*. PhD thesis, Lund University.
- [Jiang and Chen, 2003] Jiang, Y. and Chen, Q. (2003). Buoyancy-driven single-sided natural ventilation in buildings with large openings. *International Journal of Heat and Mass Transfer*, 46:973–988.
- [Kim, 2013] Kim, M. J. (2013). *Finite Element Methods with Programming and Ansys*. Lulu.com.
- [Kirkøen, 2015] Kirkøen, C. (2015). Ventilative cooling in living lab. Master’s thesis, Norges teknisk-naturvitenskaplige universitet, Trondheim.

- [Kolokotroni and Heiselberg, 2015] Kolokotroni, M. and Heiselberg, P. (2015). Ventilative cooling. *A state-of-the art review report for the International Energy Agency, Aalborg, Denmark, EBC Programme Annex*, 62.
- [Koskela and Heikkinen, 2002] Koskela, H. and Heikkinen, J. (2002). Calculation of thermal comfort from cfd-simulation results. In *Proceedings of the International Conference on Indoor Air Quality and Climate*, volume 3, pages 712–717.
- [Koskela et al., 2001] Koskela, H., Heikkinen, J., Niemelä, R., and Hautalampi, T. (2001). Turbulence correction for thermal comfort calculation. *Building and Environment*, 36(2):247–255.
- [Larsen et al., 2012] Larsen, T. S., Jensen, R. L., and Daniels, O. (2012). The comfort houses: Measurements and analysis of the indoor environment and energy consumption in 8 passive houses 2008-2011. Technical report, Department of Civil Engineering, Aalborg University.
- [Li and Nielsen, 2011] Li, Y. and Nielsen, P. V. (2011). Cfd and ventilation research. *International Journal of Indoor Environment and Health*, 21(6):442–453.
- [Lin et al., 2011a] Lin, Z., Lee, C. K., Fong, S., Chow, T. T., Yao, T., and Chan, A. (2011a). Comparison of annual energy performances with different ventilation methods for cooling. *Energy and Buildings*, 43(1):130–136.
- [Lin et al., 2011b] Lin, Z., Tian, L., Yao, T., Wang, Q., and Chow, T. T. (2011b). Experimental and numerical study of room airflow under stratum ventilation. *Building and Environment*, 46(1):235–244.
- [Linden, 1999] Linden, P. F. (1999). The fluid mechanics of natural ventilation. *Annual Review of Fluid Mechanics*, 31(1):201–238.
- [Maxim Integrated, 2018] Maxim Integrated (2018). Ds 1920 temperature ibutton. <https://www.maximintegrated.com/en/products/digital/ibutton/DS1920.html>.
- [Meng et al., 2016] Meng, X., Wang, Y., Liu, T., and Yingxue Cao, X. X., and Zhao, J. (2016). Influence of radiation on predictive accuracy in numerical simulations of the thermal environment in industrial buildings with buoyancy-driven natural ventilation. *Applied Thermal Engineering*, 96:473–480.
- [Nilsson and Group, 2003] Nilsson, P. E. and Group, C., editors (2003). *Achieving the Desired Indoor Climate : Energy Efficiency Aspects of System Design*. Lund: Studentlitteratur.
- [Norton et al., 2007] Norton, T., Sun, D.-W., Grant, J., Fallon, R., and Dodd, V. (2007). Applications of computational fluid dynamics (cfd) in the modelling and design of ventilation systems in the agricultural industry: A review. *Bioresource technology*, 98(12):2386–2414.

- [Novakovic et al., 2007] Novakovic, V., Hanssen, S., Thue, J., Skarstein, Ø., and Gjerstad, F. (2007). Enøk i bygninger-effektiv energibruk. *Oslo: Gyldendal undervisning*, 63.
- [NS-EN ISO 7730, 2006] NS-EN ISO 7730, S. N. (2006). Ergonomics of the thermal environment - analytical determination and interpretation of thermal comfort using calculation of the pmv and ppd indices and local thermal comfort criteria (iso 7730:2005).
- [Orme et al., 2003] Orme, M., Palmer, J., and Irving, S. (2003). Control of overheating in well-insulated housing. In *Proceedings of the CIBSE/ASHRAE Conference (24-26 September 2003) in Building Sustainability, Value & Profit, Edinburgh*.
- [Pletcher et al., 2013] Pletcher, R. H., Tannehill, J. C., and Anderson, D. A. (2013). *Computational Fluid Mechanics and Heat Transfer*. CRC Press, 3 edition.
- [Ramponi and Blocken, 2012] Ramponi, R. and Blocken, B. (2012). Cfd simulation of cross-ventilation flow for different isolated building configurations: validation with wind tunnel measurements and analysis of physical and numerical diffusion effects. *Journal of Wind Engineering and Industrial Aerodynamics*, 104:408–418.
- [Riedy et al., 2011] Riedy, C., Lederwasch, A., and Ison, N. (2011). Defining zero emission buildings-review and recommendations.
- [Risnes, 2016] Risnes, A. (2016). Indoor environment in zeb living lab. Master's thesis, Norges teknisk-naturvitenskaplige universitet, Trondheim.
- [Rodriguez-Ubinas et al., 2014] Rodriguez-Ubinas, E., Montero, C., Porteros, M., Vega, S., Navarro, I., Castillo-Cagigal, M., Matallanas, E., and Gutiérrez, A. (2014). Passive design strategies and performance of net energy plus houses. *Energy and buildings*, 83:10–22.
- [Romano and Duval, 2012] Romano, V. A. and Duval, A. S. (2012). *Ventilation : Types, Standards, and Problems*. New York : Nova Science Publishers.
- [Ryaben'kii and Tsynkov, 2006] Ryaben'kii, V. S. and Tsynkov, S. V. (2006). *An introduction to numerical analysis*. CRC Press.
- [Santamouris and Allard, 1998] Santamouris, M. and Allard, F. (1998). *Natural ventilation in buildings: a design handbook*. Earthscan.
- [Santamouris et al., 1996] Santamouris, M., Asimakopoulos, D., et al. (1996). *Passive cooling of buildings*, volume 1. James & James London;
- [Sensor Electronic, 2018] Sensor Electronic (2018). Airdistsys 5000. http://www.sensor-electronic.pl/pdf/KAT_AirDistSys5000.pdf.

- [S+S Regeltechnik, 2018] S+S Regeltechnik (2018). Thermasgard®. <https://spluss.de/en/products/temperature/temperature-passive/room-temperature-sensor/1101-40a0-1003-000-rtf1-pt100/>.
- [Stavrakakis et al., 2008] Stavrakakis, G. M., Koukou, M. K., Vrachopoulos, M. G., and Markatos, N. C. (2008). Natural cross-ventilation in buildings: Building-scale experiments, numerical simulation and thermal comfort evaluation. *Energy and Buildings*, 40(9):1666–1681.
- [Stavridou and Prinos, 2017] Stavridou, A. D. and Prinos, P. E. (2017). Unsteady cfd simulation in a naturally ventilated room with a localized heat source. *Procedia Environmental Sciences*, 38:322–330.
- [Versteeg and Malalasekera, 2007] Versteeg, H. K. and Malalasekera, W. (2007). *An Introduction to Computational Fluid Dynamics: The Finite Volume Method*. Pearson Education.
- [Woods and Samdal, 2017] Woods, R. and Samdal, M. (2017). Zeb final report 2009-2017. <https://xmedia.no/zeb-final-report/mobile/index.html#p=1>.
- [Zhai and Chen, 2006] Zhai, Z. J. and Chen, Q. Y. (2006). Sensitivity analysis and application guides for integrated building energy and cfd simulation. *Energy and buildings*, 38(9):1060–1068.
- [Ziskind et al., 2002] Ziskind, G., Dubovsky, V., and Letan, R. (2002). Ventilation by natural convection of a one-story building. *Energy and Buildings*, 34:91–102.

Appendix A

Living Lab

Table A.1: Integrated sensors in Living Lab

Name	Brand	Parameter	Range	Accuracy
THERMasgard®	S+S Regeltechnik	Air Temperature Indoor	-30...+70°C	±0.1°C
RTF1 PT100 FRIJA II 1/3 DIN	S+S Regeltechnik	Air Temperature Indoor	0...+50°C	±0.2°C
HD52.3D	Delta OHM	Wind Speed Wind Direction Air Temperature Outdoor	0...60m/s 0...360° -40...+60°C	±0.2m/s ±2°RMSE from 1.0 m/s ±0.15°C
LP PYRA 03 pyranometers	Delta OHM	Global Solar Irradiance	0...2000 W/m ²	±5%

[Goia et al., 2015, S+S Regeltechnik, 2018, Delta OHM, 2018, Delta OHM, 2007]

Table A.2: Measuring Equipment for the Full-scale experiment

Name	Brand	Parameter	Range	Accuracy
SensoAnemo5100SF	Sensor Electronic	Air Speed	0.05...5m/s	±0.02m/s ±1% of readings
		Air Temperature	-10...+50°C	±0.2°C
DS1920 iButton	Maxim Integrated Products	Air Temperature	-55...+100°C	±0.5°C

[Blandkjenn, 2017, Sensor Electronic, 2018, Maxim Integrated, 2018]

Appendix **B**

Material Setup Information

B.1 Material properties

Table B.1: Material properties

Fluids				
Type of material	Property	Value		
		(T=20°C)	(T=10°C)	(T=0°C)
Air	ρ (kg/m ³)	1.205	1.249	1.293
	C_p (J/kg-K)	1005	1005	1005
	k (W/m-K)	0.0243	0.025	0.0257
	μ (kg/m-s)	1.820755e-05	1.774205e-05	1.71969e-05
	β (1/K)	0.00341	0.00353	0.00366
Solids				
Type of material	Properties	Value		
Glass		South window	North window	Skylight
	ρ (kg/m ³)	2500		
	C_p (J/kg-K)	800		
	k (W/m-K)	0.0585*/0.0621**	0.0582	0.03
Wood		Floor	Roof	Walls
	ρ (kg/m ³)	700		
	C_p (J/kg-K)	2310		
	k (W/m-K)	0.05050	0.05050	0.05555

* South window(s) closed

** South window(s) open

B.2 North window point measurement coordinates

Table B.2: Overview of the north window point location in coordinates

Point location	Coordinates			Point location	Coordinates				
	x (m)	y (m)	z (m)		x (m)	y (m)	z (m)		
A	1	3.638	0.800	3.705	E	1	1.638	0.800	3.705
	2	3.638	1.050	3.705		2	1.638	1.050	3.705
	3	3.638	1.300	3.705		3	1.638	1.300	3.705
B	1	3.138	0.800	3.705	F	1	2.638	0.100	3.705
	2	3.138	1.050	3.705		2	2.638	0.350	3.705
	3	3.138	1.300	3.705		3	2.638	0.600	3.705
C	1	2.638	0.800	3.705	G	1	2.138	0.100	3.705
	2	2.638	1.050	3.705		2	2.138	0.350	3.705
	3	2.638	1.30	3.705		3	2.138	0.600	3.705
D	1	2.138	0.800	3.705	H	1	1.638	0.100	3.705
	2	2.138	1.050	3.705		2	1.638	0.350	3.705
	3	2.138	1.300	3.705		3	1.638	0.600	3.705

Window Opening Calculations

Certain simplifications to the window geometries have been performed to make a more cost-efficient simulation. [Blandkjenn, 2017] measured the maximum opening area of the different windows in the building. These opening areas are used in the sections below, to calculate the angles the windows must be rotated so the simulated cases can be compared with measurements from [Blandkjenn, 2017].

C.1 Skylight windows

The skylight windows are pivot windows, located high up on the north facing walls of the building. [Blandkjenn, 2017] calculated a surface area of 0.338 m^2 to be the maximum opening area for each of these windows. In the simulation model, the window opening geometry is assumed to have little meaning on the air flow inside the room. Therefore, in the model, the windows have a surface area equal to the maximum opening area. For the simulations where one or more skylight windows are open, the given windows are "removed", and the entire area acts like an outlet. For all the ventilative cooling measurements [Blandkjenn, 2017] performed with skylight windows, the windows were fully open.

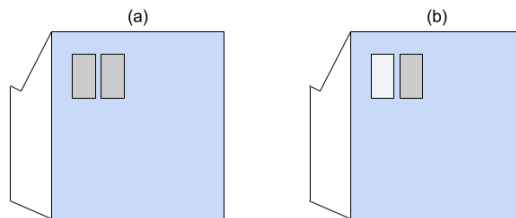
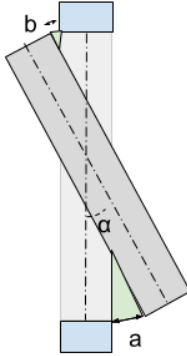


Figure C.1: (a) The skylight windows are closed, (b) The skylight window to the left is open

C.2 North windows

C.2.1 Opening area found in [Blandkjenn, 2017]



The lengths **a** and **b** were measured to 0.23m and 0.09m, respectively, for the maximum opening angle $\alpha=51^\circ$ [Blandkjenn, 2017].

This gives a maximum opening area of the north window to be 0.786 m^2 , when the length of the window is $L=2.21 \text{ m}$. The method used for the opening area calculation are given in Eq.(C.1).

$$A_{opening} = L * (a + b) + \frac{a^2}{\sin\alpha} + \frac{b^2}{\sin\alpha} \quad (\text{C.1})$$

Figure C.2: North window cross section from [Blandkjenn, 2017]

C.2.2 Opening angle calculations for the model

The original opening (Figure C.2) will cause problems for the simulation model when the mesh is created. Small angles and sharp, skewed surfaces will characterize the mesh around the top and bottom of the north window. By rotating the window at the top, the model reduces the number of elements required to achieve an appropriate mesh quality. The alteration in the window opening method is assumed to have only a small effect on the predicted flow pattern, and is therefore acceptable.

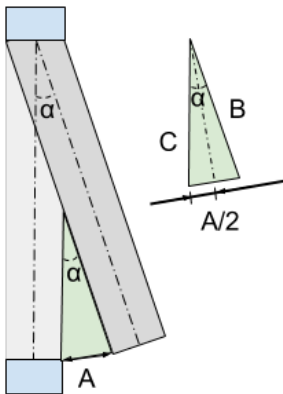


Figure C.3: North window cross section of simulation model

With a maximum opening area of 0.786 m^2 , the maximum opening angle will be calculated with a trial and error method. The length of sides **A**, **B**, and **C** (illustrated in Figure C.3) are measured for different angles in Workbench DesignModeler, and then used to calculate the opening area. Each of the triangle areas are calculated with Eq.(C.2).

$$A_{triangle} \approx \frac{A * (B + C)}{2} \quad (\text{C.2})$$

The opening area is calculated with Eq.(C.3)

$$A_{opening} = 2 * A_{triangle} + L * A \tag{C.3}$$

where L=2.21 m.

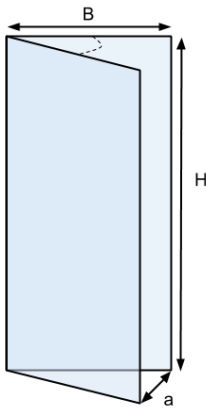
The opening areas used in the experimental measurements from [Blandkjenn, 2017] for the north windows were 25% and 50% of $A_{opening,max}$. Table C.1 lists the calculated angles that will produce similar opening areas for the CFD model.

Table C.1: Calculated opening angles for the north window

[%]	[m ²]	α [°]
25	0.197	16
50	0.393	25

C.3 South windows

C.3.1 Opening area found in [Blandkjenn, 2017]



The double-skin window were calculated to have a maximum window opening area of 1.13 m², for B = 0.85 m, H = 1.965 m and $a_{max} = 0.405$ m. Equation (C.4) calculates the opening area.

$$A_{opening} = a * H + 2 * \sqrt{p(p - a)(p - B)(p - B)} \tag{C.4}$$

where

$$p = (B + B + a)/2$$

The opening areas used in the experimental measurements from [Blandkjenn, 2017] for the south windows were 12.5%, 25%, 37.5%, 50% and 70% of $A_{opening,max}$.

Figure C.4: South window opening from [Blandkjenn, 2017]

